TOWARDS EFFICIENT MODELS FOR LITHIUM ION BATTERIES

A Dissertation

Presented to

the Faculty of the Graduate School

Tennessee Technological University

by

Vinten D. Diwakar

In Partial Fulfillment

of the Requirements for the Degree

DOCTOR OF PHILOSOPHY

Engineering

May 2009

CERTIFICATION OF APPROVAL OF DISSERTATION

TOWARDS EFFICIENT MODELS FOR LITHIUM ION BATTERIES

by

Vinten D. Diwakar

Graduate Advisory Committee:

Venkat R. Subramanian, Chairperson — Date: 04/29/09

Joseph J. Biernacki — Date: 04/30/09

Pedro E. Arce — Date: 04-30-09

Jie Cui — Date: 4-30-09

Jane Liu — Date: 04/29/09

Subramanian Deivanayagam — Date: 5/4/09

Approved for the Faculty:

Francis Otuonye
Associate Vice President of
Research and Graduate Studies

5/6/09
Date

AN ABSTRACT OF A DISSERTATION

TOWARDS EFFICIENT MODELS FOR LITHIUM ION BATTERIES

Vinten D. Diwakar

Doctor of Philosophy in Engineering

Lithium ion (Li-ion) batteries offer excellent cycle life, no memory effect, and high energy density when compared to competing chemistries like NiCd, NiMH, etc. These characteristics make Li-ion batteries the preferred power source for next generation hybrid vehicles. Models for Li-ion batteries have primarily focused on transport and reaction mechanisms for the first-principles prediction of their electrochemical behavior. For better understanding and better applicability of these models, Li-ion battery systems need to be considered both from a component and a system point of view. The present work demonstrates three different aspects related to model simulation of Li-ion batteries. Firstly, a simplification of an electrochemical engineering model is presented, that can be used to predict the electrochemical behavior of batteries. Secondly, a novel numeric symbolic solution (NSS) is presented to predict AC impedance response of electrodes. Thirdly, a novel Monte Carlo method with a simple framework is presented that can evaluate the performance characteristics of a Li-ion battery cathode material. The methods developed form a common theme of providing accurate results by way of a simpler computational framework with significant reduction in computational time and resources.

DEDICATION

To Amma and Appa

ACKNOWLEDGEMENTS

A grateful heart beats in me as I think of the days that I have spent at Tennessee Tech. First of all, thanks and praise be to my Lord and Savior Jesus for His grace and mercy that has sustained me, it's His infinite grace, mercy and love that allows me to live each day.

A heartfelt gratitude to my advisor Dr. Venkat Subramanian, He has been a mentor, a friend, and a guide to me. His patience and his confidence in my abilities has been a great source of encouragement and motivation. I shall always be thankful.

A note of thanks to my committee members: Dr. Joe Biernacki, Dr. Pedro Arce, Dr. Jie Cui, Dr. Jane Lui, and Dr. Deivy for valuable suggestions, support, and encouragement. I also feel the need to acknowledge the faculty at the Department of Chemical Engineering, including, Dr. Visco, Dr. Carpen, Dr. Oyanader, Dr. York, and Dr. Stretz for being a source of inspiration and models to follow.

A note of thanks also to my current group mates, Dr. Vijay, Venkat Sailainathan, and Mounika for all the fruitful discussions, encouragement, and friendship. Dr. Harinipriya and Kartik, my former colleagues for their support, friendship and insight.

To the Department of Chemical Engineering, which I have considered home for the past 6 years, thank you ever so much and a special word of gratitude to Becky Asher and Christy Huddleston for being caring, honest, extremely helpful, and patient with me.

To the Center for Energy Systems Research for financial support and a special word of thanks to Dr. Munukutla, Linda Lee, Sandy Garrison, Tony Greenway, and Etter Staggs who have always been kind, patient, and extremely helpful.

To my friends from Cookeville, Arul, "maama" Karthik, Guru, Pravin, Siva, Barath, Adrian, Sam, my Sunday school family at SSBC. Your friendship has meant the world to me and I thank the Lord for having provided friends such as you.

A debt of gratitude I owe to Dr. Daniel Badoe and Dr. Craig Henderson from the Department of Civil Engineering for their friendship, for as *Iron sharpeneth Iron*, so has your counsel pointed me in the right direction.

Last but not the least, my parents, my Mother, Mary E. Poornakumari, and my Father, Dr. Joseph E. Diwakar, who have always been a constant source of strength, encouragement and love; your prayers, have carried me! Thank you for your sacrifice and unconditional support.

"Laus Deo"

TABLE OF CONTENTS

Page

LIST OF TABLES..... x

LIST OF FIGURES..... xi

LIST OF SYMBOLS..... xiv

Chapter

1. INTRODUCTION..... 1

1.1. Lithium Ion Batteries..... 1

1.2. Components of a Lithium Ion battery..... 4

1.3. Working Mechanism..... 6

1.4. Characteristics of Battery Materials..... 8

1.5. Lithium Ion Battery Applications..... 11

1.6. Battery Management Systems..... 15

1.6.1. Types of battery management systems..... 17

1.6.1.1. Direct measurement systems..... 17

1.6.1.2. Bookkeeping systems..... 18

1.6.1.3. Adaptive systems..... 18

Chapter Page

1.6.2. Summary..... 18

2. MODELING OF LITHIUM ION BATTERIES..... 21

2.1. Cathode Governing Equations and Boundary Conditions..... 23

2.2. Separator Governing Equations and Boundary Conditions..... 27

2.3. Governing Equations and Boundary Conditions..... 28

2.4. Other Equations and Parameters Required..... 31

3. LITHIUM ION BATTERY MODEL SIMPLIFICATION AND SIMULATION..... 36

3.1. A Finite Difference Stencil for Numerical Simulation..... 36

3.2. Solution of the System of Differential Algebraic Equations..... 42

3.3. Electrolyte Concentration: Proof of Concept..... 45

3.4. Discharge Profiles..... 52

3.5. Intrinsic Variables..... 54

3.5.1. Solution Phase Concentration..... 54

3.5.2. Solid Phase Concentration..... 56

3.5.3. Solid Phase Potential..... 57

3.5.4. Solution Phase Potential..... 58

Chapter Page

4. IMPEDANCE RESPONSE – A NOVEL SYMBOLIC SOLUTION METHOD..... 61

4.1. Introduction..... 61

4.2. Example – Diffusive Impedance..... 62

4.2.1. Analytical Approach..... 64

4.2.2. Numerical Approach..... 64

4.2.3. Numeric Symbolic Solution..... 65

4.3. Comparison of Methods..... 69

4.4. Discussion..... 73

4.5. Future Work..... 76

5. NOVEL MONTE CARLO STRATEGY – LITHIUM ION CATHODE PERFORMANCE CHARACTERISTICS..... 78

5.1. Introduction..... 79

5.2. Methodology..... 81

5.3. Parameters Employed..... 84

5.4. Results and Discussion..... 84

5.4.1. Discharge Behavior of $LiCoO_2$..... 86

5.4.2. Discharge Behavior of $LiFePO_4$..... 88

Chapter Page

5.5. Perspectives..... 91

5.6. Conclusions from this Work..... 92

5.7. Scope for Future Work..... 93

6. PERSPECTIVES AND CONCLUSIONS..... 94

6.1. Multiscale Simulation of Battery Systems – Design of New Materials Using Simulation..... 95

6.2. Hybrid Systems Modeling – Coupled Modeling of Various Power Sources..... 97

6.3. Monitoring and Control of Battery Systems – Extending the Life-time of Battery Systems..... 98

6.4. Conclusions..... 99

BIBLIOGRAPHY..... 100

APPENDIX A: Summary of Governing equations and boundary conditions for a Li-ion Battery..... 112

VITA..... 113

LIST OF TABLES

Table		Page
1.1	Advantages of disadvantages Li-ion battery	3
1.2	Requirements for a cathode material	9
1.3	Requirements for a separator	9
1.4	Requirements for an anode material	11
1.5	The advantages and disadvantages of current state-of-art in BMS	19
2.1	Parameters used for the simulation ($LiCoO_2$ and LiC_6 system)	35
4.1	Comparison of computational times for different approaches for the simulation of AC impedance response	70
4.2	Comparison of estimated parameter values and computation time for different approaches	74
5.1	The parameters employed in the simulation strategy for $LiCoO_2$ and $LiFePO_4$	85

LIST OF FIGURES

Figure		Page
1.1	Typical commercially available cylindrical Li-ion battery showing the various components	4
1.2	Schematic representation of a typical Lithium Ion cell	5
1.3	Schematic of the electrochemical process in a Li-ion cell. M represents the metal species, for e.g., Cobalt	7
1.4	Schematic representation of the components of a Plug-in Hybrid Electric Vehicle (PHEV). The vehicle uses an electric motor and an internal combustion engine to propel the wheels	12
1.5	A proposed representation of a stationary hybrid power source for residential use. The power sources are a hybrid of Batteries, Fuel cells and super capacitors	14
1.6	A general architecture of a Battery Management System	15
2.1	Pictorial representation of a Li-ion cell. L_P, L_S, L_N represent the length of the positive electrode (cathode), separator and negative electrode (anode) respectively. 0, l_p, l_p+l_s, $l_p+l_s+l_n$ represent the interfaces at the cathode/current collector, cathode/separator, separator/anode and anode/current collector respectively	21
2.2	Open circuit potential of Li_xCoO_2 as a function of state-of-charge relative to potential of solid Li at the same electrolyte concentration	32
2.3	Open circuit potential of Li_xC_6 as a function of state-of-charge relative to potential of solid Li at the same electrolyte concentration	33
3.1	A Li-ion battery discretized stencil. Both the micro-scale and the macro-scale have been discretized	37
3.2	Different solvers available for use based on different discretization methods is shown	43

Figure Page

3.3 Schematic representation of the steps involved in the simplification of the Li-ion battery model..... 45

3.4 Comparison of electrolyte concentration distributions obtained by rigorous numerical and simplified model for a case of uniform current distribution..... 49

3.5 Discharge voltage as a function of time is plotted at different C rates for a galvanostatic case. The solid lines represent the full numeric model and the open symbols represent the simplified model..... 53

3.6 Solution phase concentration as a function of time is plotted at different interfaces rates for a galvanostatic case. The solid lines represent the full numeric model and the open symbols represent the simplified model..... 55

3.7 Solid phase concentration as a function of time is plotted at different interfaces rates for a galvanostatic case. The solid lines represent the full numeric model and the open symbols represent the simplified model..... 57

3.8 Comparison of solid phase potential (Φ_1) obtained from simulating the simplified model and rigorous finite difference model at different interfaces.. 58

3.9 Comparison of solution phase potential (Φ_2) obtained from simulating the simplified model and rigorous finite difference model at different interfaces.. 59

4.1 Computational procedure for numeric symbolic solution (NSS)..... 68

4.2 Impedance response of diffusion in a planar electrode (Nyquist plot). Solid line:-Analytical method, Dotted line (boxed):-Numerical method, Dotted line (circled):-Numeric symbolic solution, Solid line (thin line):- synthetic experimental data. Numerical and NSS data points coincide..... 71

4.3 Number of node points required for NSS for various values of Ω..... 75

5.1 Schematic representation of the Lithium ion battery cell assumed for the simulation purpose, The cathode is either $LiFePO_4$ or $LiCoO_2$, where lp, ls, ln represent the thickness(length) of cathode, separator and the anode respectively..... 82

Figure Page

5.2 Scheme 1 - The scheme for the proposed simulation methodology for the discharge behavior of $LiFePO_4$ and $LiCoO_2$ battery..... 83

5.3 The discharge behavior of (potential vs time) for $LiCoO_2$ (current applied in mA/cm^2)..... 87

5.4 Scheme 2 - Schematic representation of the processes occurring in the discharge process of $LiCoO_2$ as lithium ion battery cathode material, Li foil is employed as the anode and reference electrode for simulation purpose. Insert represents the discharge behavior of $LiCoO_2$ from simulations, identical with the results of ref. [61]..... 88

5.5 The discharge behavior (potential vs time) for $LiFePO_4$ (current applied in mA/cm^2)..... 90

5.6 Scheme 3 - Schematic representation of the processes occurring in the discharge process of $LiFePO_4$ as lithium ion battery cathode material, Li foil is employed as the anode and reference electrode for simulation purpose. Insert represents the discharge curve from simulation of results employing the above mechanism, identical with the results of ref. [86]..... 91

6.1 Simulation methods at varying time and length scales. Each method has its own independent attributes and can be used for specific purposes. Length scale and time scale overlap constitutes that there is flow of information between scales..... 96

LIST OF SYMBOLS

a_i	specific surface area of electrode i (i=p, n), m^2/m^3
$brugg_i$	Bruggman coefficient of region i (i=p, s, n)
c	electrolyte concentration, mol/m^3
c_0	initial electrolyte concentration, mol/m^3
$c_{s,i}$	concentration of lithium ions in the intercalation particle of electrode i (i=p, n), mol/m^3
$c_{s,i,0}$	initial concentration of lithium ions in the intercalation particle of electrode i (i=p, n), mol/m^3
$c_{s,i,max}$	maximum concentration of lithium ions in the intercalation particle of electrode i (i=p, n), mol/m^3
D	electrolyte diffusion coefficient, m^2/s
$D_{s,i}$	lithium ion diffusion coefficient in the intercalation particle of electrode i (i=p, n), m^2/s
F	Faraday's constant, C/mol
I	applied current density, A/cm^2
i_1	solid phase current density, A/m^2
i_2	solution phase current density, A/m^2
$i_{s,0}$	exchange current density for the solvent reduction reaction, A/m^2
j_s	solvent reduction current density, mol/m^2
j_i	wall flux of Li^+ on the intercalation particle of electrode i (i=n, p), mol/m^2

k_i intercalation/deintercalation reaction rate constant of electrode i (i=p,n), $mol/(mol/m^3)^{1.5}$

l_i thickness of region i (i=p, s, n), m

M_s molar weight of the solvent reaction product, g/mol

n negative electrode

p positive electrode

r radial coordinate, m

R universal gas constant, J/(mol·K)

R_i radius of the intercalation particle of electrode i (i=p, n), m

s separator

t_+ Li^+ transference number in the electrolyte

T absolute temperature, K

U_i open circuit potential of electrode i (i=p, n), V

U_s standard potential of the solvent reduction reaction, V

x spatial coordinate, m

δ thickness of the solvent reduction product film, m

δ_0 initial thickness of the solvent reduction product film, m

ε_i porosity of region i (i=p, s, n)

$\varepsilon_{f,i}$ volume fraction of fillers of electrode i (i=p, n)

θ_i dimensionless concentration of lithium ions in the intercalation particle of electrode i ($\theta_i = c_{s,i}/c_{s,i,max}$)

κ ionic conductivity of the electrolyte, S/m

$\kappa_{eff,i}$ effective ionic conductivity of the electrolyte in region i (i=p, s, n), S/m

ρ_s density of the solvent reduction product film, g/m^3

σ_i electronic conductivity of the solid phase of electrode i (i=p, n), S/m

$\sigma_{eff,i}$ effective electronic conductivity of the solid phase of electrode i (i=p, n), S/m

Φ_1 solid phase potential, V

Φ_2 electrolyte phase potential, V

CHAPTER 1

INTRODUCTION

Batteries are electrochemical energy storage devices that are able to convert chemical energy to electrical energy by means of an electrochemical reaction at an electrode site [1]. Batteries can be classified into two main categories, namely, the primary type and the secondary type. The primary battery is defined as a battery that cannot be recharged, or, it can be thought of as a single use battery, once the 'fuel' within the battery is used the battery needs to be replaced with a new one. The secondary battery can be used multiple times by recharging the battery by applying an external current to it. Of late, secondary batteries are in prime demand because of its wide spread use in the consumer electronics industry, for example in digital cameras, cellular phones, global positioning systems (GPS) etc.

1.1. Lithium Ion Batteries

Interest in Lithium ion batteries started with dissertation work by W. S. Harris in 1958 [2]. Work preceding Harris' dissertation ultimately led to the development of a variety of primary lithium cells during the 1970s. Early attempts at developing rechargeable (secondary) lithium cells were plagued by safety concerns because of venting and flames emanating from the cell at relatively lower discharge rates. The reactivity of the lithium metal was found to be the cause of venting and flames, this eventually led to research in lithium insertion compounds. The first groups to develop

lithium insertion compounds and use them in battery systems were Exxon and Moli energy with the Li/TiS_2 and Li/MoS_2 systems.

A large volume of work followed specifically from S. Wittingham and J. B. Goodenough et al. [3,4,5]. The use of lithium ion batteries were revolutionized and marketed by Matsushita electronics (Sony corporation) in the year 1991[6] with the use of a $LiCoO_2$, based, cathode. These batteries were also called 'rocking chair' batteries, because of the 'to' and 'fro' shuttling of lithium ions from cathode to anode during discharge and anode to cathode during charge. With decrease in the size and weight of portable electronic devices, the need of the hour was a battery that would be both light and be able to provide high power for a relatively smaller size. Lithium has a distinct advantage in that it is has the lightest weight, highest voltage and greatest energy density of any metal. These days the Li-ion battery is expected to power the next generation of Hybrid Electric Vehicles (HEVs) and a lot of research in the materials aspect has taken place. The advantages and disadvantages of the Li-ion battery chemistry are summarized and tabulated in Table 1.1.

Table 1.1. Advantages of disadvantages Li-ion battery (*ref.* 1)

Advantages	Disadvantages
Sealed cells; no maintenance required	Moderate initial cost
Long cycle life	Degrades at high temperature
Broad temperature range of operation	Need for protective circuitry
Long shelf life	Capacity loss or thermal runaway when overcharged
Low self discharge rate	
Rapid charge ability	Venting and possible thermal runaway when crushed
High rate and high power discharge capability	Cylindrical designs typically offer lower power density than NiCd or NiMH
High coulombic and energy efficiency	
High specific energy and energy density	
No memory effect	

1.2. Components of a Lithium Ion Battery

A typical cylindrical Li-ion battery construction is shown below in Figure 1.1. Li-ion batteries are packaged in four formats: prismatic, cylindrical, pouch, and button. Along with these four formats, coin cells or T cells are popular designs for laboratory use because of their ease in construction. The prismatic cells are wound in a rectangular fashion. Prismatic cells are mostly custom-made for cell phones and other high volume items. Prismatic cells have no venting system. Cylindrical cells, similar to the one shown in Figure 1.1, are wound in a coil like fashion. The cylindrical construction can withstand high internal pressures.

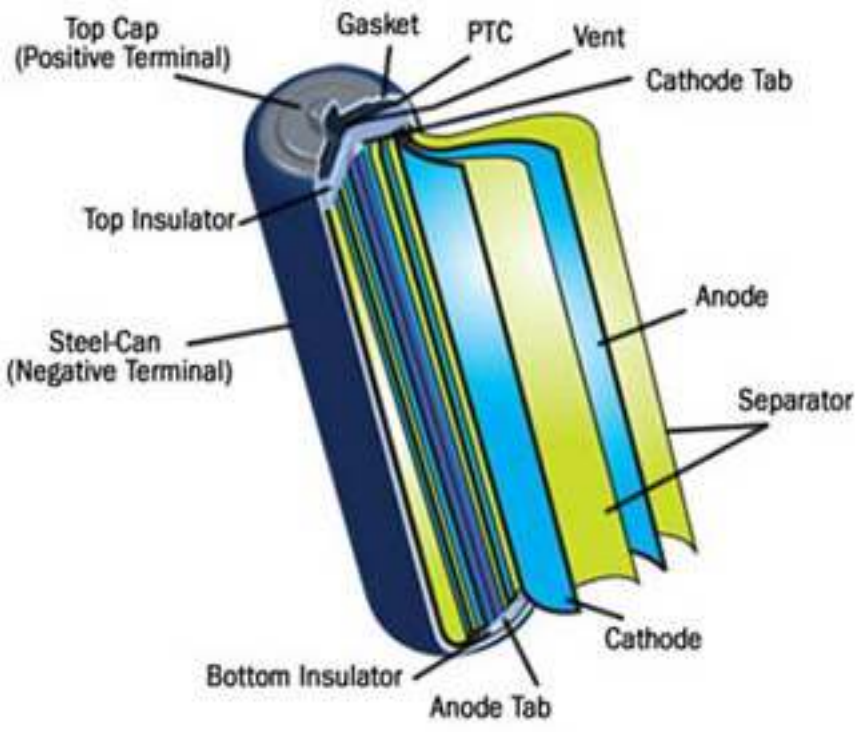

Figure 1.1: Typical commercially available cylindrical Li-ion battery showing the various components (source: Hitachi online – August 2008)

Typical applications are wireless communication, mobile computing, biomedical instruments, power tools, and applications that do not demand micro-packaging. Cylindrical cells are the design choice for making battery packs for HEV applications. The pouch cells are a less expensive alternative to the metal-cased batteries. They can be tailor-made to fit the application. The drawback of pouch cells is the factor of bulging during higher rates of discharge, which needs to be accounted for during the design.

The heart of the Li-ion battery is a unit called the 'cell' or 'cell-sandwich', depicted pictorially in Figure 1.2, which consists of the cathode, separator, and the anode. Batteries have many of these cells in series or have a single cell wound into the particular format. The main components of the Li-ion cell are; (i) Cathode, (ii) Anode, (iii) Separator, and (iv) Current collector.

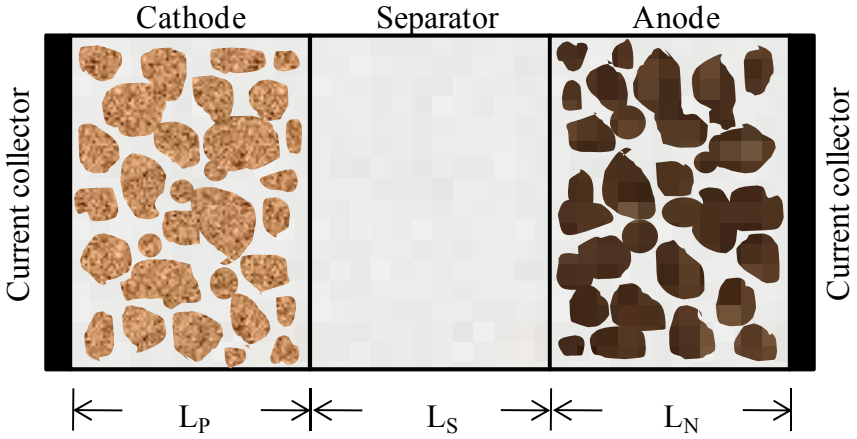

Figure 1.2: Schematic representation of a typical Lithium Ion cell.

1.3. Working Mechanism

The active materials in Li-ion cells operate by reversibly incorporating lithium in an intercalation process, a topotactic (insertion) reaction where lithium ions are reversibly removed or inserted into a host without a significant structural change to the host [7]. The positive material in a Li-ion cell is usually a metal oxide, with either a layered or tunneled structure. The graphitic carbon negative materials have a layered structure similar to graphite. Thus the metal oxide, graphite, and other materials act as hosts, incorporating lithium ions, reversibly to form ‘‘sandwich’’-like structures.

When a Li-ion cell is charged, the positive material is oxidized and the negative material is reduced. In this process, lithium ions are de-intercalated from the positive material and intercalated into the negative material, as illustrated in the reaction scheme (Equations 1.1 – 1.3) described below [1]. In this scheme, $LiMO_2$ represents the metal oxide positive material (cathode), such as $LiCoO_2$, and C the carbonaceous negative material (anode), such as graphite (Li_xC_6). The reverse happens during discharge.

Cathode (positive electrode): $$LiMO_2 \underset{\text{discharge}}{\overset{\text{charge}}{\rightleftharpoons}} Li_{1-x}MO_2 + xLi^+ + xe^- \quad (1.1)$$

Anode (negative electrode): $$C + xLi^+ + xe^- \underset{\text{discharge}}{\overset{\text{charge}}{\rightleftharpoons}} Li_xC \quad (1.2)$$

Overall: $$LiMO_2 + C \underset{\text{discharge}}{\overset{\text{charge}}{\rightleftharpoons}} Li_xC + Li_{1-x}MO_2 \quad (1.3)$$

Figure 1.3 further pictorially illustrates the working mechanism of the Li-ion battery. The electrode material is shown attached to current collectors, usually a high electronic conductor, this helps in moving the electrons to the load (represented by the Voltmeter).

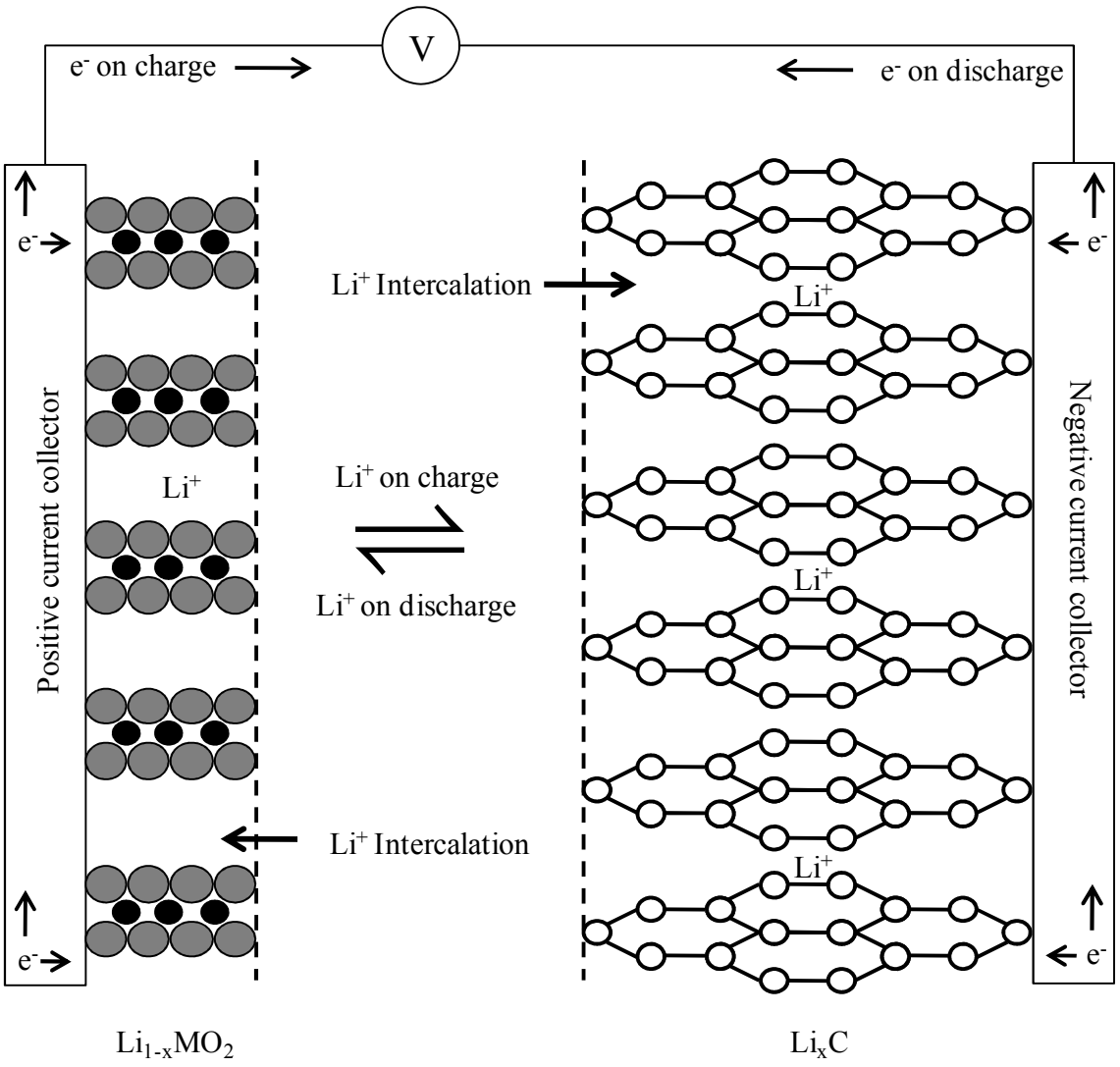

Figure 1.3: Schematic of the electrochemical process in a Li-ion cell (Adapted from *ref.* 1). M represents the metal species, for e.g., Cobalt.

1.4. Characteristics of Battery Materials

Possible electrode materials must satisfy a number of requirements which are summarized in Table 1.2. These factors guide the selection and development of positive electrode materials [7,8,9]. To enable high capacity, materials must incorporate a large amount of lithium. Further, the materials must reversibly exchange that lithium with little structural change to permit long cycle life, high coulombic efficiency, and high energy efficiency. To achieve high cell voltage and high energy density, the lithium exchange reaction must occur at a high potential relative to lithium. When a cell is charged or discharged, an electron is removed or returned to the positive material. So that this process can occur at a high rate, the electronic conductivity and Li^+ mobility in the material must be high. Also, the material must be compatible with the other materials in the cell; in particular it must not be soluble in the electrolyte. It is highly desired that the material must be of acceptable cost. To minimize cost, preparation from inexpensive materials in a low-cost process is preferred. The important requirements for cathode material are tabulated in Table 1.2.

Table 1.2: Requirements for a cathode material

- High free energy of reaction with Lithium
- Should be able to incorporate large quantity of lithium within its structure
- The material should reversible incorporate lithium with very minimal structural changes
- Should have high lithium ion diffusivity
- Good electronic conductivity
- Insoluble in the electrolyte
- Prepared from inexpensive reagents
- Low cost of synthesis

The principal function of a separator in a Li-ion battery is to keep the positive and negative electrodes apart. This is needed to prevent electrical short circuits and at the same time allow for rapid transport of ionic charge carriers that are critical to complete the circuit during the passage of current in the battery.

Table 1.3: Requirements for a separator

- It should be a good electronic insulator
- The electrolyte (ionic) resistance should be minimal
- The separator should offer mechanical and dimensional stability
- Sufficient physical strength to allow easy handling
- Chemical resistance to degradation by electrolyte, impurities, and electrode reactants and products
- It should be an effective barrier to prevent migration of particles or colloidal or soluble species between the two electrodes
- The separator has to be easily wet by electrolyte
- Uniform in thickness and other properties

The considerations that are important and influence the selection of the separator are tabulated in Table 1.3 [10,11]. For effective operation and stability of lithium-ion batteries require electrolyte solution consisting of linear combination of alkyl carbonates including organic solvents of ethylene carbonate (EC), propylene carbonate (PC), Dimethyl carbonate (DMC), diethyl carbonate (DEC), ethyl-methyl carbonate (EMC), etc., [12] and commonly used $LiClO_4$ or $LiPF_6$ as electrolyte salt. The electrolyte solution should have good ionic conductivity, have low electronic permittivity to prevent self discharge and remain stable over a wide potential widow. Additionally EC is a necessary component because of its thermal stability and its ability to form an effective protective surface film over the negative anode (graphite) to protect it from further reduction by the electrolyte. Hence, Li^+ ion insertion and the stability of graphite anode in salt solution is strongly dependent on the composition of the electrolyte solution [13,14,15].

Pure lithium metal itself, as the anode, provides the best capability, energy density, and lightest weight [16]. However, due to its highly reactive nature, it is usually unsafe and potentially explosive and flammable; irreversible dendrites can also be formed after many cycles. The commercial battery uses graphitic carbon as the anode. It has a relatively low theoretical capacity of 372 mAh/g, and may pose safety problems, especially at a high current rate. It cannot meet the demand for the system of the next generation and new materials to replace graphite are explored. The following criteria have to be met for new anode materials and are tabulated below in Table 1.4:

Table 1.4: Requirements for an anode material (*ref.* 1,7,9)

- High capacity and energy density.
- Excellent capacity retention.
- Low irreversible capacity loss during first cycle.
- Good discharge voltage vs Li, preferably between 0.3 and 0.5V.
- No co-intercalation of solvent molecules into the structure.
- Low price and environmentally benign
- Good rate capability and performance at low temperature.

1.5. Lithium Ion Battery Applications

One way of classifying Lithium ion batteries can be classified based on the type of application it is manufactured for: (1) Stationary Applications and (2) Transportation Applications. There is also another way to classify these batteries based on whether they are used by the military or by civilians. It is important to make a clear distinction between civilian and military applications because, the usage characteristics vary very markedly and the demands on the battery for each of these applications are very different. It can be argued that some batteries can be used both for civilian and military applications but most military batteries have to pass a stringent quality control policy over and above that required for civilian applications in order for it to be declared fit to be used in military applications. Stationary applications range from powering portable electronics to powering long-range communications, locating (GPS) and data gathering devices used by foot soldiers in war zones. Another important projected use of lithium ion batteries in stationary applications is in back-up power units for small homes and offices.

Of late the push towards finding an alternative energy source to replace internal combustion engines has propelled the Lithium-ion battery as the prime candidate. The United States Council for Automotive Research in their freedom car and fuel partnership program has set requirements and goals for the use of batteries in vehicular applications [17]. The desirable characteristics that need to be met by the advanced battery technologies include (but are not limited to) high power density, long cycle life, and wide range of operating variables. Figure 1.4 shows the various components of a hybrid vehicle's propulsion system.

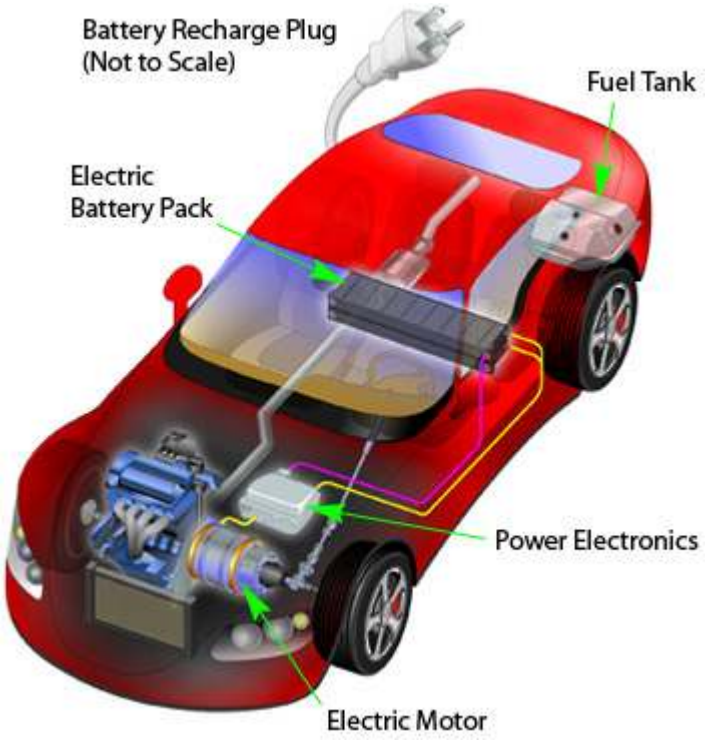

Figure 1.4: Schematic representation of the components of a Plug-in Hybrid Electric Vehicle (PHEV). The vehicle uses an electric motor and an internal combustion engine to propel the wheels (Picture source: National Renewable Energy laboratory).

The important components are the brushless electric motors, the battery pack, an internal combustion engine, and a power electronics module. Current hybrid vehicles use Nickel Metal Hydride batteries (NiMH), and as previously noted, suffer from memory effect losses and poor power to weight ratios. Lithium ion batteries are expected to replace the NiMH batteries on the next generation of hybrid vehicles. The hybrid vehicles use regenerative braking and IC engine power to charge the batteries while the vehicle is in operation. The power electronics module is used to monitor the battery's state-of-charge and state-of-health; this forms a very important component of the hybrid vehicle.

The PHEV is the next generation of hybrid vehicles that are to be launched shortly into the market. The main advantages of a PHEV over conventional hybrids are the ability to charge the battery packs from an external power source and the increase in driving range on battery power. Lithium-ion battery packs provide the most power and life for a given weight and are hence being installed on next generation PHEVs. A much anticipated example of a PHEV is the Chevy Volt, which is expected to enter commercial markets in the year 2011 [18]. The volt uses lithium ion batteries to power its electric motor.

Figure 1.5 depicts a proposed residential auxiliary power supply unit. The principal idea is to replace conventional uninterupted power supply (UPS) system with ones similar to the design shown in the figure. Conventional UPS systems use IC engine coupled to a generator to provide uninterupted power supply during failure of the city's power supply. It should be noted that the system consists of a hybrid of electrochemical power sources, namely, a battery pack, fuel cell, and a supercapacitor. Depending on the load on the system, any one of the power sources or a combination or all three can be in

use. This requires monitoring and control; the computer-based control center would be used for this operation.

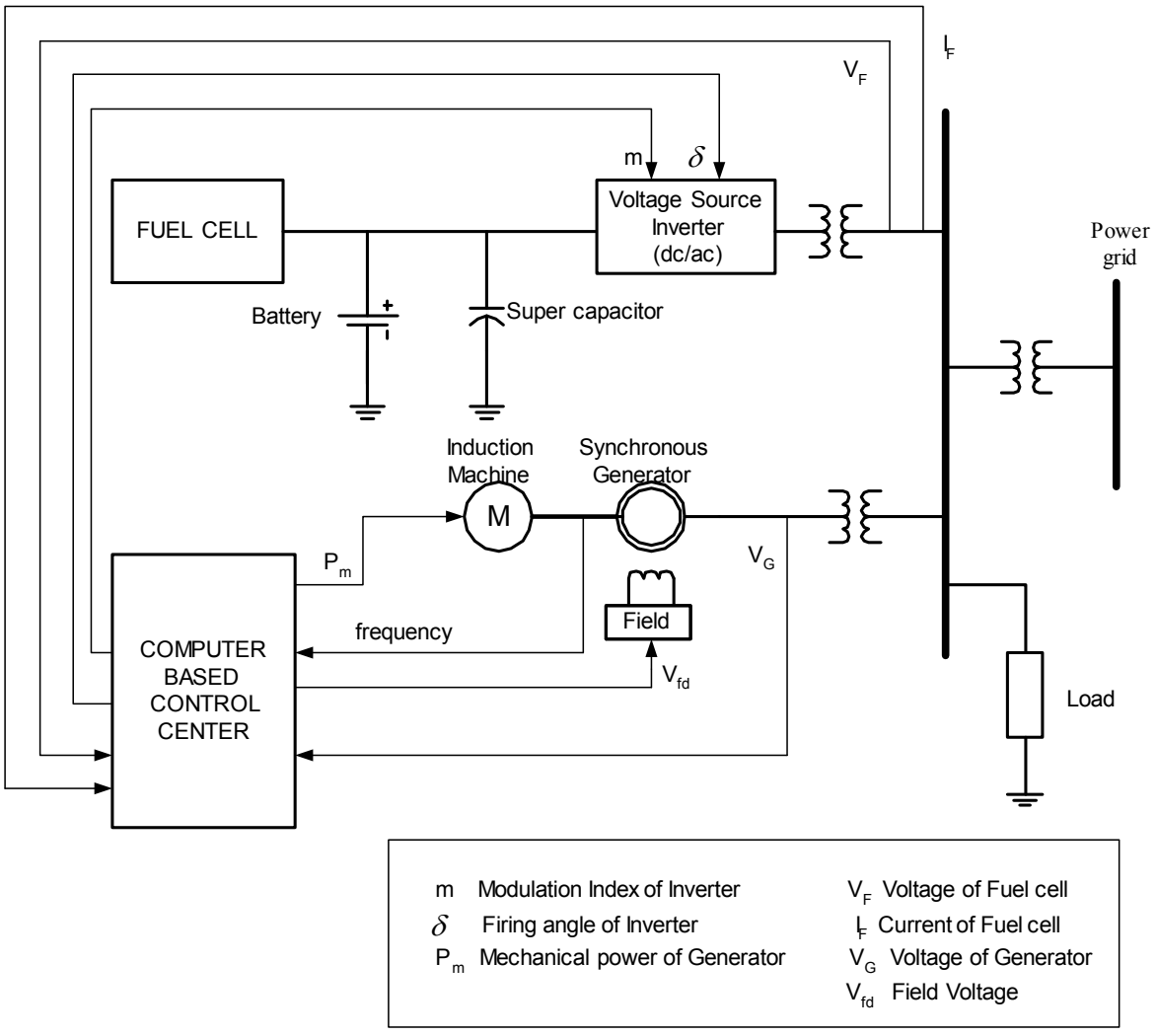

Figure 1.5: A proposed representation of a stationary hybrid power source for residential use. The power sources are a hybrid of Batteries, Fuel cells and supercapacitors. (Source: Dr. Gadhir Radman, Tennessee Technological University)

1.6. Battery Management Systems

It is evident from the previous section that the devices that run on Li-ion batteries are varied and complex. The power demands on these systems are not constant in real world applications and the variations need to be accounted for. Some applications, especially those that require accurate remaining run-time information, monitoring of battery capacity, etc., for example, satellite electronics and military GPS systems, require super accurate data from the battery to make important battery usage/management decisions. This requires the use of a Battery Management System (BMS). A BMS can be envisioned as an arrangement that ensures that optimum use is made of the energy available inside the battery powering the device and that the risk of damage to the battery is prevented. This is achieved by monitoring and controlling the battery's charging and discharging process. A general block diagram of a BMS is shown in Figure 1.5 [19].

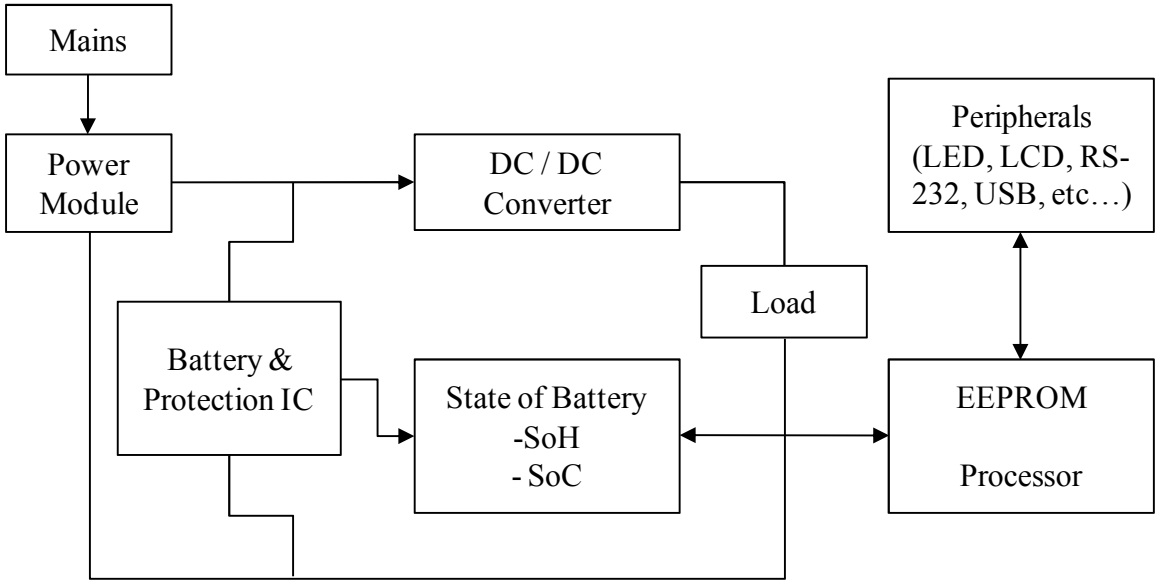

Figure 1.5: A general architecture of a battery management system (*ref.* 19).

The basic task of the power module (PM) is to charge the battery by converting electrical energy from the mains (external power supply) into electrical energy suitable for charging the battery. The PM can either be a separate external device, for example, a travel charger, or it can be integrated within the portable device, for example, in shavers. A protection Integrated Circuit (IC) connected in series with the battery is generally needed for Li-ion batteries. The reason for this is that battery suppliers are particularly concerned about safety issues due to liability risks. Discharging the Li-ion battery below 3.0V may cause irreversible damage to the cell because of dendritic growth which may eventually lead to shorting. Shorting causes the battery to explode or catch fire. The battery voltage, current, and temperature have to be monitored and the protection IC ensures that the battery is never operated under unsafe conditions. The battery manufacturer determines the operating conditions under which it is assumed to be safe to use Li-ion batteries. Outside the safe region, the battery may not be very stable and may cause it to behave in a destructive manner.

The DC/DC converter is used to efficiently condition the unregulated battery voltage (commonly, 4.2–3.0 V in Li-ion chemistry) for compatibility with stringent load requirements. The load converts the electrical energy supplied by a battery into an energy form that will fulfill the load's function, such as mechanical energy (as in electrical motors used in HEVs), light, sound, heat, etc. The battery status can be indicated by a display system (LCD, LED, etc.) that point to the State-of-Charge (SoC) and the battery's condition (e.g., the State-of-Health (SoH)). The processor is used to run the battery-management software, including the SoC algorithm. Communication between the BMS and other devices is another important task of the BMS. Depending on the application,

various systems can be used for data exchange, such as an inter-integrated-circuit bus interface (I^2C) or some other form of serial interface [20]. The battery state is used as an input parameter for the portable device's electrical management and it is an important parameter for the user. The battery state can be used to estimate the battery's expected lifetime. It can be simply described by two parameters: SoC and SoH. Both parameters depend on each other and influence the battery performance.

SoC is defined as the percentage of the maximum possible charge that is present inside a rechargeable battery and SoH is a 'measure' that reflects the general condition of a battery and its ability to deliver the specified performance in comparison with a fresh battery (fully charged new battery).

1.6.1. Types of battery management systems

Battery management systems are classified into three main categories in literature [21,22]; they are

- Direct measurement
- Book-keeping method
- Adaptive systems

1.6.1.1. Direct measurement systems. As the name suggests, these systems, are based on measurement of battery variables such as voltage (V), battery impedance, and the voltage relaxation time after the battery is subject to a step input of current. The direct measurement based systems can be further classified into three types: (1)

voltage measurements, (2) the Electro-Motive Force (EMF) method and (3) Impedance measurement.

1.6.1.2. Bookkeeping systems [22]. This system is based on measuring and integrating the current. This method is sometimes also referred to as 'coulomb counting', since it involves literally counting the charge that is entering and exiting the battery. These Coulomb counting data of the battery and other relevant data of the battery such as self-discharge rate of the battery, temperature, charge/discharge efficiency, history (i.e., cycle life), etc., are used as input for the book-keeping system.

1.6.1.3. Adaptive systems. Due to the unpredictability of user behavior, the battery response to user behavior is rarely linear. Designing an accurate SoC indicator therefore is not a simple task. An adaptive system that uses a combination of direct measurement and book-keeping methods is a reasonable solution for the problem. Many methods such as using artificial neural networks (ANN), Fuzzy logic, Kalman filters, etc., have been used to design adaptive battery management systems [23,24,25,26,27]. The advantages and drawbacks of these systems are tabulated in Table 1.3.

1.6.2. Summary

Although, the adaptive systems are advanced and can perform complex calculations for a more efficient BMS, it cannot be ignored that their computational,

memory and implementation requirements are very high. Another point of contention is the use of circuit models in these BMS systems. Circuit models can be effectively used when considering average quantities over time or length scales and can show very promising results in limiting conditions; however, the nonlinear behavior of the battery response to external user loads can cause drastic deviations from limiting cases and cause the circuit models to fail.

Table 1.5: The advantages and disadvantages of current state-of-art in BMS (*ref.* 21)

BMS Technique	Advantages	Disadvantages
Discharge test	Easy and accurate	Offline, time intensive, modifies the battery state, loss of energy
Impedance spectroscopy	Gives information about SoH and quality	Temperature sensitive, cost intensive
EMF	Online, cheap, EMF prediction	Needs long rest time (current = 0)
Coulomb counting	Accurate if enough re-calibration points are available and with good current measurements	Sensitive to parasite reactions; needs regular re-calibration points
ANN	Online	Needs training data of a similar battery, expensive to implement
Fuzzy logic	Online	Memory required in real-word application in very high
Kalman filters	Online, dynamic	Difficult to implement the filtering algorithm that considers all features such as, for e.g., abnormalities and nonlinearities

Engineering (continuum) models for batteries encompass transport phenomena, thermodynamics, and kinetics, defining the working principles of the battery and providing a strong, robust, and accurate predictive tool for engineers to work with. Engineering models are usually defined by a set of partial differential equations (PDE) and solving them could be tedious depending on the models. Reformulating these engineering models to enable quick and efficient simulation could prove a valuable tool in the next generation of BMS. The motivation for the current work stems from the failure of circuit models to capture all the physics and the expensive nature of adaptive systems preventing their implementation in certain applications. One of the primary objectives of the group has been in coming up with reformulation strategies, specifically, reformulated models that are computationally extremely fast 'real-time', robust, and extremely accurate. To come up with reformulated models one needs to first identify the right mathematical model(s) for the Li-ion battery system. The following chapter walks through the development of a Li-ion battery model.

CHAPTER 2

MODELING OF LITHIUM ION BATTERIES

Mathematical modeling of lithium ion batteries involves defining the dependant variables and their respective governing equations along with necessary boundary and initial conditions [28,29,30,31,32]. These models can be derived by considering basic chemical engineering principles such as material balances, reaction kinetics, and thermodynamics. Li-ion battery models use concentrated solution theory, porous electrode theory, and Butler-Volmer type of kinetics in their formulation [33,34,35,36]. Figure 2.1 shows the geometry that is being modeled.

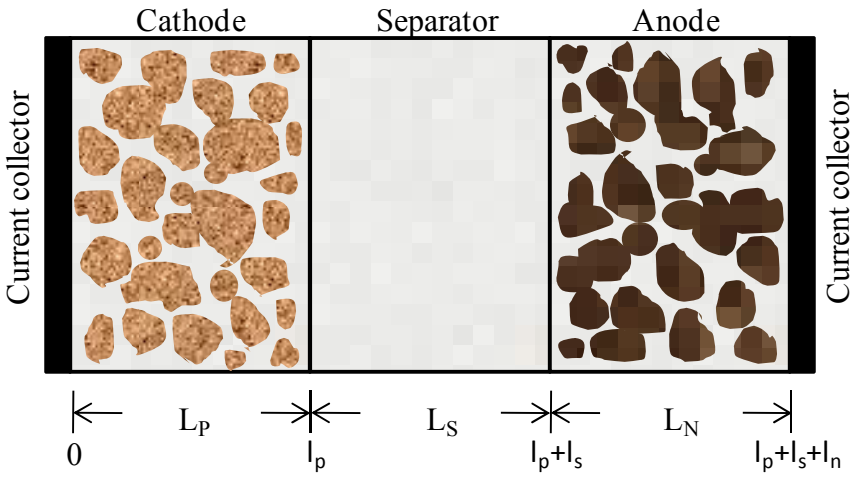

Figure 2.1: Pictorial representation of a Li-ion cell. L_P, L_S, L_N represent the length of the positive electrode (cathode), separator and negative electrode (anode) respectively. 0, l_p, l_p+l_s, $l_p+l_s+l_n$ represent the interfaces at the cathode/current collector, cathode/separator, separator/anode and anode/current collector respectively.

The electrodes as described in Chapter 1 are porous in nature and are preferred over solid (non-porous) electrodes because it provides large interfacial area for the electrode reaction. The porous nature of the electrode helps in significantly reducing the distance required by the reactants to reach the surface. Newman developed the first model to describe the porous electrode in which he treated the porous electrode as a super-position of electrode and solution phases for a priory known volume fractions [37]. This simplifies the model from having to use detailed pore geometries and using instead the specific interfacial area, a_i, and volume fractions of each phase or porosity, ε [38,39,40,41].

Li-ion batteries usually use binary electrolytes. These electrolytes have a high salt concentration >1M. The use of concentrated solution theory is therefore of prime importance to describe the transport of electrolyte within the Li-ion cell. At constant temperature and pressure the concentration solution theory defines the driving force for mass transfer as being the gradient of electrochemical potential for the ionic species (Li^+).

The following sections define and explain the governing equations, constraint equations, and initial and boundary conditions that are needed to solve continuum models to predict battery discharge behavior [42,43,44,45].

2.1. Cathode Governing Equations and Boundary Conditions

The potential drop in the solid phase of the positive electrode is governed by Ohm's law:

$$i_1 = -\sigma_{\text{eff,p}} \frac{\partial \Phi_1}{\partial x} \tag{2.1}$$

At the current collector/electrode interface, i.e., $x = 0$, the entire current density is carried by the solid phase. Hence we have

$$\left.\frac{\partial \Phi_1}{\partial x}\right|_{x=0} = -\frac{I}{\sigma_{\text{eff,p}}} \tag{2.2}$$

where I is the applied current density (the current which is divided by the projected electrode area). I is positive when charging the cell. The potential drop in the solution phase is given by the modified Ohm's law:

$$i_2 = -\kappa_{\text{eff,p}} \frac{\partial \Phi_2}{\partial x} + \frac{2\kappa_{\text{eff,p}} RT}{F}\left(1 - t_+\right)\frac{\partial \ln c}{\partial x} \tag{2.3}$$

Setting the value for the solution phase potential equal to zero, as a reference value, at $x = 0$ provides the necessary constraint for this equation:

$$\Phi_2\big|_{x=0} = 0 \tag{2.4}$$

The current densities in the solid phase and the solution phase total up to the applied current density:

$$i_1 + i_2 = I \tag{2.5}$$

and the divergence of the solution phase current is related to the pore wall flux at the cathode through

$$a_{\mathrm{p}} F j_{\mathrm{p}} = \frac{\partial i_2}{\partial x} \tag{2.6}$$

These two equations provide the distribution of the current in the solution and the solid phase, respectively. All the current that enters the separator is assumed to be through the solution phase; i.e., we have

$$i_2\big|_{x=l_{\mathrm{p}}} = I \tag{2.7}$$

This provides the additional constraint required to solve Equation 2.6.

The flux j_p is related to the potentials in the solid and solution phases through the Butler-Volmer type kinetics equation:

$$j_{\mathrm{p}} = 2k_{\mathrm{p}} \left(c_{s,\mathrm{p,max}} - c_{\mathrm{s,p}}\big|_{r=R_{\mathrm{p}}} \right)^{0.5} \left(c_{\mathrm{s,p}}\big|_{r=R_{\mathrm{p}}} \right)^{0.5} c^{0.5} \sinh\left[\frac{0.5F}{RT} \left(\Phi_1 - \Phi_2 - U_{\mathrm{p}} \right) \right] \tag{2.8}$$

The concentration of lithium at the solid/solution interface, $c_{\mathrm{s,p}}\big|_{r=R_{\mathrm{p}}}$, is obtained by solving the Fick's law in spherical coordinates. The active cathode material is assumed to be made up of spherical particles of radius R_p with diffusion being the mechanism of transport of the lithium. If r is the direction normal to the surface, then for the concentration of lithium inside the solid phase we have

$$\frac{\partial c_{\mathrm{s,p}}}{\partial t} = D_{\mathrm{s,p}}\left(\frac{\partial^2 c_{\mathrm{s,p}}}{\partial r^2} + \frac{2}{r}\frac{\partial c_{\mathrm{s,p}}}{\partial r}\right) \tag{2.9}$$

The initial condition for Equation 2.9 is given by

$$c_{\mathrm{s,p}}\Big|_{t=0} = c_{\mathrm{s,p,0}} \tag{2.10}$$

Here $c_{\mathrm{s,p,0}}$ is the initial solid concentration. Since the diffusion coefficients are assumed to be constants we have by symmetry

$$\left.\frac{\partial c_{\mathrm{s,p}}}{\partial r}\right|_{r=0} = 0 \tag{2.11}$$

The second boundary condition is given by accounting for the relationship between the pore wall flux j_{p} and the rate of diffusion of lithium ions into the surface of the cathode material:

$$-D_{\mathrm{s,p}}\left.\frac{\partial c_{s,p}}{\partial r}\right|_{r=R_{\mathrm{p}}} = j_{\mathrm{p}} \tag{2.12}$$

Finally, the solution phase concentration is given by the material balance on the electrolyte phase [41]:

$$\varepsilon_{\mathrm{p}}\frac{\partial c}{\partial t} = D_{\mathrm{eff,p}}\frac{\partial^2 c}{\partial x^2} + \left(1-t_{+}\right)a_{\mathrm{p}}j_{\mathrm{p}} - \frac{i_2}{F}\frac{dt_{+}}{dx} \tag{2.13a}$$

The transference number, t_{+}, is a transport property that is function of concentration. For most practical simulation purposes and lack of experimental data it is assumed to be a

constant, this eliminates the third term on the right-hand side of Equation 2.13a. The equation then becomes

$$\varepsilon_{\mathrm{p}} \frac{\partial c}{\partial t} = D_{\mathrm{eff,p}} \frac{\partial^2 c}{\partial x^2} + \left(1 - t_{+}\right) a_{\mathrm{p}} j_{\mathrm{p}} \qquad 2.13\mathrm{b}$$

The initial concentration of the electrolyte is set to a known constant value, c_0:

$$c\big|_{t=0} = c_0 \text{ for all } x \qquad 2.14$$

The flux at the electrode/current collector interface is zero:

$$\left.\frac{\partial c}{\partial x}\right|_{x=0} = 0 \text{ for all } t \qquad 2.15$$

and the flux is continuous at the separator/electrode interface:

$$D_{\mathrm{eff,p}} \left.\frac{\partial c}{\partial x}\right|_{x=l_{\mathrm{p}}^{-}} = D_{\mathrm{eff,s}} \left.\frac{\partial c}{\partial x}\right|_{x=l_{\mathrm{p}}^{+}} \qquad 2.16$$

To summarize this section, there are seven dependent variables in the cathode region: the solid and solution phase potentials (Φ_1 and Φ_2), solid and solution phase concentrations ($c_{\mathrm{s,p}}$ and c), solid and solution phase currents (i_1 and i_2) and the flux at the cathode (j_{p}).

2.2. Separator Governing Equations and Boundary Conditions

There are two dependent variables in the separator: the solution phase concentration (c) and the solution phase potential (Φ_2). The solution phase concentration is governed by the material balance for lithium in the solution phase of the separator:

$$\varepsilon_s \frac{\partial c}{\partial t} = D_{\text{eff,s}} \frac{\partial^2 c}{\partial x^2} \tag{2.17}$$

The initial concentration of the electrolyte is set to a known constant, c_0:

$$c\big|_{t=0} = c_0 \text{ for all } x \tag{2.18}$$

and the flux is continuous at either separator/electrode interface:

$$D_{\text{eff,p}} \left.\frac{\partial c}{\partial x}\right|_{x=l_p^-} = D_{\text{eff,s}} \left.\frac{\partial c}{\partial x}\right|_{x=l_p^+} \tag{2.19}$$

$$D_{\text{eff,n}} \left.\frac{\partial c}{\partial x}\right|_{x=\left(l_p+l_s\right)^+} = D_{\text{eff,s}} \left.\frac{\partial c}{\partial x}\right|_{x=\left(l_p+l_s\right)^-} \tag{2.20}$$

The potential distribution in the separator is given by

$$I = -\kappa_{\text{eff,s}} \frac{\partial \Phi_2}{\partial x} + \frac{2\kappa_{\text{eff,s}} RT}{F}\left(1-t_+\right)\frac{\partial \ln c}{\partial x} \tag{2.21}$$

The solution phase current density is continuous across the separator/electrode interface:

$$\left[-\kappa_{\text{eff,p}}\frac{\partial\Phi_2}{\partial x}+\frac{2\kappa_{\text{eff,p}}RT}{F}\left(1-t_+\right)\frac{\partial\ln c}{\partial x}\right]_{x=l_{\text{p}}^-} = \left[-\kappa_{\text{eff,s}}\frac{\partial\Phi_2}{\partial x}+\frac{2\kappa_{\text{eff,s}}RT}{F}\left(1-t_+\right)\frac{\partial\ln c}{\partial x}\right]_{x=l_{\text{p}}^+} \quad 2.22$$

2.3. Anode Governing Equations and Boundary Conditions

There are nine dependent variables in the anode: the solid and solution phase potentials (Φ_1 and Φ_2), solid and solution phase concentrations ($c_{\text{s,n}}$ and c), solid and solution phase current densities (i_1 and i_2) and the flux at the anode for the intercalation reaction (j_{n}) are governed by equations similar to those in the cathode. In addition there are two other variables, namely, the side reaction flux (j_{s}) and the thickness of the film (δ), which grows on the anode particle due to solvent reduction. The following equations are used to describe the profiles of all these variables:

The potential drop in the solid phase of the positive electrode is governed by Ohm's law:

$$i_1=-\sigma_{\text{eff,n}}\frac{\partial\Phi_1}{\partial x} \quad 2.23$$

At the current collector/electrode interface, i.e., x = $l_{\text{p}}+l_{\text{s}}+l_{\text{n}}$, the entire current is carried by the solid phase. Hence we have

$$\left.\frac{\partial \Phi_1}{\partial x}\right|_{x=l_p+l_s+l_n} = -\frac{I}{\sigma_{\text{eff,n}}} \tag{2.24}$$

The potential drop in the solution phase is given by the modified Ohm's law:

$$i_2 = -\kappa_{\text{eff,n}} \frac{\partial \Phi_2}{\partial x} + \frac{2\kappa_{\text{eff,n}} RT}{F}\left(1-t_+\right)\frac{\partial \ln c}{\partial x} \tag{2.25}$$

and the ionic current is continuous across the separator/electrode interface:

$$\begin{aligned}&\left[-\kappa_{\text{eff,n}} \frac{\partial \Phi_2}{\partial x} + \frac{2\kappa_{\text{eff,n}} RT}{F}\left(1-t_+\right)\frac{\partial \ln c}{\partial x}\right]_{x=\left(l_p+l_s\right)^+} = \\ &\left[-\kappa_{\text{eff,s}} \frac{\partial \Phi_2}{\partial x} + \frac{2\kappa_{\text{eff,s}} RT}{F}\left(1-t_+\right)\frac{\partial \ln c}{\partial x}\right]_{x=\left(l_p+l_s\right)^-}\end{aligned} \tag{2.26}$$

The current densities in the solid phase and the solution phase total up to the applied current density:

$$i_1 + i_2 = I \tag{2.27}$$

and the solution phase current is related to the flux at the anode as follows:

$$a_n F\left(j_n + j_s\right) = \frac{\partial i_2}{\partial x} \tag{2.28}$$

These two equations provide the distribution of the current in the solution and the solid phase, respectively. At the interface of the separator and the anode, the solution phase current density is equal to the applied current density; i.e., we have

$$i_2\big|_{x=l_p+l_s} = I \tag{2.29}$$

This provides the additional constraint required to solve Equation 2.25. The intercalation flux j_n is related to the potentials in the solid and solution phases through the Butler-Volmer type kinetic equation:

$$j_{\mathrm{n}} = 2k_{\mathrm{n}}\left(c_{s,n,\max} - c_{\mathrm{s,n}}\big|_{r=R_n}\right)^{0.5}\left(c_{\mathrm{s,n}}\big|_{r=R_n}\right)^{0.5} c^{0.5}\sinh\left[\frac{0.5F}{RT}\left(\Phi_1 - \Phi_2 - U_{\mathrm{n}}\right)\right] \tag{2.30}$$

The concentration of lithium at the solid/solution interface, $c_{\mathrm{s,n}}\big|_{r=R_{\mathrm{n}}}$, is obtained by solving the Fick's law in the spherical coordinates, for the concentration of lithium inside the solid phase [42,43]:

$$\frac{\partial c_{\mathrm{s,n}}}{\partial t} = D_{\mathrm{s,n}}\left(\frac{\partial^2 c_{\mathrm{s,n}}}{\partial r^2} + \frac{2}{r}\frac{\partial c_{\mathrm{s,n}}}{\partial r}\right) \tag{2.31}$$

The initial and boundary conditions for this equation are given by

$$c_{\mathrm{s,n}}\big|_{t=0} = c_{\mathrm{s,n},0} \tag{2.32}$$

$$\left.\frac{\partial c_{\mathrm{s,n}}}{\partial r}\right|_{r=0} = 0 \tag{2.33}$$

$$-D_{\mathrm{s,n}}\left.\frac{\partial c_{\mathrm{s,n}}}{\partial r}\right|_{r=R_{\mathrm{n}}} = j_{\mathrm{n}} \tag{2.34}$$

Finally, the solution phase concentration is given by the material balance on the electrolyte phase:

$$\varepsilon_{\mathrm{n}} \frac{\partial c}{\partial t} = D_{\mathrm{eff,n}} \frac{\partial^2 c}{\partial x^2} + \left(1 - t_+\right) a_{\mathrm{n}} j_{\mathrm{n}} \qquad 2.35$$

The initial concentration of the electrolyte is set to a known constant, c_0:

$$c\big|_{t=0} = c_0 \text{ for all } x \qquad 2.36$$

The flux at the electrode/current collector interface is zero:

$$\left.\frac{\partial c}{\partial x}\right|_{x=0} = 0 \qquad 2.37$$

and the flux is continuous at the separator/electrode interface:

$$D_{\mathrm{eff,n}} \left.\frac{\partial c}{\partial x}\right|_{x=\left(l_{\mathrm{p}}+l_{\mathrm{s}}\right)^+} = D_{\mathrm{eff,s}} \left.\frac{\partial c}{\partial x}\right|_{x=\left(l_{\mathrm{p}}+l_{\mathrm{s}}\right)^-} \qquad 2.38$$

2.4. Other equations and Parameters Required

U_{p} is defined as the anode theoretical open circuit potential. The open-circuit potential is obtained by a coulometric titration (measuring the potential of the insertion material versus a Li reference electrode at a very-low-rate discharge at room temperature (25$^{\mathrm{o}}$C)) [49,50]. The magnitude and dependence of U_{p} on solid phase concentration vary considerably among different insertion materials. The shape of the open-circuit potential profile has a large effect on the simulation results, and accurate data for this property is very important. The expression is obtained by fitting to experimental data and also varies on the manufacturing technique used and the manufacturer. θ_{p} is the SoC of the system.

For a $LiCoO_2$ system in Equation 2.8, U_p depends on θ_p ($= c_{s,p}\big|_{r=R_p} / c_{s,p,max}$) according to the following equation:

$$U_p = \frac{-4.656 + 88.669\theta_p^{\,2} - 401.119\theta_p^{\,4} + 342.909\theta_p^{\,6} - 462.471\theta_p^{\,8} + 433.434\theta_p^{\,10}}{-1.0 + 18.933\theta_p^{\,2} - 79.532\theta_p^{\,4} + 37.311\theta_p^{\,6} - 73.083\theta_p^{\,8} + 95.96\theta_p^{\,10}} \qquad 2.39$$

Figure 2.2 shows the open-circuit potential as a function of x in Li_xCoO_2.

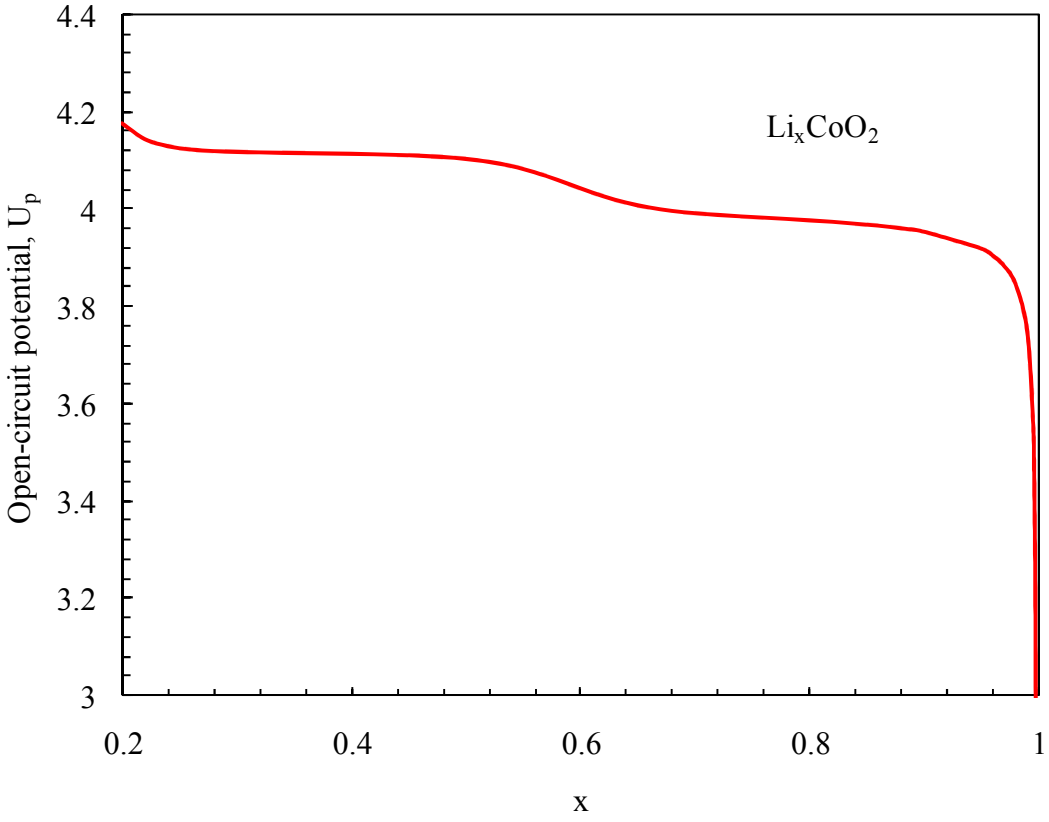

Figure 2.2: Open circuit potential of Li_xCoO_2 as a function of state-of-charge relative to potential of solid Li at the same electrolyte concentration.

Similarly for the negative electrode we have expression 2.40 also plotted in Figure 2.3;

In Equation 2.30, U_n depends on θ_n ($= c_{s,n}\big|_{r=R_n} / c_{s,n,max}$) according to the following equation:

$$U_n = 0.7222 + 0.1387\theta_n + 0.029\theta_n^{0.5} - \frac{0.0172}{\theta_n} + \frac{0.0019}{\theta_n^{1.5}} + 0.2808\exp(0.90 - 15\theta_n) - 0.7984\exp(0.4465\theta_n - 0.4108) \quad 2.40$$

U_n is defined as the anode theoretical open circuit potential.

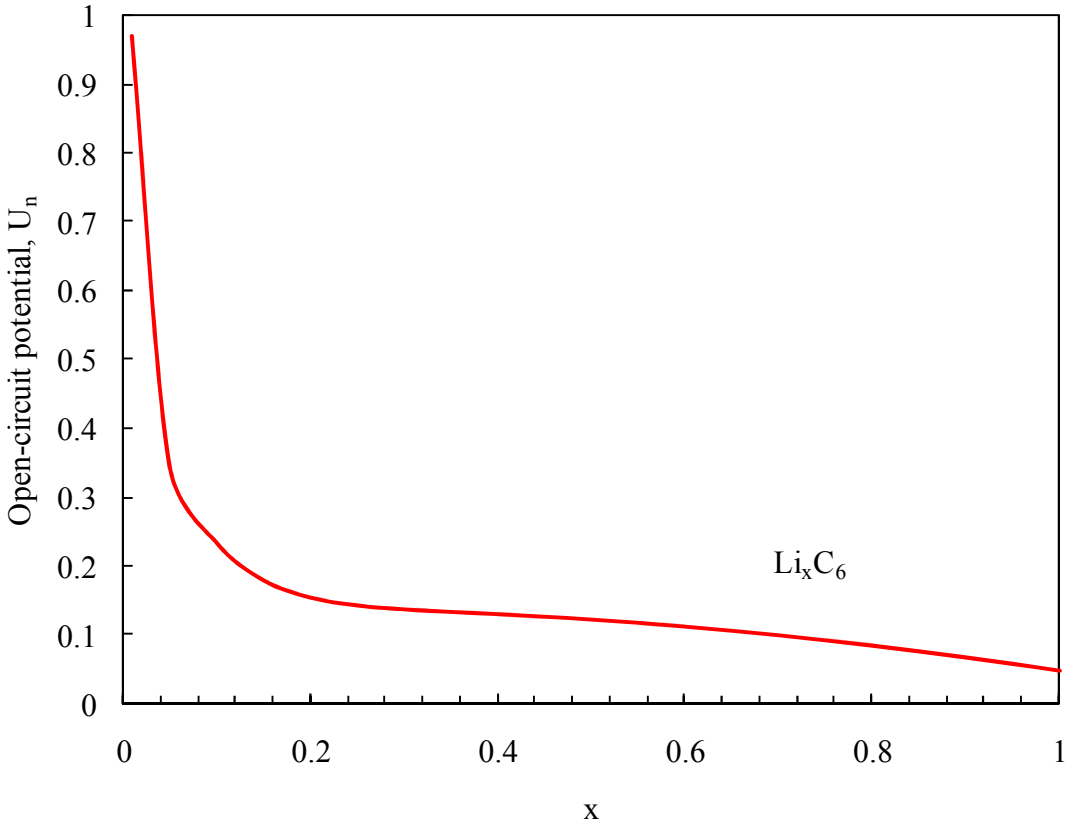

Figure 2.3: Open circuit potential of Li_xC_6 as a function of state-of-charge relative to potential of solid Li at the same electrolyte concentration.

The following relationships are used in the equations presented in the previous sections:

$$\sigma_{\text{eff,i}} = \sigma_{\text{i}}\left(1-\varepsilon_{\text{i}}-\varepsilon_{\text{f,i}}\right), \quad \text{i=p, n} \tag{2.41}$$

Equation 2.41 defines the effective electronic conductivity.

$$\kappa_{\text{eff,i}} = \begin{pmatrix} 4.1253\times10^{-2} + 5.007\times10^{-1}c - 4.7212\times10^{-1}c^2 \\ +1.5094\times10^{-1}c^3 - 1.6018\times10^{-2}c^4 \end{pmatrix} \varepsilon_{\text{i}}^{\ \text{brugg}_{\text{i}}}, \quad \text{i=p, s, n} \tag{2.42}$$

Equation 2.42 defines the effective ionic conductivity distribution at each domain, which is a function of ion concentration in each of the modeling domains [40]. The conductivity is measured for a system consisting of 2:1 v/v mixture of EC/DMC and reported at 25$^{\text{o}}$C. This expression is obtained by fitting to experimental values.

$$D_{\text{eff,i}} = D\varepsilon_{\text{i}}^{\ \text{brugg}_{\text{i}}}, \ \text{i=p, s, n} \tag{2.43}$$

The effective diffusion co-efficient is given by Equation 2.43. It is the product of the average diffusion coefficient and tortuosity, ε. The factor brugg_{i} is defined as the Bruggemann coefficient and accounts for the porosity of the medium.

$$a_{\text{i}} = \frac{3}{R_{\text{i}}}\left(1-\varepsilon_{\text{i}}-\varepsilon_{\text{f,i}}\right), \ \text{i=p, n} \tag{2.44}$$

These effective transport properties, i.e., $\kappa_{\text{eff,i}}$, $D_{\text{eff,i}}$, and $\sigma_{\text{eff,i}}$, given by the above expressions account for the tortuous path the ions in solution need to trace around the solid particles or the electrons must take around the electrolyte filled pores within the electrode [49].

The governing equations are tabulated and summarized in Appendix A. A list of electrode and design parameter used in modeling the system is given in Table 2.1. Electrode parameters include, diffusion coefficients, conductivity data, etc. Design parameters include; electrode thickness, particle size, etc.

Table 2.1: Parameters used for the simulation ($LiCoO_2$ and LiC_6 system)

Symbol	*Units*	*Positive Electrode*	*Separator*	*Negative Electrode*
σ_i	S/m	100		100
$\varepsilon_{f,i}$		0.025		0.0326
ε_i		0.385	0.724	0.485
Brugg		4		
$D_{s,i}$	m^2/s	1.0×10^{-14}		3.9×10^{-14}
D	m^2/s	7.5×10^{-10}		
k_i	$Mol/(s\cdot m^2)/(mol/m^3)^{1+\alpha a,i}$	2.334×10^{-11}		5.0307×10^{-11}
$c_{s,i,max}$	mol/m^3	51554		30555
$c_{s,i0}$	mol/m^3	0.4955×51554		0.8551×30555
c_0	mol/m^3	1000		
R_p	m	2.0×10^{-6}		2.0×10^{-6}
l_i	m	80×10^{-6}	25×10^{-6}	88×10^{-6}
R_{SEI}	$\Omega\cdot m^2$	0.0		
t_+		0.363		
F	C/mol	96487		
R	J/(mol·K)	8.314		
T	K	298.15		

CHAPTER 3

LITHIUM ION BATTERY MODEL SIMPLIFICATION AND SIMULATION

3.1. A Finite Difference Stencil for Numerical Simulation

The finite different method (FDM) is used to discretize the spatial co-ordinate in 1D/2D/3D partial differential equations with initial and boundary conditions [51]. FDM generates a regular grid over the computational domain. The finite difference method has been used extensively in Lithium ion battery modeling due to its simplicity and accuracy. Finite difference is used in conjunction with time-stepping solvers for better accuracy. Applying finite difference on the governing equations (usually a combination of partial differential equations and or differential equations with algebraic equations) converts the governing equations to a set of differential algebraic equations by discretizing in the spatial coordinate. At this point since most of the simulation is done using finite difference formulation, it is important to derive the display the discretized equations. This forms the ready-to-solve set of DAEs that need to solved for obtaining the discharge profiles.

The discretized stencil for the battery is shown in Figure 3.1. The Boundaries are at 0 and 3N+3. The two interfaces are at N+1 and 2N+2. We use M node points for the solid phase concentration. At the current collector end of the cathode, the flux for the electrolyte and solid phase potentials are zero and applied charge/discharge current density, respectively. Since there is no flow to the left of this region the flux for the electrolyte concentration is also equal to zero.

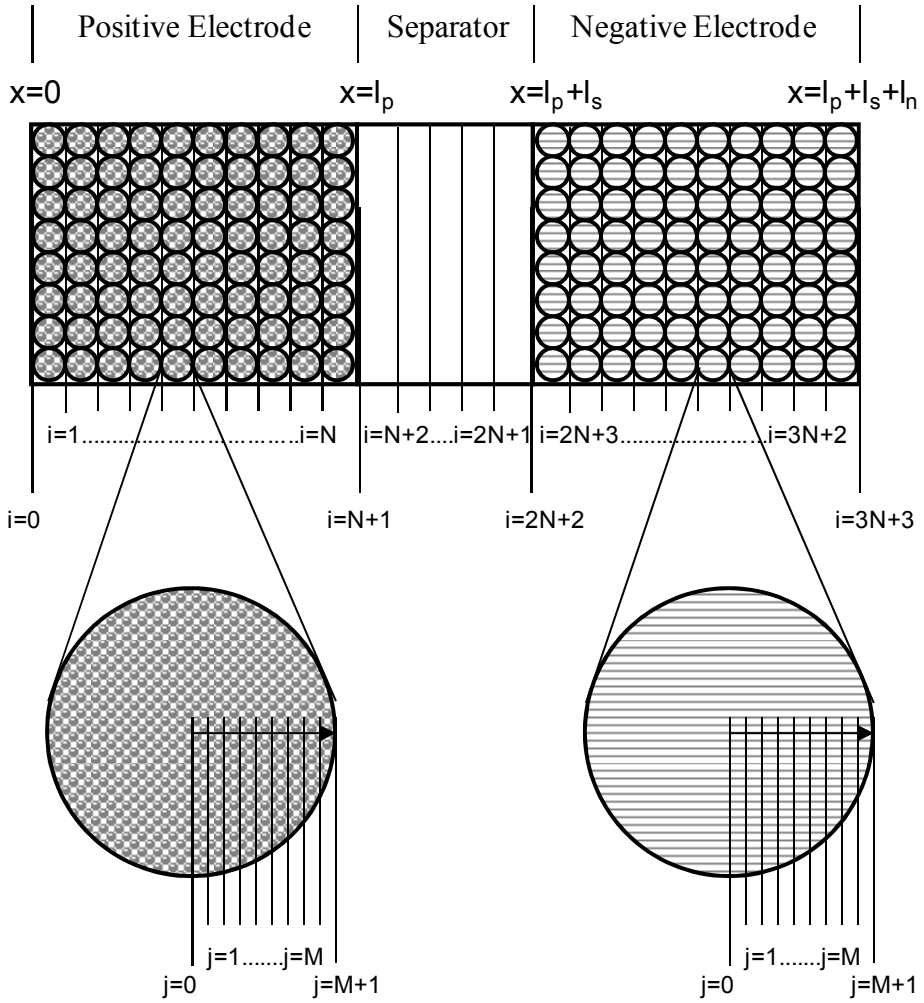

Figure 3.1: A Li-ion battery discretized stencil. Both the micro-scale and the macro-scale have been discretized.

At x = 0, i = 0 and thus the discretized equations are

$$-D_{\text{eff,p}}\left[\frac{-c_2+4c_1-3c_0}{2h_1}\right]=0 \tag{3.1}$$

$$-\kappa_{\text{eff,p}}\left[\frac{-\Phi 2_2+4\Phi 2_1-3\Phi 2_0}{2h_1}\right]=0 \tag{3.2}$$

$$-\sigma_{\text{eff,p}}\left[\frac{-\Phi 1_2+4\Phi 1_1-3\Phi 1_0}{2h_1}\right]=I \tag{3.3}$$

These three boundary conditions at x = 0 account for three algebraic equations to the resulting system of DAEs. The model equations for electrolyte concentration and solid-phase concentration have an explicit time derivative, they constitute differential equations in time. The direct approach to handle this situation of two different length scales is discretization in both x and r and is shown below,

For $0 < x < l_p$, $0 < i < N+1$

$$\varepsilon_{\text{p}}\frac{dc_i}{dt}=D_{\text{eff,p}}\frac{c_{i+1}-2c_i+c_{i-1}}{h_1^2}+\left(1-t_+\right)a_{\text{p}}j_{\text{p}i} \tag{3.3}$$

$$-\sigma_{\text{eff,p}}\left[\frac{\Phi 1_{i+1}-\Phi 1_{i-1}}{2h_1}\right]-\kappa_{\text{eff,p}}\left[\frac{\Phi 1_{i+1}-\Phi 1_{i-1}}{2h_1}\right]+\frac{2\kappa_{\text{eff,p}}RT}{F}\left(1-t_+\right)\frac{1}{c_i}\left[\frac{c_{i+1}-c_{i-1}}{2h_1}\right]=I \tag{3.4}$$

$$\sigma_{\text{eff,p}}\frac{\Phi 1_{i+1}-2\Phi 1_i+\Phi 1_{i-1}}{h_1^2}=a_{\text{p}}Fj_{\text{p}} \tag{3.5}$$

The solid-phase transport equation is discretized in r with M internal node points as follows:

At r = 0, j = 0

$$\left[\frac{-cs_2+4cs_1-3cs_0}{2\Delta r}\right]=0 \tag{3.6}$$

For $0 < r < R_p$, $0 < j < M+1$

$$\frac{dcs_j}{dt}=D_{\text{s,p}}\left(\frac{cs_{j+1}-2cs_j+cs_{j-1}}{\Delta r^2}+\frac{2}{j\Delta r}\left[\frac{cs_{j+1}-cs_{j-1}}{2\Delta r}\right]\right) \tag{3.7}$$

At $r = R_p$, $j = M+1$

$$j_p = -D_{s,p}\left[\frac{3cs_{M+1} - 4cs_M + cs_{M-1}}{2\Delta r}\right] \tag{3.8}$$

The discretized form of the expressions for effective electrolyte conductivity in cathode, separator and anode can be obtained by simply replacing the variable c with its respective discrete form $c_{(i)}$.

The fluxes for electrolyte concentration and potential are continuous at the interfaces between the porous cathode-separator and separator-porous anode. This needs a careful mathematical step because this situation demands application of both forward and backward differences in x and node spacing in two different regions of interest.

At $x = l_p$, $i = N+1$,

$$-D_{eff,p}\left[\frac{c_{N-1} - 4c_N + 3c_{N+1}}{2h_1}\right] = -D_{eff,s}\left[\frac{-3c_{N+1} + 4c_{N+2} - c_{N+3}}{2h_2}\right] \tag{3.9}$$

$$-\kappa_{eff,p}\left[\frac{\Phi 2_{N-1} - 4\Phi 2_N + 3\Phi 2_{N+1}}{2h_1}\right] = -\kappa_{eff,s}\left[\frac{-3\Phi 2_{N+1} + 4\Phi 2_{N+2} - \Phi 2_{N+3}}{2h_2}\right] \tag{3.10}$$

$$-\sigma_{eff,p}\left[\frac{\Phi 1_{N-1} - 4\Phi 1_N + 3\Phi 1_{N+1}}{2h_1}\right] = 0 \tag{3.11}$$

Meanwhile, the two governing equations for the separator are also discretized using central difference formulae.

For $l_p < x < l_p + l_s$, $N+1 < i < 2N+2$

$$\varepsilon_{\mathrm{s}} \frac{dc_i}{dt} = D_{\mathrm{eff,s}} \frac{c_{i+1} - 2c_i + c_{i-1}}{h_2^2} \tag{3.12}$$

$$-\kappa_{\mathrm{eff,s}} \left[\frac{\Phi 2_{i+1} - \Phi 2_{i-1}}{2h_2} \right] + \frac{2\kappa_{\mathrm{eff,s}} RT}{F} \left(1 - t_+\right) \frac{1}{c_i} \left[\frac{c_{i+1} - c_{i-1}}{2h_2} \right] = I \tag{3.13}$$

The discretized of governing equations at the second interface are derived similar to the first interface.

At $x = l_p + l_s$, $i = 2N+2$,

$$-D_{\mathrm{eff,s}} \left[\frac{c_{2N} - 4c_{2N+1} + 3c_{2N+2}}{2h_2} \right] = -D_{\mathrm{eff,n}} \left[\frac{-3c_{2N+2} + 4c_{2N+3} - c_{2N+4}}{2h_3} \right] \tag{3.14}$$

$$-\kappa_{\mathrm{eff,s}} \left[\frac{\Phi 2_{2N} - 4\Phi 2_{2N+1} + 3\Phi 2_{2N+2}}{2h_2} \right] = -\kappa_{\mathrm{eff,n}} \left[\frac{-3\Phi 2_{2N+2} + 4\Phi 2_{2N+3} - \Phi 2_{2N+4}}{2h_3} \right] \tag{3.15}$$

$$-\sigma_{\mathrm{eff,n}} \left[\frac{-3\Phi 1_{2N+2} + 4\Phi 1_{2N+3} - \Phi 1_{2N+4}}{2h_3} \right] = 0 \tag{3.16}$$

The anode equations are formulated in a similar fashion to the cathode equations using central difference formulae.

For $l_p + l_s < x < l_p + l_s + l_n$, $2N+2 < i < 3N+3$

$$\varepsilon_{\mathrm{n}} \frac{dc_i}{dt} = D_{\mathrm{eff,n}} \frac{c_{i+1} - 2c_i + c_{i-1}}{h_3^2} + \left(1 - t_+\right) a_{\mathrm{n}} j_{\mathrm{n}i} \tag{3.17}$$

$$-\sigma_{\mathrm{eff,n}} \left[\frac{\Phi 1_{i+1} - \Phi 1_{i-1}}{2h_3} \right] - \kappa_{\mathrm{eff,n}} \left[\frac{\Phi 2_{i+1} - \Phi 2_{i-1}}{2h_3} \right] + \frac{2\kappa_{\mathrm{eff,n}} RT}{F} \left(1 - t_+\right) \frac{1}{c_i} \left[\frac{c_{i+1} - c_{i-1}}{2h_3} \right] = I \tag{3.18}$$

$$\sigma_{\mathrm{eff,n}} \frac{\Phi 1_{i+1} - 2\Phi 1_i + \Phi 1_{i-1}}{h_3^2} = a_{\mathrm{n}} F j_{\mathrm{n}i} \tag{3.19}$$

The solid-phase transport equation is discretized in r with M internal node points as follows:

At r = 0, j = 0

$$\left[\frac{-cs_2 + 4cs_1 - 3cs_0}{2\Delta r}\right] = 0 \tag{3.20}$$

For $0 < r < R_n$, $0 < j < M+1$

$$\frac{dcs_j}{dt} = D_{s,n}\left(\frac{cs_{j+1} - 2cs_j + cs_{j-1}}{\Delta r^2} + \frac{2}{j\Delta r}\left[\frac{cs_{j+1} - cs_{j-1}}{2\Delta r}\right]\right) \tag{3.21}$$

At $r = R_n$, $j = M+1$

$$j_{n(i)} = -D_{s,n}\left[\frac{3cs_{M+1} - 4cs_M + cs_{M-1}}{2\Delta r}\right] \tag{3.22}$$

The equations at the extreme boundary are obtained using backward differences formulae.

At $x = l_p + l_s + l_n$, $i = 3N+3$,

$$-D_{eff,n}\left[\frac{c_{3N+1} - 4c_{3N+2} + 3c_{3N+3}}{2h_3}\right] = 0 \tag{3.23}$$

$$\Phi 2_{3N+3} = 0 \tag{3.24}$$

$$-\sigma_{eff,n}\left[\frac{\Phi 1_{3N+1} - 4\Phi 1_{3N+2} + 3\Phi 1_{3N+3}}{2h_3}\right] = I \tag{3.25}$$

The above system of DAEs, Equations 3.26 – 3.51 can readily be solved by a mathematician using any DAE solver to simulate charge or discharge behavior as shown in Figure 3.1. This approach forms the basis for battery simulation.

3.2. Solution of the System of Differential Algebraic Equations

There are many commercially available solvers for solving a system of PDEs or DAEs. They involve discritizing the spatial variables in one of three forms; finite differences, finite elements and finite volumes. A few of the methods available are shown in Figure 3.2 below. Finite differences is the preferred discretization method for Li-ion battery models since the battery model is pseudo 2D, and the stencil for which is shown in the previous chapter. For the current work, the rigorous numerical model was simulated using BANDJ, DASSL, BESRIK, and COMSOL [52,53,54,55]. Although COMSOL has a strong multiphysics engine and a robust solver, it still did not prove to be very effective when compared against DASSL and BESIRK. BESIRK was chosen finally because of its robustness, ease of interface with FORTRAN and MAPLE (our GUI of choice), and ease of use for this particular problem. Having said that it is important to note that an initialization problem needed to be addressed while using BESIRK and an initializing solver DAEIS was used to mitigate the problem by other researchers from of the group [56].

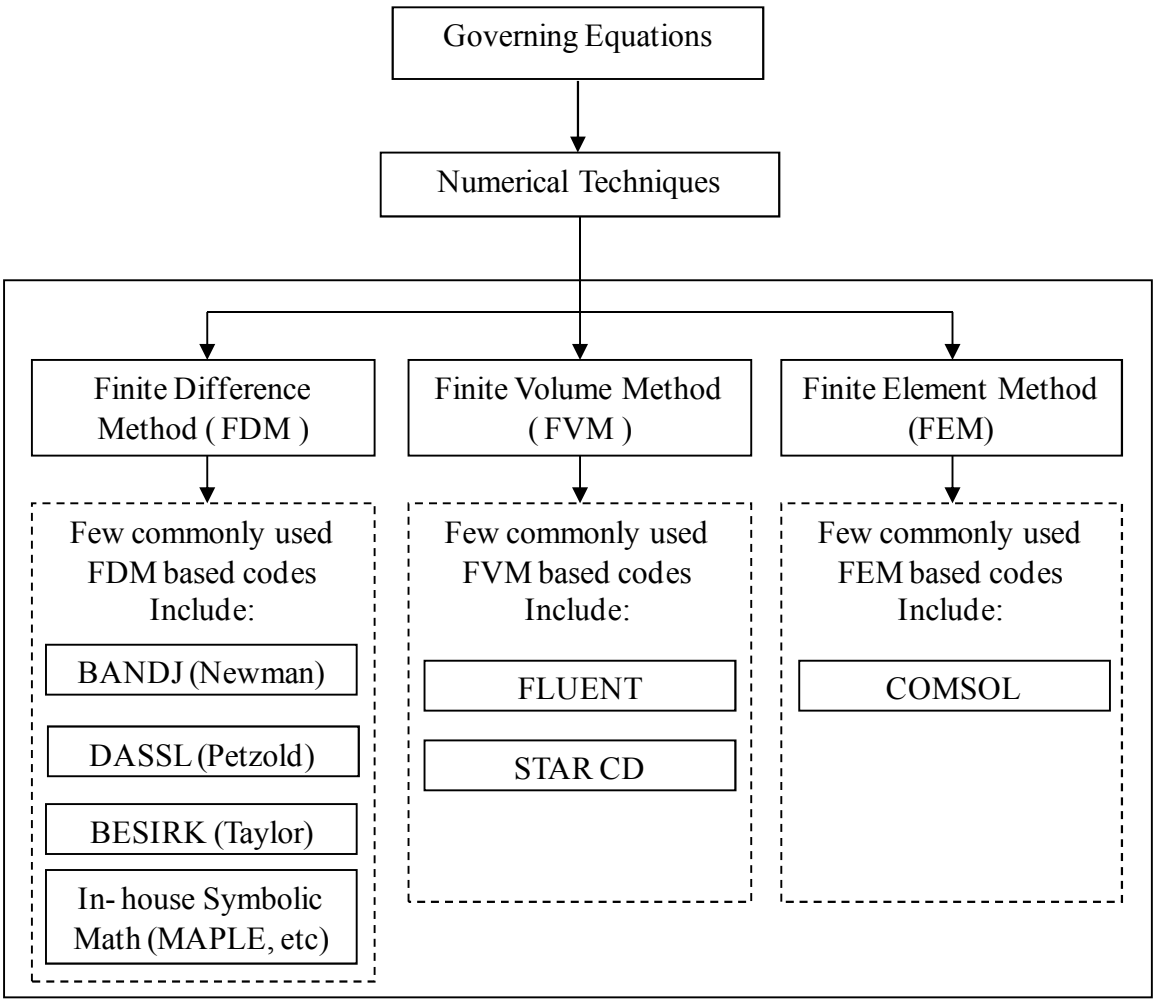

Figure 3.2: Different solvers available for use based on the different discretization methods is shown.

Model simplification for any modeling system depends on the model complexity and order of the models. In the literature, order reduction based on volume-averaging, Liapunov-Schmidt technique, etc., has been illustrated for various systems including monolith reactors [57-59]. Even classical perturbation techniques can help in simplifying the models and hence the number of equations to be solved. However, to our knowledge, these methods have been applied only for models in which the independent variable, x for

example, varies between 0 and 1 or L (constant physical properties across the entire domain of interest). Lithium-ion batteries have three regions of different physical properties with different number of equations in each region (positive electrode/separator/negative electrode). In addition, standard order reduction techniques require a parameter (for example aspect ratio, time-constant, etc.) based on which the order of PDEs is reduced (for example, 2D to 1D or 1D PDE to ODE).

The following sections show a simplified model that has been arrived at for Li-ion battery model. Figure 3.3 shows the different steps developed in the simplification strategy. Given the number of space discritized equations involved, real-time simulation of the lithium-ion battery model is impractical as of today. Real-time optimization and feedback control of sensitive Lithium-ion battery where the health of the battery is vital to the very operation of the device requires quick solving models that give an accurate account of the battery variables. The full physics model described in Chapter 2 is therefore not the best candidate for real-time optimization and control. To facilitate real-time simulation, more than one mathematical concept has to be used. In the present study volume averaging, approximation methods, Liapunov-Schmidt based simplification of the variables are explored.

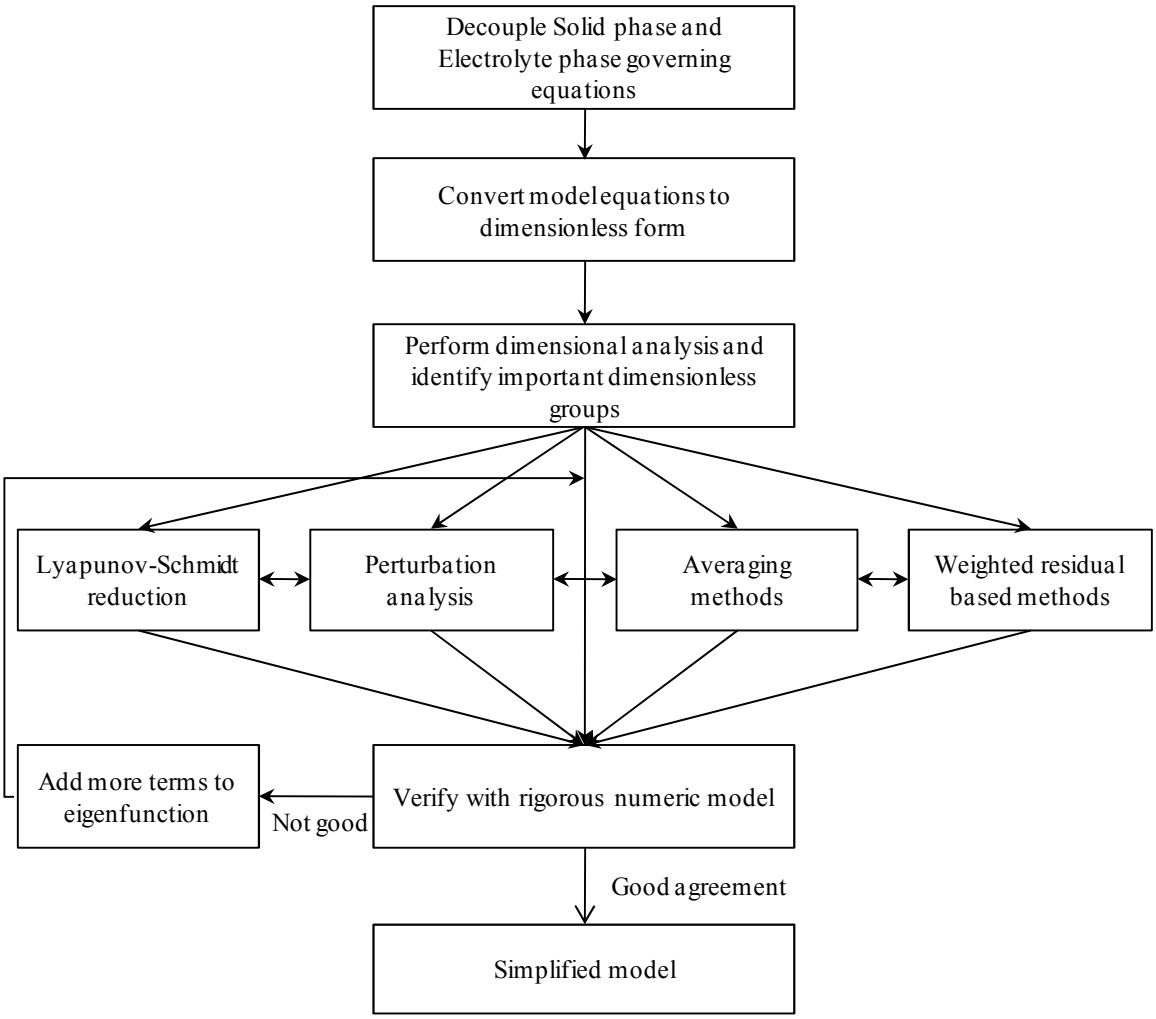

Figure 3.3: Schematic representation of the steps involved in the simplification of the Li-ion battery model.

3.3. Electrolyte Concentration: Proof of Concept

Consider the case of uniform current distribution, the electrolyte concentration governing equations in the three regions are [60]

$$\varepsilon_p \frac{\partial c}{\partial t} = D\varepsilon_p^{bruggp} \frac{\partial^2 c}{\partial x^2} + a_p \left(1-t_+\right) j_p \qquad 3.26$$

$$\varepsilon_s \frac{\partial c}{\partial t} = D\varepsilon_s^{bruggs} \frac{\partial^2 c}{\partial x^2} \quad 3.27$$

$$\varepsilon_n \frac{\partial c}{\partial t} = D\varepsilon_n^{bruggn} \frac{\partial^2 c}{\partial x^2} + a_n \left(1\text{-}t_+\right) j_n \quad 3.28$$

j_n and j_p are the pore wall flux at the negative electrode and positive electrode respectively, and for uniform current distribution they are given by

$$j_n = \frac{I}{a_n F l_n} \text{ and } j_p = \frac{I}{a_p F l_p} \quad 3.29$$

Equations 3.26-3.28 are rewritten in dimensionless form as follows:

$$\frac{\partial C}{\partial \tau} = \varepsilon_p^{bruggp\text{-}1} \frac{\partial^2 C}{\partial X^2} + J_p \quad 3.30$$

$$\frac{\partial C}{\partial \tau} = \varepsilon_s^{bruggs\text{-}1} \frac{\partial^2 C}{\partial X^2} \quad 3.31$$

$$\frac{\partial C}{\partial \tau} = \varepsilon_n^{bruggn\text{-}1} \frac{\partial^2 C}{\partial X^2} + J_n \quad 3.32$$

where the dimensionless variables are

$\tau = \frac{D}{L^2} t$, $C = \frac{c}{c_0}$, $X = \frac{x}{L}$ with the dimensionless groups $J_p = \frac{L^2(1\text{-}t_+)}{c_0 D \varepsilon_p} \frac{I}{F l_p}$ and

$J_n = \frac{L^2(1\text{-}t_+)}{c_0 D \varepsilon_n} \frac{I}{F l_n}$ where $L = l_p + l_s + l_n$.

The electrolyte concentration can be volume-averaged over the respective region as follows:

$$C_{ave}^{Cathode}=\frac{1}{L_p}\int_0^{L_p} CdX,\quad C_{ave}^{separator}=\frac{1}{L_s}\int_{L_p}^{L_p+L_s} CdX \text{ and } C_{ave}^{anode}=\frac{1}{L_n}\int_{L_n+L_s}^{L_p+L_s+L_n} CdX \qquad 3.33$$

where, $L_p=\frac{l_p}{L}$, $L_s=\frac{l_s}{L}$ and $L_n=\frac{l_n}{L}$. Applying Equations 3.33 to the governing equations 3.30, 3.31, and 3.32, yield

$$\frac{\partial C_{ave}^{Cathode}}{\partial \tau}=\varepsilon_p^{bruggp-1}\left(\frac{\partial C}{\partial X}\right)\Big|_{X=l_p}+J_p \qquad 3.34$$

$$\frac{\partial C_{ave}^{separator}}{\partial \tau}=\varepsilon_s^{bruggs-1}\left[\left(\frac{\partial C}{\partial X}\right)\Big|_{X=l_p+l_s}-\left(\frac{\partial C}{\partial X}\right)\Big|_{X=l_p}\right] \qquad 3.35$$

$$\frac{\partial C_{ave}^{anode}}{\partial \tau}=-\varepsilon_n^{bruggn-1}\left(\frac{\partial C}{\partial X}\right)\Big|_{X=l_p+l_s}+J_n \qquad 3.36$$

Note that Equations 3.34 - 3.36 are ordinary differential equations in time (ODE) as opposed to the original model Equations 3.5 – 3.7 which are partial differential equations (PDE). Equations 3.34 – 3.36 are exact and are as good as the original model equations. Hence, order reduction can be done easily. However, to solve Equations 3.34 – 3.36 we need to know what the concentration derivatives (flux) are at the two interfaces x = lp and x = lp + ls. This is where various approximations come into the picture. By assuming the concentration profile to be a parabolic profile, fluxes at the interfaces can be approximated and Equations 3.34 – 3.36 are converted as (for $brugg_p$ = $brugg_s$ = $brugg_n$ = 4)

$$\frac{dC_{ave}^{separator}}{dt}=\frac{-6\varepsilon_s^3\left(2C_{ave}^{separator}-C_1-C_3\right)}{L_s^2} \qquad 3.37$$

At the positive electrode, the governing equation for $C_{ave}^{cathode}$ is given by

$$\frac{dC_{ave}^{cathode}}{dt} = \frac{3\varepsilon_p^3 \left(C_1 - C_{ave}^{cathode}\right)}{L_p^2} + J_p \tag{3.38}$$

At the negative electrode, the governing equation for C_{ave}^{anode} is given by

$$\frac{dC_{ave}^{anode}}{dt} = \frac{3\varepsilon_n^3 (C_3 - C_{ave}^{anode})}{L_n^2} \frac{\left(1 - L_p - L_s\right)}{L_n} + J_n \tag{3.39}$$

where

$$C_1 = \frac{3\varepsilon_p^4 C_{ave}^{cathode} L_s + 6\varepsilon_s^4 L_p C_{ave}^{separator} - 2\varepsilon_s^4 L_p C_3}{3\varepsilon_p^4 L_s + 4\varepsilon_s^4 L_p} \tag{3.40}$$

$$C_3 = \frac{-2\varepsilon_s^4 L_n \varepsilon_p^4 C_{ave}^{cathode} L_s + 4\varepsilon_s^8 L_n L_p C_{ave}^{separator} + 6\varepsilon_s^4 L_n C_{ave}^{separator} L_s \varepsilon_p^4 + 3\varepsilon_n^4 C_{ave}^{anode} L_s^2 \varepsilon_p^4 + 4\varepsilon_s^4 C_{ave}^{anode} L_s \varepsilon_s^4 L_p}{4\varepsilon_s^8 L_n L_p + 4\varepsilon_s^4 L_n L_s \varepsilon_p^4 + 3\varepsilon_n^4 L_s^2 \varepsilon_p^4 + 4\varepsilon_n^4 L_s \varepsilon_s^4 L_p} \tag{3.41}$$

More details about the finding the constants are illustrated elsewhere for solid-phase diffusion approximations [61]. Note that Equations 3.37 - 3.41 can be solved exactly (linear equations) to obtain the transient response of the model equations. The accuracy of the reduced-order Equations 3.37 – 3.39 depend on the system parameters and the complexity of the original model equations. This is a very simple model and hence a parabolic profile approximation is sufficient for rates up to 1C rate of discharge. Adding more terms to the polynomial profiles improves accuracy, but at higher computation costs, higher number of equations and needs more work in deriving the reduced-order equations. The method proposed here differs from standard collocation procedures in a

subtle manner, as we do physics based averaging and volume averaging on physical variables first.

The simplified model now has three ordinary differential equations (which are initial value problems). Figure 3.4 gives a comparison of the predictive capability of the simplified model for predicting the electrolyte concentration. It can be seen that the simplified model is able to predict with no loss in accuracy compared to the rigorous numerical solution using the governing equation for electrolyte concentration in the three regions.

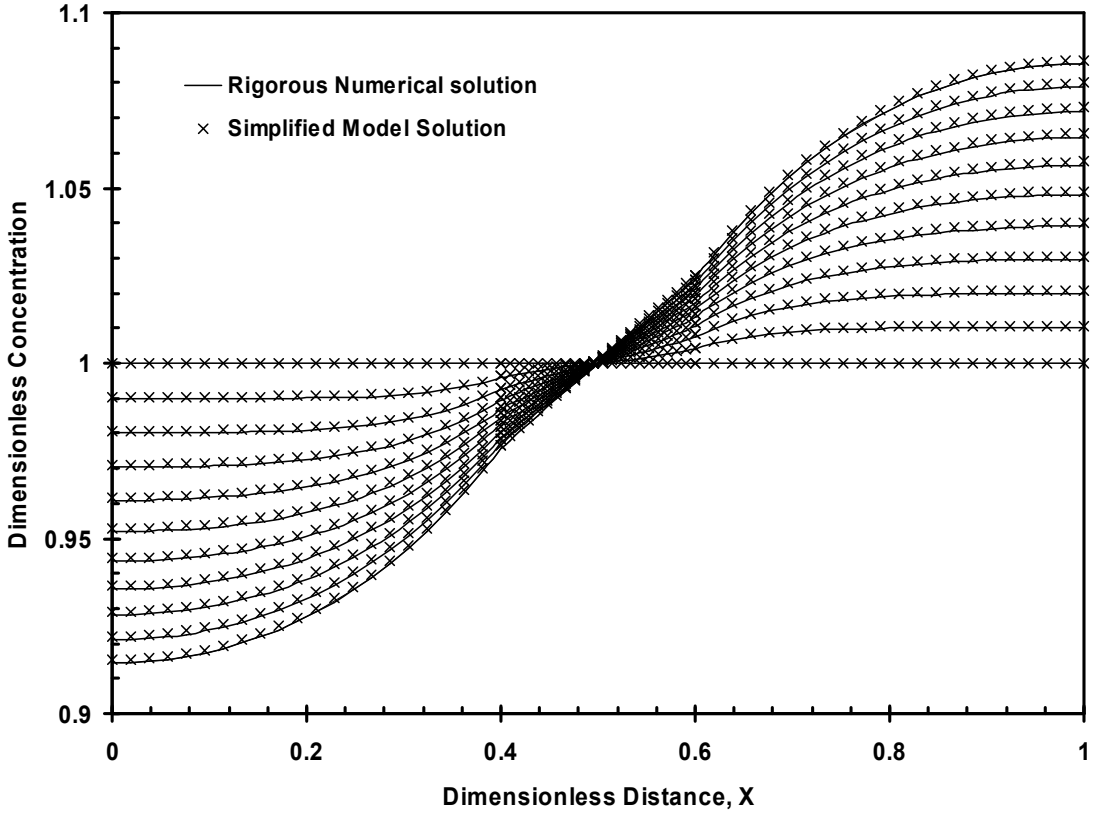

Figure 3.4: Comparison of electrolyte concentration distributions obtained by rigorous numerical and simplified model for a case of uniform current distribution.

For the simple case shown above, parabolic profile was used. For lithium-ion battery models, this approach is not the optimized approach. Any dependent variable can be approximated by

$$y(x,t)=\sum_{i=0}^{N_1} a_i(t)\xi_i(x) \qquad 3.42$$

where y(x,t) is the dependant variable of interest, $a_i(t)$ is a time-varying co-efficient that needs to be determined, and $\xi_i(x)$ is a space dependant function. The function $\xi_i(x)$ can be chosen based on mathematical intuition, experience, and research and can take one of the following forms or a combination of them: linear form (x, 1/x, etc.), nonlinear form (exp(x), ln(x), etc.), trigonometric form (sin(x), sinh(x), etc.). Clearly as we keep increasing N_1 in Equation 3.42, standard collocation procedures will converge and yield accurate results. The objective is to not to minimize N_1 for a particular variable. The objective is to minimize the total number of differential algebraic equations (DAEs) that result from equations similar to Equation 3.42 for all the dependent variables in all the regions to predict the discharge curves accurately (*i.e.,* $\sum N_i$). This is obtained by combining standard collocation schemes with volume-averaging, Liapunov-Schmidt technique, perturbation, Green's function theory, etc.

The system of partial differential equations (PDE) defined in Chapter 2 and summarized in Appendix 1 form the core of governing equations for battery simulation for a $LiCoO_2$ (positive electrode) – LiC_6 (negative electrode)- based system. Supposing we discretize the positive electrode, separator, and negative electrode into 100 equally spaced node points in linear length scale i.e., in x, the positive electrode now has 100

differential equations for the electrolyte concentration, 100 algebraic equations for the electrolyte potential (potential in the electrolyte phase), and 100 algebraic equations for the solid-phase potential. If we take 20 solid particles present in every node point in x, then for the solid phase concentration we have 1x100x20 differential equations. Thus for a single porous electrode (say for positive electrode) we have 2300 DAEs. Following the same number of node points in x the separator now has 100 differential equations for the electrolyte concentration and 100 algebraic equations for the electrolyte phase potential. The negative electrode is discretized similar to the positive electrode and has a total of 3x100+1x100x20 = 2300 DAEs to solve. Thus, the number of differential algebraic equations to be solved for the rigorous model is 3x100+1x100x20 + 2x100 + 3x100+1x100x20 = 4800 DAEs. By using parabolic profile and other approximations solid-phase diffusion can be approximated and the number of DAEs are reduced to 302 DAEs as shown by Subramanian et al. [61].

By using the approximations discussed in this work, we are able to predict the discharge curves accurately with just 47 DAEs. Note that 47 DAEs are needed for matching for all the intrinsic variables. With this approach we can choose to go "approximate" in the intrinsic variables and solve only for discharge curves accurately with only 27 DAEs. The next section elucidates the extension of the model to the full electrolyte concentration equation.

Chapter 2 discussed the governing equations, additional equations, and boundary conditions that define a Li-ion battery model. The inimitable strength of battery modeling is the ability to predict the distribution of potential and concentration across the full cell during operation of the battery. This often provides valuable information that is either

difficult or impossible to determine experimentally, not forgetting the enrichment of our understanding of the phenomena occurring inside the cell.

To validate the simplified models, a rigorous numerical model based on finite difference as shown in section 3.1 was solved. The rigorous numerical model is benchmarked with experimental results from literature. MAPLE® with the BESIRK solver was the preferred choice of programming environment. The codes developed were then ported to FORTRAN and solved using a FORTRAN version of BESIRK. The desktop personal computer used for this work had a 3.0 GHz processor with 2 GB of RAM, it is also noteworthy to report that these models were run on a personal laptop computer with a 1.7 GHz dual core processor with 1 GB of RAM. The run-times on both computers were identical.

The most important information from a battery system is the output voltage. It defines the available current with respect to time and can be used as an accurate measure of state-of-health and state-of-charge of the battery. The voltage from the battery is the only measurable quantity and hence the most important.

3.4. Discharge Profiles

Figure 3.5 shows that the simplified models show excellent accuracy when predicting the discharge voltage at different C rates. This implies that the physics of the system is not compromised by simplifying the governing equations. It is of prime importance to note that the voltage is one of the few measurable quantities in real world applications. Using simplified models to predict discharge voltage in conjunction with

simple book-keeping methods can be used powerfully to determine exact state-of-charge and state-of-health of the battery.

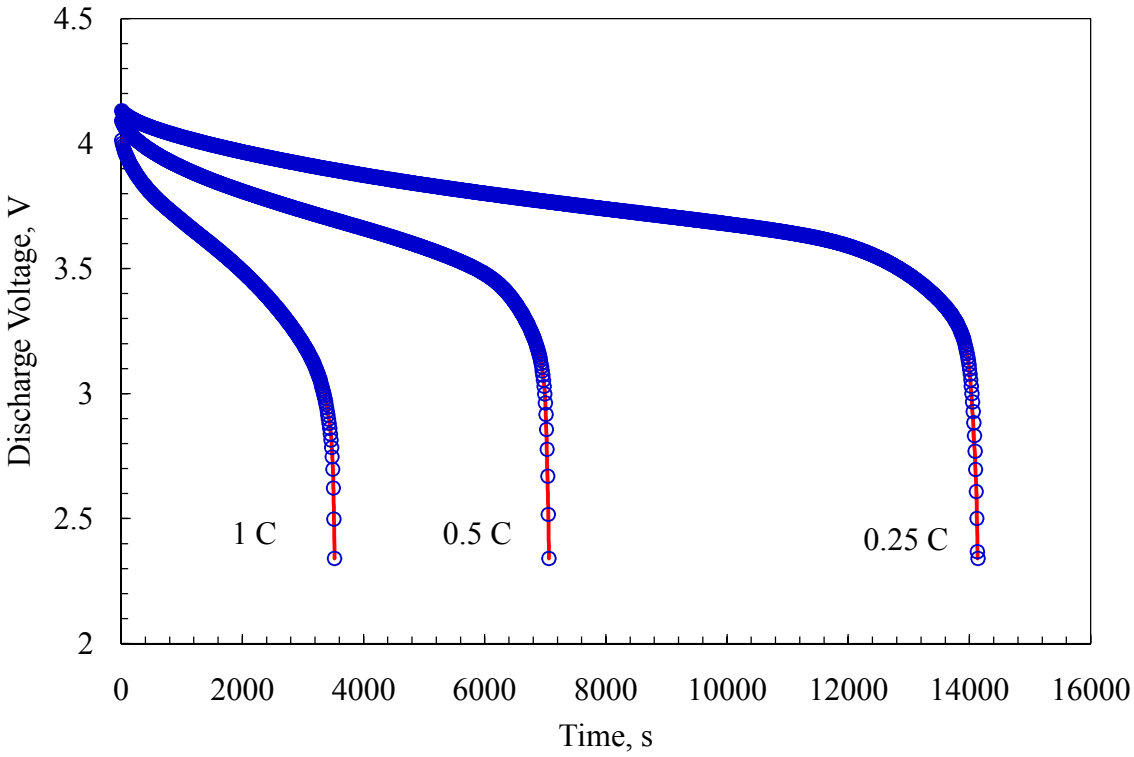

Figure 3.5: Discharge voltage as a function of time is plotted at different C rates for a galvanostatic case. The solid lines represent the full numeric model and the open symbols represent the simplified model.

3.5. Intrinsic variables

Discharge curves themselves do not explain the state of the battery, in other words, it is important to keep track of other variables that cannot be measured easily. Making key battery usage policies based on remaining power may not be viable by just keeping track of the voltage. The simplified model also predicts the intrinsic variables accurately. This is an important characteristic that needs to be considered when trying to estimate transport and kinetic parameters, for example, diffusion constants, reaction constants, etc. The intrinsic variables namely, over-potential (η), solution phase potential (Φ_2), solid phase potential (Φ_1), and electrolyte concentration determined by the simplified model are plotted and compared with a rigorous finite difference code. The interfaces are positive electrode-current collector junction (x=0), the positive electrode-separator (electrolyte) junction (x=lp), the separator-negative electrode junction (x=lp+ls), and the negative electrode-current collector junction (x=lp+ls+ln).

3.5.1. Solution Phase Concentration

Figure 3.6 gives the variation of salt concentration in the electrolyte phase with time at the four interfaces for a 1C rate of discharge. During this process the Li de-intercalates from the carbon electrode and intercalates into the $LiCoO_2$ electrode. At the separator interfaces, l_p and l_p+l_s, we can see nearly constant concentration gradient; this is due to the electrolyte anions not being involved in the reaction and at steady state the flux becomes zero. The other current collector interfaces, 0 and lp+ls+ln, show nonlinear

gradients as expected. There is a quick initial increase in the concentration at current collector anode interface; this initial increase then reduces to a very small increase until the stop condition is reached. Conversely, at the current collector cathode interface we observe a quick decrease in concentration followed by a gradual decrease until the stop condition is reached. This is the expected behavior for the solution phase concentration. The simplified model predicts the variation with nearly zero error to the rigorous numerical model. This validates the use of Equation 3.18 in simplifying the solution phase concentration equation.

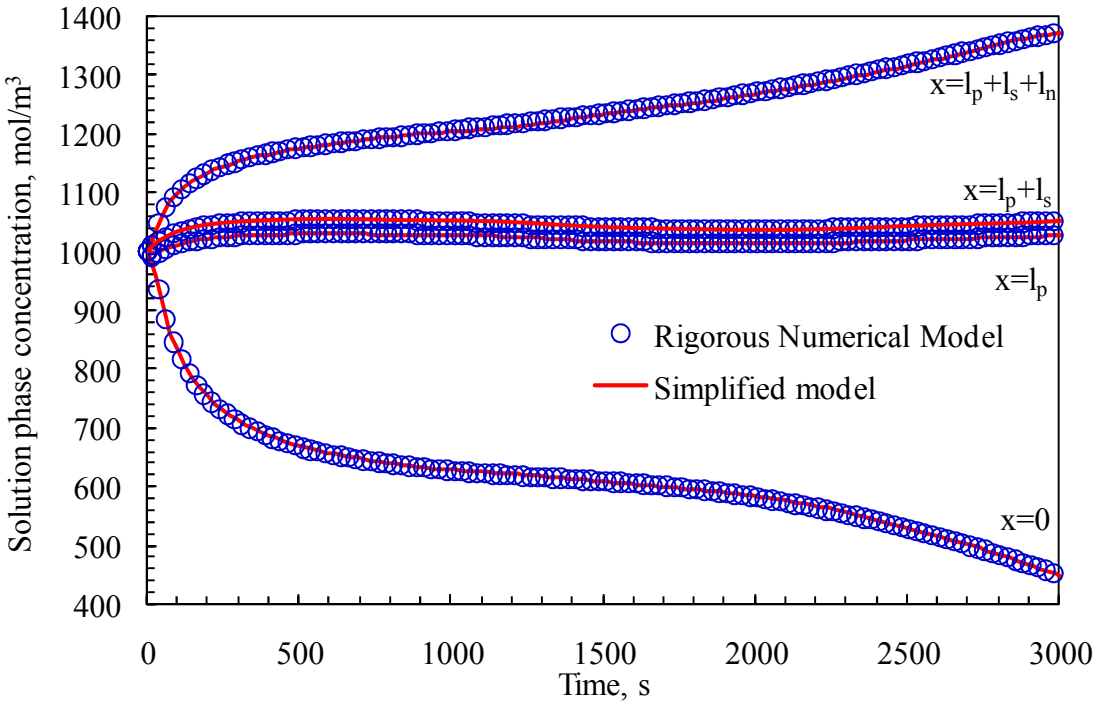

Figure 3.6: Solution phase concentration as a function of time is plotted at different interfaces rates for a galvanostatic case. The solid lines represent the full numeric model and the open symbols represent the simplified model.

3.5.2. Solid Phase Concentration

There is good agreement between the simplified model and the finite difference model for the solid phase concentration. It is interesting to note that there is deviation between the models at the two current collector junctions of the Li-ion cell at short times, but at long times they converge to have no error. Solid phase limitations are the most important factor to consider when operating at high discharge rates (>1C), treatment of the solid phase has to be considered carefully to avoid applying restrictions on the predictive ability of the solid phase diffusion equation. The error deviation can be attributed to the approximations on the solid phase diffusion equation and not the solution phase concentration equation. It is suggested that obtaining a closed form solution would be the best possible scenario to reduce the deviation at short times. In a previous work on solid phase simplification, it was suggested and proved that using higher order polynomials provides much more accurate results and does not make the solid phase concentration from being the limiting factor [61].

In another study, Wang and Srinivasan, define a correction term for the treatment of short time solutions for the solid phase diffusion equation, which can be incorporated here, but this would involve specifying an additional algebraic equation at every node point and would prove counterproductive to the overall objective of this kind of work [62,63]. The short time solution is also empirical in nature and is specific to the discharge rate. The future direction of this research attempt would involve resolving the issues associated with the computational limitations of solid phase concentration.

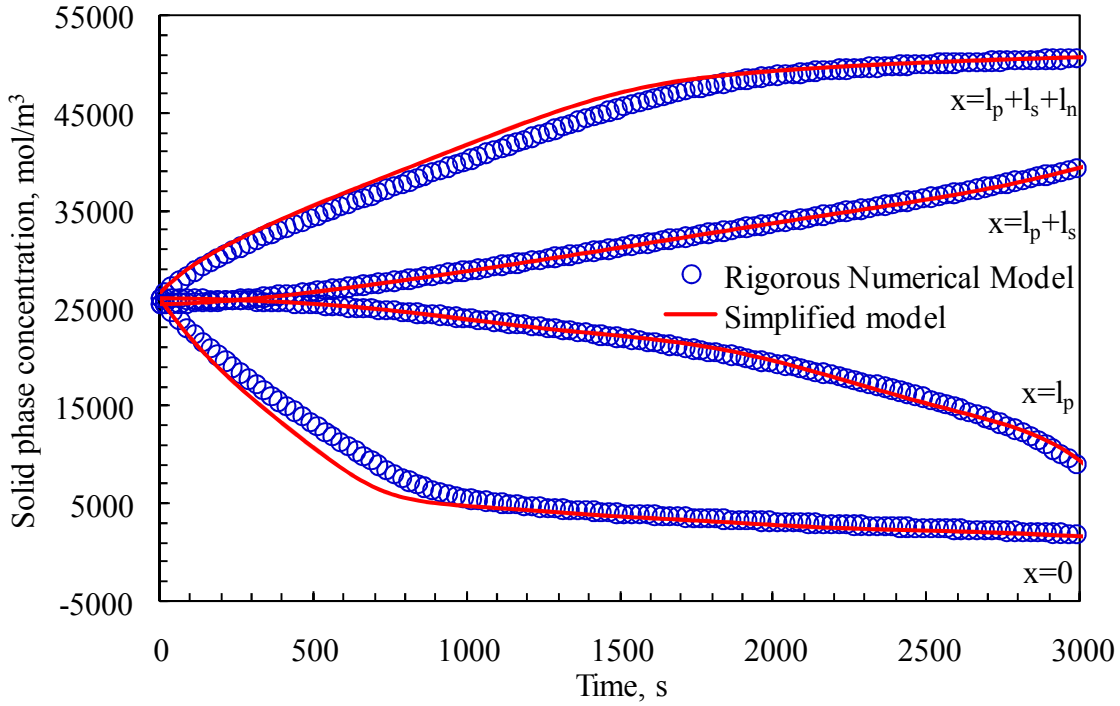

Figure 3.7: Solid phase concentration as a function of time is plotted at different interfaces rates for a galvanostatic case. The solid lines represent the full numeric model and the open symbols represent the simplified model.

3.5.3. Solid Phase Potential

The solid phase potential defines the charge carried by the solid particles in either electrode. It is expected that during discharge most solid phase potential would be measured at the anode, with values near the open-circuit voltage (4.2V). It is interesting to note that the potential measured at the two anode interfaces and two cathode interfaces are identical, this can be attributed to the fact that the current is transferred very quickly in the solid phase and hence there is no measureable potential drop between the current collector/electrode and electrode/separator interface at both electrodes. The simplified model and the rigorous numerical model show excellent agreement between them.

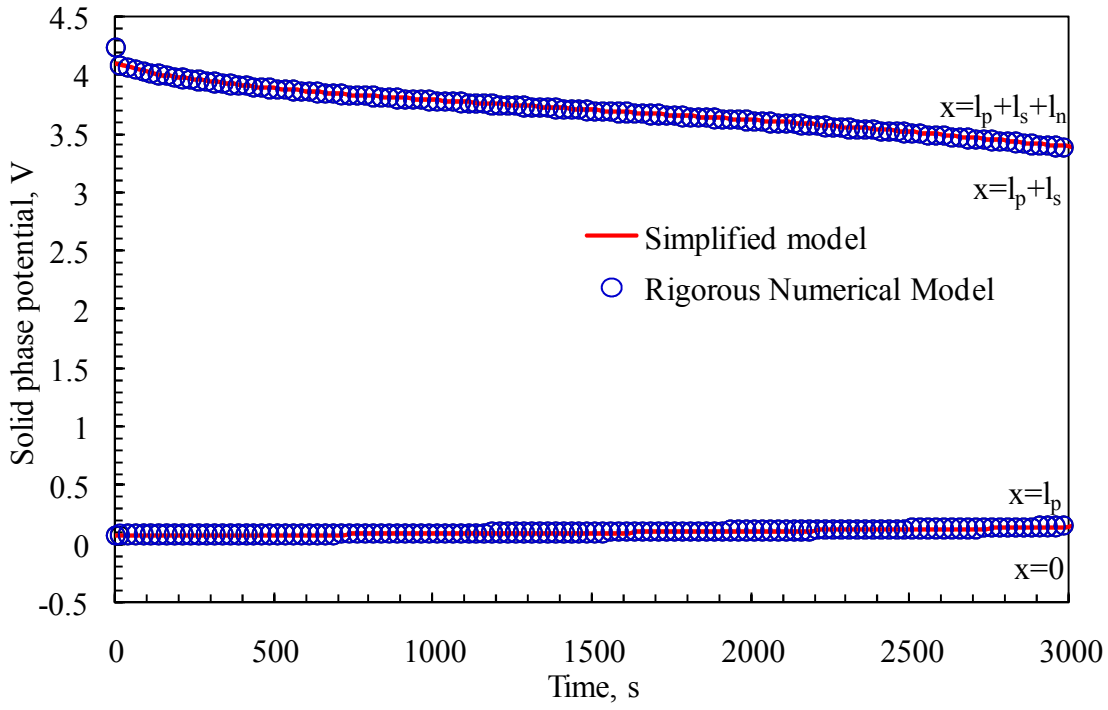

Figure 3.8: Comparison of solid phase potential (Φ_1) obtained from simulating the simplified model and rigorous finite difference model at different interfaces.

3.5.4. Solution Phase Potential

The solution phase potential is compared in Figure 3.9. Contribution from the solution phase potential is minimal since most of the current is carried by the solid phase. There is good correlation between the rigorous numerical model and the simplified model.

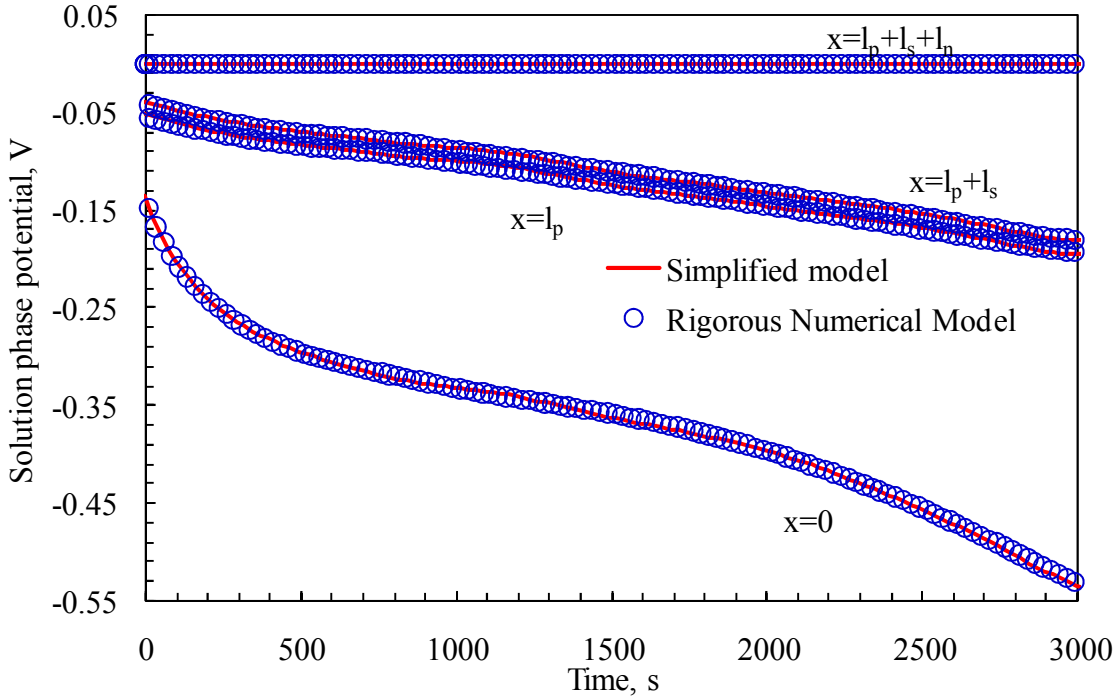

Figure 3.9: Comparison of solution phase potential (Φ_2) obtained from simulating the simplified model and rigorous finite difference model at different interfaces.

The merit of the approach is evident when comparing the number of governing equations that are solved. The simplified model specifies 47 DAEs as opposed to 302 DAEs for the rigorous code. It is also noteworthy that 302 DAEs is the minimum number of equations required for a converged finite difference solution. The simplified model for all practical situations (rates of discharge) uses a maximum of 47 specified equations for a converged solution which compares very well even with 302 DAEs based finite difference code.

The simplified models in this study have been evaluated only at C rates 1 and below, these are relative low yet practical values. It is expected that the simplified models would be able to predict very well even at very high rates of discharge, > 4C. These high

rates are rarely seen but are expected in batteries that power communication devices, especially in satellites. The demand for batteries that can tolerate abuse is on the rise given their use in HEVs. This also creates another scenario where the load is constantly varying. Varying loads cannot be modeled using galvanostatic condition, a new method needs to be developed and implemented that can handle the real world power demands on the batteries. It is expected that using simplified models would play a lot more important role in such scenarios given the very complicated nature of the model.

Beyond the model simplification, the work started in this thesis has resulted in efficient simulation of battery models without compromising on the accuracy. This work was initiated in this thesis and is currently pursued to further improve, validate and apply in a wide range of applications for batteries by other group members. The process of efficient simulation without compromising on accuracy is currently termed as "Mathematical Model Reformulation" [95].

CHAPTER 4

IMPEDANCE RESPONSE – A NOVEL SYMBOLIC SOLUTION METHOD

In Chapter 1, the use of direct measurement for accurate battery state predictions was surveyed. AC Impedance is a powerful direct measurement technique and is extensively used by experimentalists to gain valuable physical data [35]. AC impedance provides valuable insight into the working of the any battery system. AC Impedance analysis is usually done offline, which makes it difficult for 'real-time' purposes. This also makes it a prime candidate for simulation work, especially, predicting important parameters that could throw light into the state of the battery. Simulating AC Impedance for complete continuum models is not an easy task as will be explained in the following sections, hence, a need for an easier method for simulation needs to be explored.

4.1. Introduction

Various transport and reaction limitations restrict the cost effectiveness, utilization and efficiency of electrochemical devices. AC impedance is a powerful technique used by various researchers to understand electrochemical systems [35,64,65]. Understanding and extracting useful information from AC impedance data is a formidable task. The main drawback with using circuit approach for simulating AC impedance response is that it only gives lumped-parameters for the system of interest and does not involve all the meaningful quantitative system parameters such as the Fickian diffusion coefficient, rate constants, etc. Rigorous physics based models for simulating

AC impedance response involves solving multiple partial differential equations (PDEs) in multiple domains making the models prohibitive because of numerical and computational constraint [65]. Typically only single PDE has been solved analytically in the literature. Recently, an analytical solution was reported for two coupled PDEs [66]. For more than one PDE, obtaining an analytical solution involves complicated eigen value and cumbersome matrix calculations. Analytical solutions may not be easily separable to real and imaginary parts.

The purpose of this work is to develop a novel numeric symbolic solution (NSS) for simulating AC impedance response of electrochemical devices. The methodology consists of applying finite differences for the spatial coordinate and a symbolic matrix inversion method for solving the resulting system of linear algebraic equations. Thus the NSS is numerical in the spatial coordinate and closed-form in all the system parameters. In this work, this novel scheme is demonstrated by simulating diffusive impedance response of a planar electrode. This novel approach will be extended in the future to multiple PDEs in multiple spatial coordinates in multiple domains that govern the electrochemical behavior of various devices. The efficiency and superiority of NSS is compared with both analytical and numerical solutions.

4.2. Example – Diffusive Impedance

Diffusion in a planar electrode is given by Fickian diffusion as

$$\frac{\partial c}{\partial t} = D\frac{\partial^2 c}{\partial x^2} \tag{4.1}$$

The boundary conditions are

$$\text{at } x = 0, c = 0 \tag{4.2a}$$

$$\text{at } x = L, D\frac{\partial c}{\partial x} = \frac{i(t)}{nF} \tag{4.2b}$$

The electrode is in contact with the bulk-liquid at x = 0 and the electrochemical behavior is governed by the surface concentration at x = L. The electrochemical reaction takes place at the electrode surface. Since impedance experiments are performed about an operating point with a small perturbation, c in Equation 4.1 can be thought of as a perturbation in concentration with initial condition being zero.

To get the AC impedance response for the electrode, Equation 4.1 is converted from the time domain to the Laplace domain s, and expressed in dimensionless form as

$$\frac{d^2C}{dX^2} = SC \tag{4.3}$$

subject to the boundary condition

$$X = 0, C = 0 \ \ and \ \ X = 1, \frac{dC}{dX} = \delta(S) \tag{4.4}$$

where X = x/L, C = c/c_{ref}, $\delta(S) = i(s)L/nFDC_{ref}$, and S = sL^2/D is the dimensionless Laplace variable. Various approaches for the simulation of diffusive impedance response of planar electrode (Equation 4.3 with the boundary conditions Equation 4.4) are described below.

4.2.1. Analytical Approach

Equation 4.3 can be analytically solved using any standard classical technique and a closed-form solution for C as a function of S (s, D and L) is obtained as [67]

$$C_{analytical} = \frac{\delta(S)\sinh\left(X\sqrt{S}\right)}{\sqrt{S}\cosh\left(\sqrt{S}\right)} \tag{4.5}$$

The surface concentration, C_s gives the over-potential and hence the impedance. C_s at the boundary X = 1 is obtained as (without losing generosity δ is assumed to be 1)

$$C_{S_{analytical}} = Z_{analytical} = \tanh\left(\sqrt{S}\right)/\sqrt{S} \tag{4.6}$$

The impedance response or the Nyquist plot is obtained by substituting S = IΩ (Ω is the dimensionless frequency and is obtained by multiplying frequency ω by L^2/D) in Equation 4.6 and by separating the real and imaginary parts. The separation of the total impedance as real and imaginary parts is simple for this case as the analytical expression does not contain complicated eigen functions and eigen values [65].

4.2.2. Numerical Approach

A numerical solution to solve Equation 4.3 is performed by applying finite difference or other discretization methods in the spatial direction, X. Since one has to find both real and imaginary parts, Equation 4.3 is typically converted to real and imaginary

parts before implementing a numerical procedure. By substituting S = IΩ, Equation 4.3 is separated for real and imaginary parts as

$$\frac{d^2 C_{re}}{dX^2} = -\Omega C_{im} \tag{4.7a}$$

$$\frac{d^2 C_{im}}{dX^2} = \Omega C_{re} \tag{4.7b}$$

The boundary conditions are also separated for real and imaginary parts as

$$X = 0, C_{re} = 0 \; ; \; C_{im} = 0 \; X = 0, C_{re} = 0 \; ; \; C_{im} = 0 \tag{4.8a}$$

$$X = 1, \frac{dC_{re}}{dX} = 1 \; ; \; \frac{dC_{im}}{dX} = 0 \tag{4.8b}$$

For a particular value of frequency Ω, the set of equations given in Equation 4.7 is solved numerically with appropriate boundary conditions given by Equation 4.8. By consecutively finding C_{re} and C_{im} at the surface (X = 1) for various values of Ω numerically, the Nyquist plot is obtained. For this purpose, Maple's dsolve numeric command is used [68].

4.2.3. Numeric Symbolic Solution

The novel numeric symbolic solution approach to solve Equation 4.3 involves applying finite differences in the spatial direction, as the primary step. Then Equation 4.3 is converted to discrete-form (system of algebraic equations) for N number of interior node points as

$$\frac{C_{i-1} - 2C_i + C_{i+1}}{h^2} = SC_i \; ; \; \mathrm{h} = \frac{1}{\mathrm{N}+1} \tag{4.9}$$

where i = 1..N. The boundary conditions governing the exterior node points are also converted to discrete-form as

$$\mathrm{C}_0 = 0 \tag{4.10}$$

$$\mathrm{C}_{\mathrm{N}+1} = -\frac{1}{3}\mathrm{C}_{\mathrm{N}-2} + \frac{4}{3}\mathrm{C}_{\mathrm{N}-1} + \frac{2\mathrm{h}}{3} \tag{4.11}$$

The above system of algebraic equations can be rewritten and solved in matrix form as [69]

$$\mathbf{AY} = \mathbf{B} \;\Rightarrow\; \mathbf{Y} = \mathbf{A}^{-1}\mathbf{B} \tag{4.12}$$

where, **Y** is the dependent variables vector, $\mathbf{Y} = [C_1\ C_2\ C_3 \ldots C_N]^T$ (for all the variables in all the interior node points), **A** is the coefficient matrix and **B** is the forcing function vector, $\mathbf{B} = [0\ 0\ 0\ \ldots\ -2/3h]^T$. If N = 2 interior node points are used the coefficient matrix **A** is given as

$$\mathbf{A} = \begin{bmatrix} -\frac{2}{h^2} - S & \frac{1}{h^2} \\ \frac{1}{3h^2} & -\frac{2}{3h^2} - S \end{bmatrix} \tag{4.13}$$

The simulation of the system is completed by inverting **A** matrix symbolically as a function of the system parameters (S or s, D and L). A flow chart describing the NSS is presented in Figure 4.1. When N = 2 interior node points are used, the resulting expression for impedance response is

$$Z_{NSS} = \frac{1+\frac{4}{27}\left(\frac{sL^2}{D}\right)+\frac{1}{243}\left(\frac{sL^2}{D}\right)^2}{1+\frac{4}{9}\left(\frac{sL^2}{D}\right)+\frac{1}{54}\left(\frac{sL^2}{D}\right)^2} = \frac{1+\frac{4}{27}S+\frac{1}{243}S^2}{1+\frac{4}{9}S+\frac{1}{54}S^2} \qquad 4.14$$

The real and imaginary parts are obtained as

$$Z_{re} = \frac{2\left[13122+567\Omega^2+\Omega^4\right]}{9\left[2916+468\Omega^2+\Omega^4\right]} \qquad 4.15$$

$$Z_{im} = \frac{8\Omega\left[324+\Omega^2\right]}{3\left[2916+468\Omega^2+\Omega^4\right]} \qquad 4.16$$

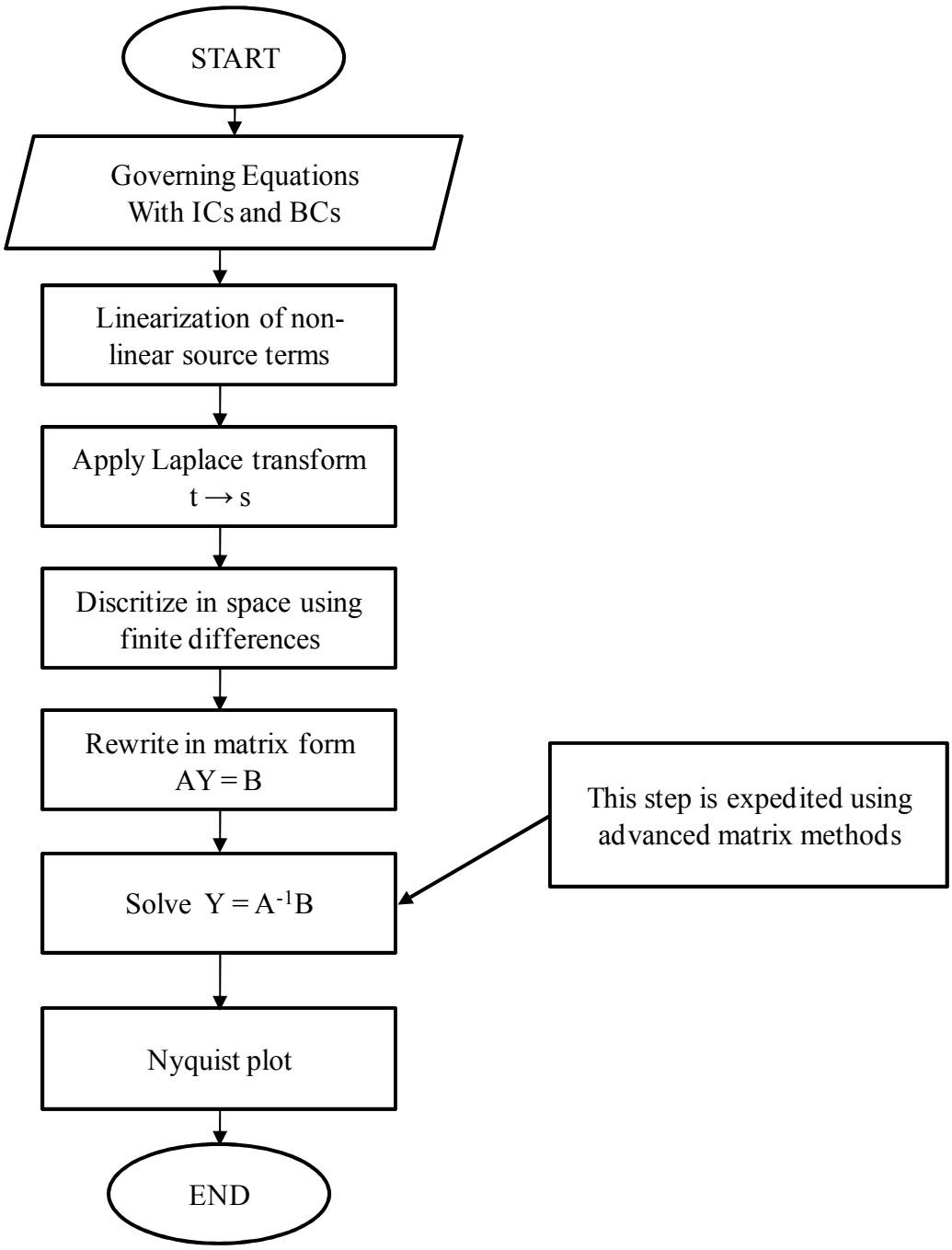

Figure 4.1: Computational procedure for numeric symbolic solution (NSS).

It can be noted from Equation 4.14 that the NSS technique yields a closed-form solution as a function of all the system parameters (S or ω or s, L and D). For illustration, we showed the results obtained with two node points. For better accuracy we need to increase the number of node points. Note that the coefficient matrix in Equation 4.12 can be a function of the Laplace variable S or the frequency, Ω. Maple can be used to invert **A** matrix. However, by following the pattern of eigen values an efficient code can be written for the inverse symbolically [67,70]. A user-friendly program has been written to obtain the matrix inverse, which does not take more than a minute to find the inverse even for N = 100 or 1000 node points. All the simulations in this work are performed in a PC with 1.7GHz processor and 1GB RAM.

4. 3. Comparison of the Methods

The impedance responses obtained using the above three approaches are plotted in Figure 4.2 and the corresponding simulation time required to obtain the curves are shown in Table 4.1. The analytical solution (solid-line in Figure 4.2) is a function of the system parameters (S or s, L, D or ω) and hence the full curve is obtained by separating the real and imaginary parts in Equation 4.6. The computation time to obtain the curve is just one second. The numerical approach (dotted line in Figure 4.2) takes more than 45 seconds to generate the plot. This is inevitable, because there is a need to solve Equation 4.7 repeatedly for every value of Ω to get one point in the curve (totally 300 points are evaluated to obtain a smooth curve). The NSS is a closed-form solution of the system

parameters S or Ω and takes only two seconds to generate the entire curve – both the numerical and NSS solutions overlap with the analytical solution in Figure 4.2.

NSS is useful for parameter estimation. There are two parameters involved in the model equations, the thickness of the electrode L, and the Fickian diffusion coefficient D. Fixing the thickness of the electrode as 10^{-6} m, the unknown parameter D is estimated using Gauss-Newton method from the synthetic experimental data. The experimental values are generated by distributing 5% randomness error to the analytical values for D = 10^{-7} m^2/s by considering 300 data points. The expression used to generate experimental values using random error is as follow,

$$Z_{experimental} = Z_{analytical}\left[0.95 + 0.01\left(\text{random number between 0 and 10}\right)\right] \quad 4.17$$

Table 4.1: Comparison of computational times for different approaches for the simulation of AC impedance response.

Method	Computation time
Analytical method	1 second
Numerical method	45 seconds
Numeric symbolic solution	2 seconds

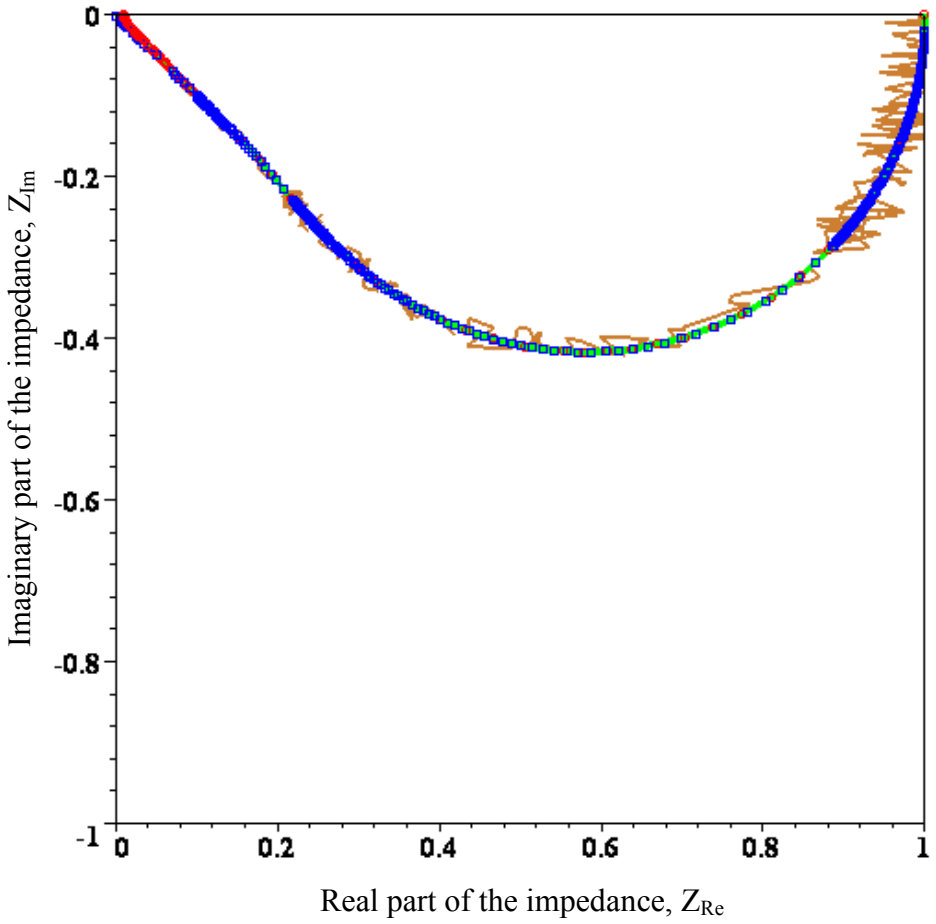

Figure 4.2: Impedance response of diffusion in a planar electrode (Nyquist plot). Solid line:-Analytical method, Dotted line (boxed):-Numerical method, Dotted line (circled):-Numeric symbolic solution, Solid line (thin line):- synthetic experimental data. Numerical and NSS data points coincide.

Figure 4.2 compares the synthetic experimental values with theoretical values. The synthetic experimental values are then provided for parameter estimation algorithm along with an initial guess based on the value used for simulating the AC impedance response. The following steps are involved in the parameter estimation of impedance data [71]: (i) start with a good initial guess for parameters, $\mathbf{k}^{(0)}$, (ii) compute the real part, imaginary part and Jacobian of both real and imaginary parts at each data point and set up

the vector with experimental values $\mathbf{Y}_{exp}$, predicted values $\mathbf{Y}_{pre}$ and the Jacobian matrix $\mathbf{J}$, (iii) the correction factor is obtained by using the expression, $\Delta\mathbf{k} = (\mathbf{J}^T\mathbf{J})^{-1}\mathbf{J}^T(\mathbf{Y}_{exp}-\mathbf{Y}_{pre})$ for both real and imaginary parts of the impedance; and (iv) using this, an improved parameter value can be obtained as $\mathbf{k}^{(i+1)} = \mathbf{k}^{(i)}+\Delta\mathbf{k}^{(i)}$, the predicted parameter for the next iteration is the arithmetic average of $\mathbf{k}^{(i+1)}$ values of real and imaginary parts. Steps (ii) to (iv) are repeated until a required accuracy is reached. The jacobian matrix $\mathbf{J}$ is defined as

$$\mathbf{J} = \begin{bmatrix} \frac{\partial Y_1}{\partial k_1} & .... & \frac{\partial Y_1}{\partial k_m} \\ .... & .... & .... \\ \frac{\partial Y_n}{\partial k_1} & .... & \frac{\partial Y_n}{\partial k_m} \end{bmatrix} \qquad 4.18$$

where m is the number of parameters and n is the number of experimental data points.

The estimated parameter values based on the three approaches (analytical, numerical and numeric symbolic solution) are shown in Table 4.2. The computation time associated with each approaches are also compared. It is clear from the simulation results that the numerical method requires more time to estimate a single system parameter. This is because the numerical approach needs additional time to solve additional differential equations (Jacobians $\mathbf{J}$) associated with both real and imaginary parts of the impedance. The inefficiency of numerical codes for predicting parameters can be overcome by the NSS. Using the closed form of symbolic solution, the jacobians involved in the parameter estimation can be exactly calculated. The comparison of computation time shows that the NSS performs as efficiently as the analytical solution for parameter estimation. All the three approaches are simulated in Maple. The NSS program that takes less than one minute to run based on advanced matrix inversion method is to be applied for software

disclosure/patents. However, Maple's inbuilt matrix inversion command can be used to obtain the NSS (this program is available upon request).

4.4. Discussion

Numerical simulation of AC impedance models is not ideal for parameter estimation. This is true because for one PDE we need 100 node points in the x-axis for a numerical simulation (for a particular value of frequency). To simulate the complete impedance spectra, for 300 different values of frequency (in the entire domain), we solved two sets (one for real and another for imaginary part of total impedance) of 100 such equations numerically 300 times. When the numerical approach is used to predict one parameter (diffusion coefficient, D) from experimental data, there is a need to solve two more sets of 100 equations for the sensitivity variable in all the 100 node points. For a model with a single PDE and a single parameter we would need to solve 2x100+2x100=4x200 equations numerically 300 times. For estimating parameters numerically using a good initial guess, we are required to iterate 10 times. Hence, for a single PDE model with one parameter we have to solve 4x200 = 800 equations 300x10 = 3000 times.

As it is evident from the previous sections, the only major step in NSS is inverting the coefficient matrix **A**. But, using advanced matrix methods, the matrix can be inverted symbolically as a function of S [67,70]. The matrix methods involve following the pattern of eigenvalues and eigenvectors of the matrix for N = 2, 3, 4 node points, etc. A recursive relationship is obtained to find the matrix inverse symbolically. Once the

recursive relationship is obtained the matrix inverse step does not take more than one minute to find the inverse of the matrix even for N = 100 or 1000 node points. Figure 4.3 shows the number of node points needed for NSS at different values of dimensionless frequency Ω, for the simulation of entire impedance response curve. It shows that at very low to fairly high values of frequency the number of node points needed is very small. Then, the number of node points steeply increases with Ω when Ω > 1000.

Table 4.2: Comparison of estimated parameter values and computation time for different approaches.

Method	Estimated value of Diffusivity	Computation time
Analytical method	$1.002803726\ 10^{-7}$	6 seconds
Numerical method	$1.005148577\ 10^{-7}$	41 minutes
Numeric symbolic solution	$1.002811529\ 10^{-7}$	35 seconds

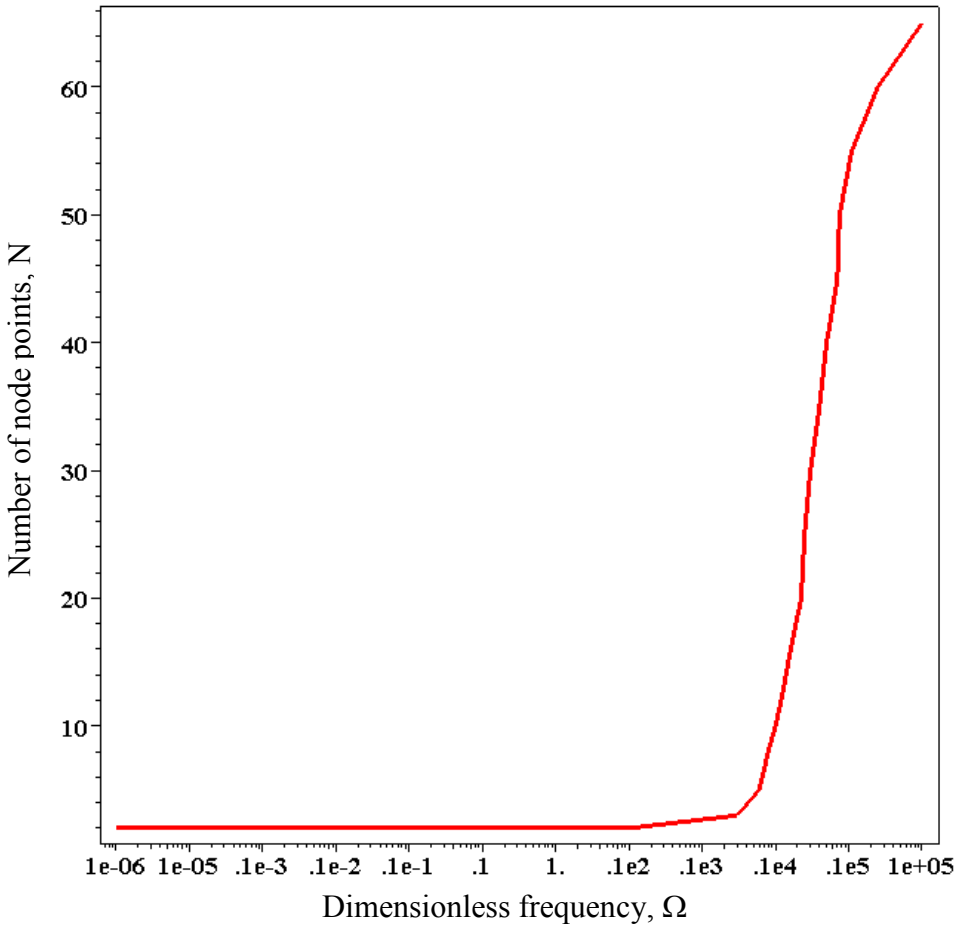

Figure 4.3: Number of node points required for NSS for various values of Ω.

The NSS can be separated into real and imaginary parts to simulate the AC impedance response without additional computation constraints. Even if more node points are used to obtain a closed form of symbolic solution; the NSS works well and simply separates the real and imaginary parts successfully. It is also interesting to realize that the computation time needed to obtain the AC impedance response using NSS is almost the same as that required by the analytical solution. Whereas the computational time taken for the simulation of impedance response using numerical solution is 45 times greater than that of the analytical solution. The NSS is expected to be superior to

analytical solutions for estimating transport and kinetic parameters if rigorous electrochemical models are considered. This means that, while rigorous analytical solutions need to be resolved/re-derived for the rigorous models for batteries or other electrochemical devices, the NSS can provide a solution independent of the boundary conditions and geometry. The NSS can also provide solutions as a function of geometry factor if Equation 4.3 has an additional term p[dC/dX] with p being 0, 1, and 2 for rectangular, cylindrical and spherical coordinates or D or other parameters as a function of X.

The advantages of NSS have been validated by comparing the time taken to obtain an impedance response curve and one parameter using the NSS, numerical and exact analytical solutions. The NSS exploits the properties of both analytical as well as numerical approaches. The computation time of NSS is several times superior to the numerical simulation.

4.5. Future Work

The proposed NSS method has been proven to be as good as the analytical solution and superior to the numerical simulation. Thus the method can be extended for the simulation of a rigorous physics based AC impedance model for electrochemical devices such as batteries, fuel cells, capacitors, sensors, etc. [65,33]. To better understand porous electrodes it is important to consider the simultaneous phenomenon of coupled gradients of concentration and potential. Real experimental data can be obtained and used for the estimation of system parameters such as diffusion coefficient, electrolyte

conductivity or exchange current for the reaction. Future communication will address the development of this novel scheme for porous electrodes to estimate parameters for Li-Ion batteries, PEM fuel cells, sensors, and other electrochemical devices. In addition other discretization methods (collocation, etc.) are also pursued and will be discussed in future communications. The closed form solution obtained can also be thought as transfer functions, thus giving hope for real-time physics based control of electrochemical devices and real time simulation of stacks and hybrids. The use of NSS for process control, stack and hybrid system modeling and control, life cycle modeling will be endeavored as future work.

CHAPTER 5

NOVEL MONTE CARLO STRATEGY – LITHIUM ION CATHODE PERFORMANCE CHARACTERISTICS

Modeling at the molecular level gives a lot of insight into the working of any chemical system. Modeling methods at this length scale vary from atomistic for e.g., ab-initio methods, quantum methods etc to more coarse grained methods such as the classical molecular dynamics approach. At this length scale most methods are computationally intensive and expensive. Although tedious, there are many excellent advantages of modeling at small length scales. One of the most important advantages is the ability to predict properties of materials. Modeling of materials with specific properties is of prime importance in meeting the emerging needs of electrochemical energy sources, particular, battery materials.

In general, Kinetic Monte Carlo codes and Molecular Dynamics simulations are very slow and time consuming, especially when several particle jumps and particle diffusion on surfaces and interfaces are considered. Most Monte Carlo and Molecular Dynamics simulations are considered when addressing very specific and isolated problems associated with electrochemical systems, for example, SEI layer growth in Li-ion batteries [93]. There have been both engineering (continuum) models and theoretical models at the molecular level to address this specific problem. Much insight has been gained from molecular level theoretical studies to study the mechanisms of SEI layer growth. The drawback however has been the lack of efficient ways to couple valuable information at the molecular level with the operation of the battery as a whole, i.e.,

predicting discharge curves. The multi-scale nature of this problem poses two important questions, 1. How do we efficiently bridge the gap between different time and length scales, and 2. Can we make the algorithms more computationally efficient?

An answer therefore could be a less time consuming and novel multistep Continuum Monte Carlo technique to solve problems created by multi-phenomena characteristics of electrochemical processes and power sources. In the case shown for a lithium ion battery cathode material three different types of Continuum Monte Carlo codes are written to solve three different electrochemical phenomena. All the codes are based on fundamental electrochemical principles, therefore invaluable physics is not lost while deriving useable data.

5.1. Introduction

The first commercially successful positive electrode was $LiCoO_2$ [72]. However, the high cost of cobalt and, potential safety hazards associated with overcharging of $LiCoO_2$ forced the hunt for more stable material under abusive conditions. Lithium iron phosphate ($LiFePO_4$) is a potential cathode candidate for the next generation of secondary lithium batteries due to low cost, environment friendly nature, cycling stability and higher theoretical capacity of 170 mAh/g [73]. However, the poor conductivity resulting from low li-ion diffusion rate and low electronic conductivity in $LiFePO_4$ phase, posed bottlenecks in their commercialization [74-80]. Several theoretical techniques like mathematical modeling, and Numerical analysis are known in literature that are employed to optimize the performance of lithium ion batteries [81,82,61,83]. The

working chemistry of $LiCoO_2$ and $LiFePO_4$ are different and hence makes it difficult to device an efficient single algorithm to investigate their performance as cathode material. Since $LiFePO_4$ has more attractive properties as a cathode material than the commercial $LiCoO_2$, lithium transition metal phosphates with ordered-olivine structures, $LiMPO_4$ (M=Co, Ni, Mn, Fe) have attracted much attention as promising new cathode material for secondary lithium battery [84]. The cycling capacity of $LiFePO_4$ is surprisingly good at low current densities or at elevated temperatures [61,85]. Lithium can be extracted from $LiFePO_4$ or inserted back into $FePO_4$ along a flat plateau at 3.4 V vs Li [85]. Increasing the current density does not lower the open circuit potential, but decreases its capacity [85]. Padhi et al., found that electrochemical extraction was limited to 0.6Li/formula unit [73]. They also suggested that the loss in capacity is because of lithium diffusion through the diminishing $LiFePO_4/FePO_4$ interface as lithium is reinserted into the structure. Goodenough et al., suggested that a large amount of lithium could be extracted and reinserted reversibly in samples with smaller grain sizes [73]. A novel multi scale and multi step Kinetic Monte Carlo strategy is developed in the present work, which can predict the performance of both $LiFePO_4$ and $LiCoO_2$ by employing appropriate input parameters corresponding to each material. As an initial stage, the solvent interactions are taken into consideration via bonding energy between the carbonyl oxygen of the EC/DEC mixture with the Li ions. In EC:DEC solvent, lithium ions are reported to hop between carbonyl oxygen bonds as $–C=O^{\delta-}…….Li^{\delta+}$ and hence solvent interaction is accounted via Li–O partial bond formation. The discharge curves obtained agree satisfactorily with existing literature for $LiCoO_2$ and $LiFePO_4$.

5.2. Methodology

The current methodology involves the assumption of the lithium ion battery as depicted in Figure 5.1. Cathode materials are $LiFePO_4$ and $LiCoO_2$ based on the case under consideration. The electrolyte employed is 1M $LiPF_6$ in binary solvents EC/DEC in the ratio 1:1. Random numbers are generated to obtain the concentration of Li^+ that gets inserted in the cathode by employing appropriate diffusion coefficients and distance criteria. From the concentration variation and the distance the Li ions have diffused, the capacity of the discharge process, and state of discharge of the battery can be predicted. The lithium ion is allowed to diffuse by the formation and breaking of the $C{=}O^{\delta-}\ldots Li^{\delta+}$ bonds. It involves the hopping mechanism of Li ions in the solvent molecules to reach the destination electrode. Depending upon the ratio of the EC/DEC mixture assumed, the type of interaction between the Li ions and the solvent will be varied to track the diffusion of the Li ions. The first Monte Carlo (MC) simulation code includes micro scale properties such as diffusion of spherical electrode particle within the periodic boundary conditions of 0<x<lp. The electrode particles are assumed as spheres and allowed to move in each step only to a distance of its nearest neighbor, employing the condition $ir(j) \geq e^{\left(\frac{-dLi1}{ds}\right)}$, where dLi1 is the nearest neighbor distance for the Li ion in the absence of solvent and ds being the thickness of the solid phase. The second MC code involves macro scale properties, namely solvation effects, diffusion coefficients, and the concentration gradient, to determine the diffusion of Li ions within the boundary conditions of lp<x<ls and employing the random number criterion $ir(j) \geq e^{\left(\frac{-dLi1}{ds_2}\right)}$, where

dLi1 is the nearest neighbor distance Li^+ can move in the presence of solvent and ds2 being the thickness of the separator. This Monte Carlo strategy is schematically represented in Figure 5.2. The potential applied is in the range of 2.4 to 4.5 Volts and the capacity is calculated from the concentration of Li ions diffusing through the separator and the distance gradient. Thus the discharge behavior of $LiCoO_2$ and $LiFePO_4$ as electrode materials in Li-ion battery can be simulated from Monte Carlo techniques employing different criteria. The present methodology helps in reduction of computation time and employs basic molecular parameters to attain the result. Monte Carlo seeds beyond 10^5 is not done because of convergence in the results from 10^2 to 10^5 seeds.

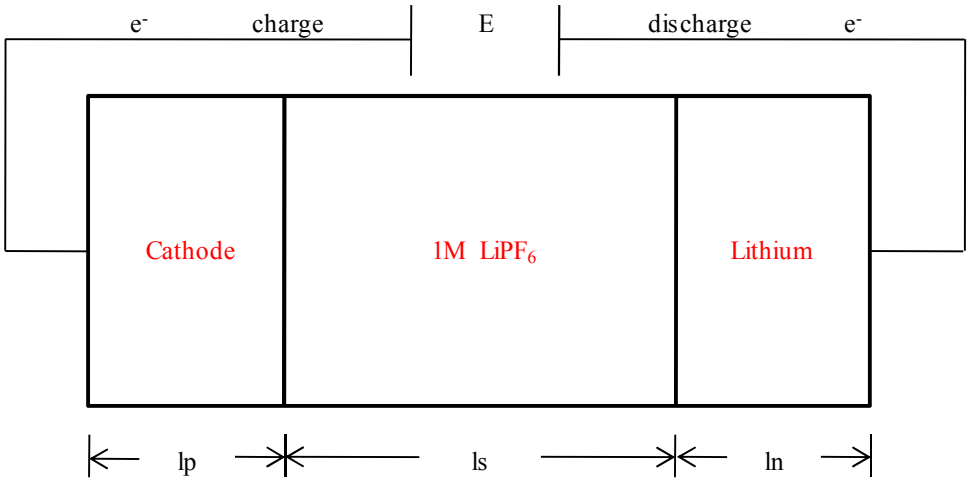

Figure 5.1: Schematic representation of the Lithium ion battery cell assumed for the simulation purpose, The cathode is either $LiFePO_4$ or $LiCoO_2$, where lp, ls, ln represent the thickness(length) of cathode, separator and the anode respectively.

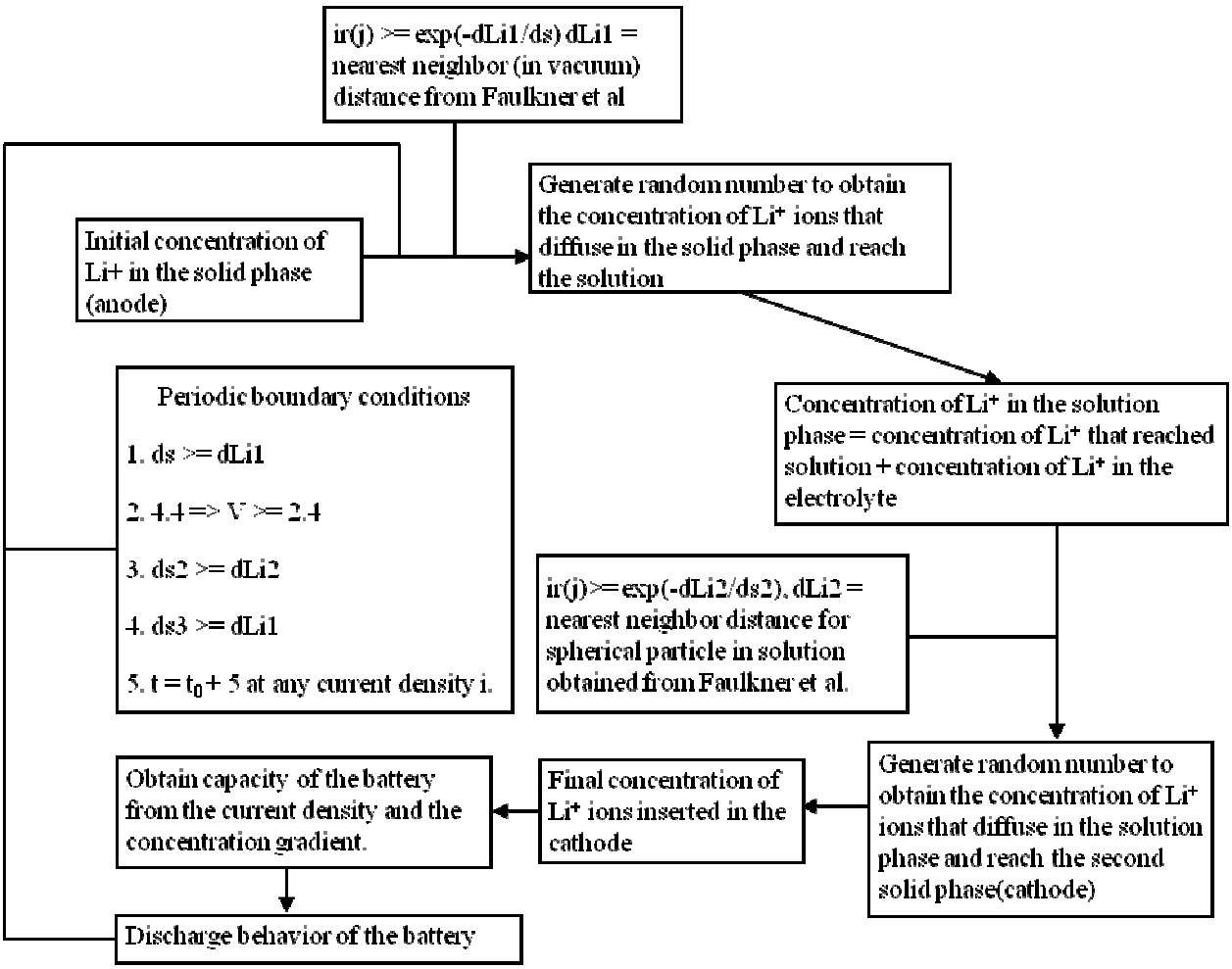

Figure 5.2: Scheme 1 - The scheme for the proposed simulation methodology for the discharge behavior of $LiFePO_4$ and $LiCoO_2$ battery

5.3. Parameters Employed

Input parameters for the Monte Carlo simulation such as diffusion coefficient of Li ions in solid phase, solution phase, porosity of the electrode, particle size, solvent interaction energy, volume fraction of the active material due to insertion and extraction of Li ions into the electrode are tabulated in Table 5.1. The values for $LiFePO_4$ are taken from Srinivasan et al and $LiCoO_2$ are from Subramanian et al [86,61].

5.4. Results and Discussion

The present Monte Carlo Simulation technique operates employing micro scale properties such as diffusion coefficient of Lithium ions in spherical electrode particle and the macro scale properties like solvation effects, diffusion coefficient of lithium ion in solution phase and the concentration gradient to determine the number of Li ions diffusing in solution and solid phase. The simulation codes are written in MATLAB version 6.5 and run in Intel centrino quadro core personal computer. The computation time consumed to get the discharge profile for the system involving 23800 moles of $LiFePO_4$ or $LiCoO_2$ at 10^5 Monte Carlo seeds is approximately 20 hours. The present simulation strategy can handle two different chemistries like $LiFePO_4$ and $LiCoO_2$ as battery material without any difficulty. These diversifying results only need to consider input parameter variation corresponding to the material under investigation.

Table 5.1: The parameters employed in the simulation strategy for $LiCoO_2$ [61] and $LiFePO_4$ [86]

Parameters employed	Values
Design parameters	
Cathode thickness	62 μm
Porosity	0.25
Volume fraction of active material	0.347
Initial salt concentration	1M
Separator thickness	25 μm
Particle size	43.3 nm
Electrode Parameters	
Diffusion coefficient of Li in $LiFePO_4$	$8*10^{-18}$ m^2/s
Diffusion coefficient of Li in $LiCoO_2$	$1*10^{-14}$ m^2/s
Diffusion coefficient of Li in 1M $LiPF_6$	$7.5*10^{-10}$ m^2/s
Contact resistance	0.0065 Ωm^2
Solvent interaction energy	
Kinetic energy contribution	1kT
Solvent interaction	$kT*\log(N_{sol}/N_{tot})$
Total number of molecules, N_{tot}	23800
Number of molecules in solvent, N_{sol}	Obtained from MC
Boltzmann constant, k	$1.38*10^{-23}$ J/K
Temperature, T	298 K

5.4.1. Discharge Behavior of $LiCoO_2$

Figure 5.3 indicates the discharge behavior of $LiCoO_2$/EC-DEC/Li half cell at different 'i' values of 0.13, 0.26, 0.52, 1.3, 2.6, and 5.2 mA/cm^2 in time. It is seen that although the discharge starts at a common potential of around 4V at higher applied current densities the discharge rate is faster. This is consistent with the existing Dynamic Monte Carlo [87], continuum models [81,82,61], Numerical analysis [83] in the literature for a given set of parameters employed. It can also be noticed that the maximum capacity attained by the half cell $LiCoO_2$/EC-DEC/Li is 140mAh/g and is in agreement with values in literature [61]. Unlike $LiFePO_4$, $LiCoO_2$ does not undergo any phase transition during the discharge process. Hence a sudden drop in capacity of the half cell does not exist even at very high applied current densities ca. 5.2 mA/cm^2. Scheme 2 represents the distribution of Lithium ion in CoO_2 structure during discharge process. No phase transition exists during the Li insertion process and the distribution is gradual. The illustration in scheme 2 is meant to describe the process via pictorial representations. It can be inferred from this scheme that as the CoO_2 is getting lithiated or discharged, the lithium gets inserted into the lattice and gradual decrease in the potential occurs with increase in the concentration of Li in the lattice. At full discharge, the potential drops suddenly, here the mole fraction of lithium (C_{Li} at that time/C_{Li} total) reaches unity implying that the electrode is totally discharged. The concentration of Li at each time step is obtained from the Monte Carlo codes and as a result the state–of–discharge (SOD) is tracked.

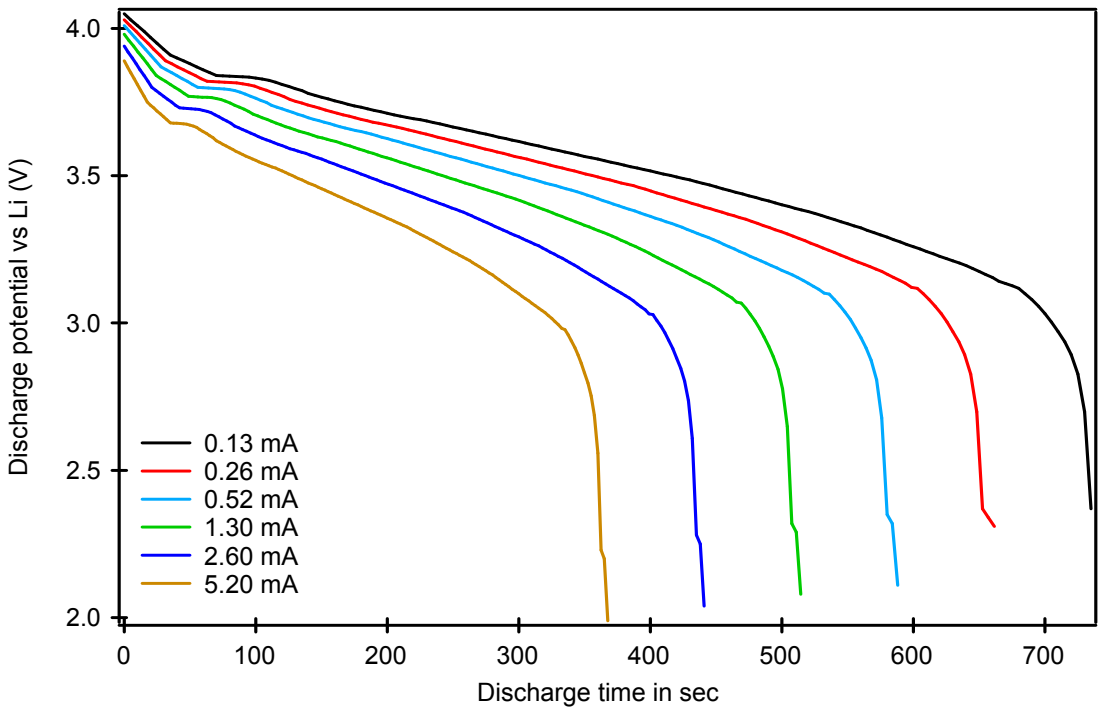

Figure 5.3: The discharge behavior of (potential vs time) for $LiCoO_2$ (current applied in mA/cm^2).

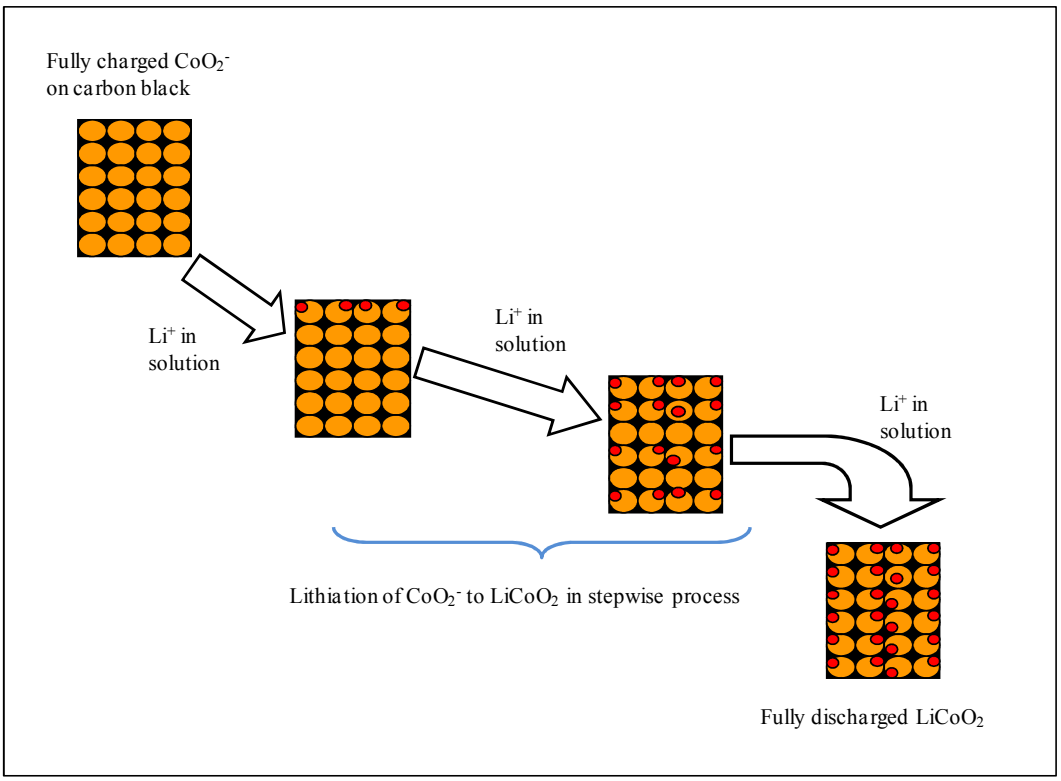

Figure 5.4: Scheme 2 - Schematic representation of the processes occurring in the discharge process of $LiCoO_2$ as lithium ion battery cathode material, Li foil is employed as the anode and reference electrode for simulation purpose. Insert represents the discharge behavior of $LiCoO_2$ from simulations, identical with the results of ref. 61.

5.4.2. Discharge Behavior of $LiFePO_4$

Figure 5.5 represents the discharge behavior of $LiFePO_4$/EC-DEC/Li half cell at different applied current densities in time. It can be inferred from these figures that two distinct features exist: (i) decrease in the utilization and (ii) decrease in the mid-plateau region with the increase in the applied current density [86]. The constancy of the potential over a wide range of time and capacity can be explained on the basis of phase transition occurring during insertion of Li into fully charged $FePO_4$. The constant behavior is mainly due to the equilibration of lithium deficient $Li_yFePO_4^{y-}$ and lithium

rich $Li_{(1-x)}FePO_4^{(1-x)-}$ phases, on continuous discharging of the fully charged $FePO_4$. As seen in Scheme 3, fully charged $LiFePO_4$ particle consists of a single $FePO_4$ phase. The discharge can be written as given by Newman et al. [86],

$$FePO_4+xLi^++xe^-\leftrightarrow xLiFePO_4+(1-x)FePO_4$$

and during the discharge process, the solid particles consists of two phases such as $FePO_4$ and $LiFePO_4$ in the proportion (1-x) and x, respectively, 'x' being the fraction of Li inserted into the solid particle of $FePO_4$. This first – order phase transition between the two species, $LiFePO_4$ and $FePO_4$, resists further lithiation of the cathode material, leading to constancy in the potential for longer time and capacity window. As the applied current density increases, the time required for the equilibration of the two phases is reduced and hence a decrease in the mid-plateau region is noticed. Thus as 'i' increases from 0.13 mA/cm^2 to 5.2 mA/cm^2 the capacity shows a drastic fall and this anomalous behavior could be attributed to the fact that the solvation energetic and the diffusion of Li ions in EC/DEC binary solvent play a vital role in the discharge process of $LiFePO_4$ -based battery materials. Since Li hops by formation and breaking of the O – Li bond in consecutive steps, the increase in current density does not allow the process to occur efficiently, thereby leading to sudden fall in the capacity. Thus the present simulation methodology explains this well known behavior of $LiFePO_4$ by employing simple random number criterion and periodic boundary conditions.

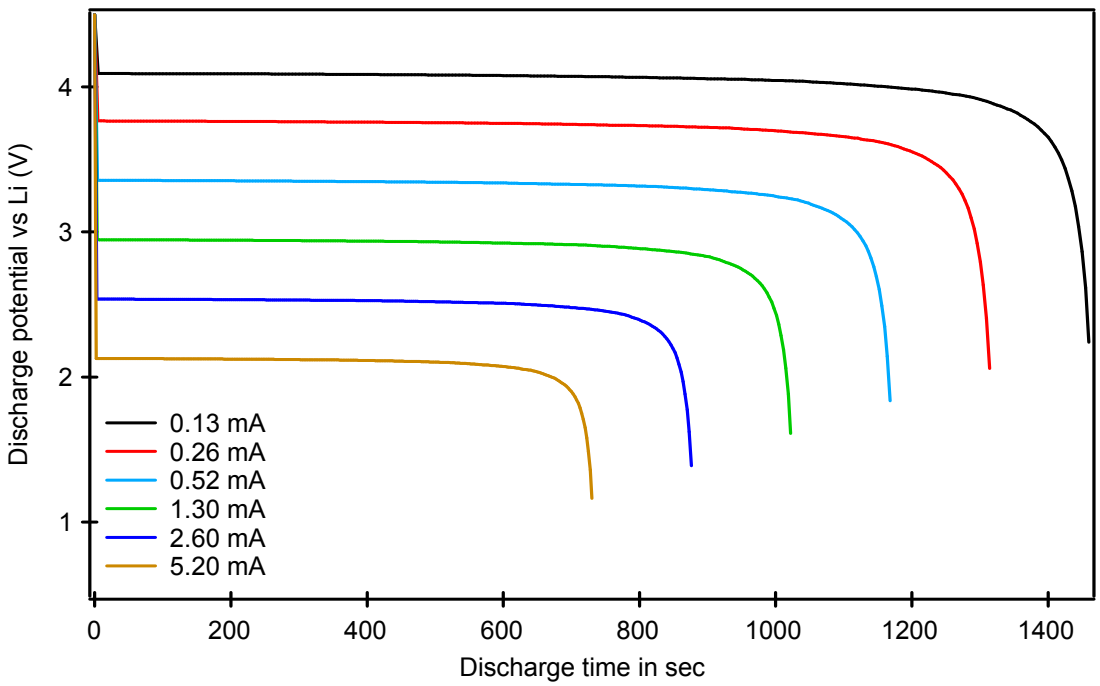

Figure 5.5: The discharge behavior (potential vs time) for $LiFePO_4$ (current applied in mA/cm^2).

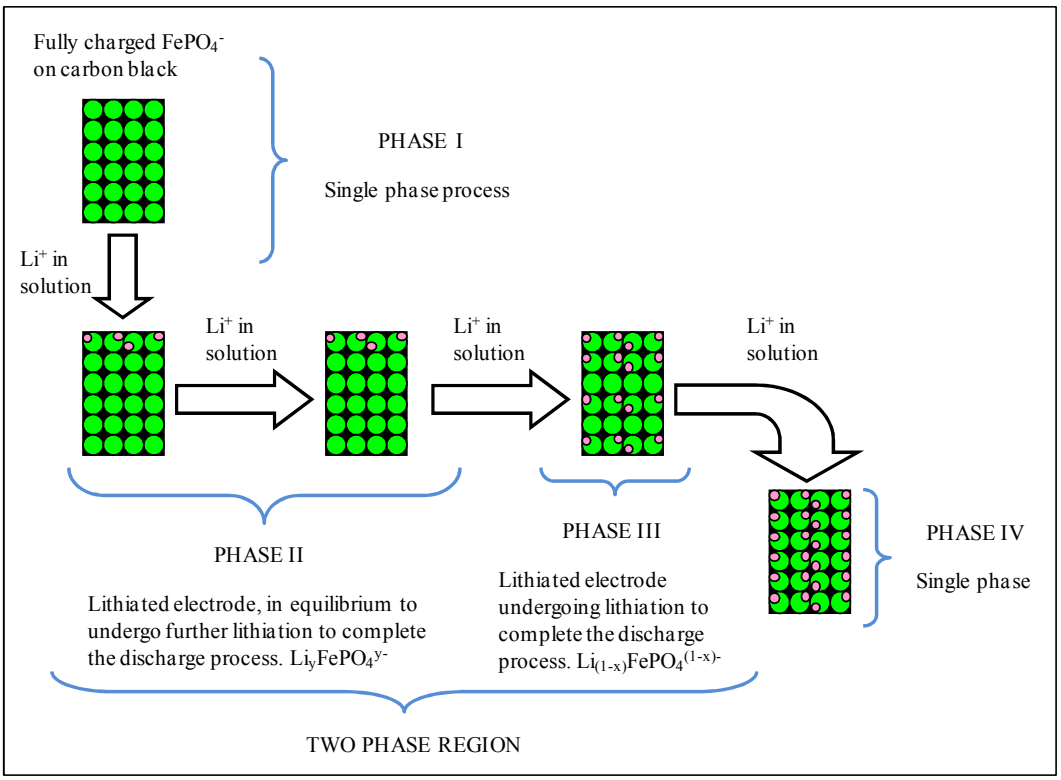

Figure 5.6: Scheme 3 - Schematic representation of the processes occurring in the discharge process of $LiFePO_4$ as lithium ion battery cathode material, Li foil is employed as the anode and reference electrode for simulation purpose. Insert represents the discharge curve from simulation of results employing the above mechanism, identical with the results of ref. [86].

5.5. Perspectives

The simulation methodology presented here possesses a simple frame work involving solvent interaction energetic, nearest neighbor distance in solid and solvent, diffusion coefficient of Li ion in solid and solution phase in evaluating the performance of $LiCoO_2$ and $LiFePO_4$ as cathode materials by invoking the hard sphere validity assumptions in conjunction with solvent interactions and transport properties. Although existing Monte Carlo Simulation techniques can handle this issue very well, inclusion of more input

parameters to account for the conceptual background makes it computationally tedious, increases the computation time and become specific to the chemistry of the material under investigation. However we can reinstate that this Monte Carlo strategy is complimentary in nature to the extensive existing literature on lithium ion battery and can easily be extended to understand the temperature effects on the battery performance, exact mechanism governing the nature of charge/discharge process, solvent interaction variations, conductivity profile of Li and methods to improve the performance of the batteries.

5.6. Conclusions from this work

The discharge behavior of $LiCoO_2$ and $LiFePO_4$ as cathode material is in agreement with existing literature on lithium ion batteries. Current methodology is multi scale in nature by taking into account micro scale properties such as diffusion of spherical electrode particle within the periodic boundary conditions of $0<x<lp$ and macro scale properties like solvation effects, diffusion coefficients and the concentration gradient to determine the diffusion of Li ions within the boundary conditions of $lp<x<ls$. The potential applied is in the range of 2.4 V to 4.5 V and the capacity is calculated from the concentration of Li ions diffusing through the separator and the distance gradient.

5.7. Scope for future work

A Monte Carlo strategy that has a generic backbone and future work in this topic will be based on applications to fuel cells, biosensors and highly electrically conducting bipolar electrode plates made of polymer composites for electrochemical studies. In the case of fuel cells the Continuum Monte Carlo codes described above can be modified based on electron – ion pathway determination. Depending on the reaction scheme and the free energy for the scheme from Monte Carlo codes, the reaction pathway and the rate determining step can be predicted. This holds good for the extension of the same to biosensors and to bipolar electrodes based on polymer composites of very high conductivity.

CHAPTER 6

PERSPECTIVES AND CONCLUSIONS

Simulation of Lithium Ion batteries has reached a mature level of understanding. Simulation of Li-ion battery systems for specific chemistries can be achieved in real-time by the use of reformulated models that have a high degree of precision and accuracy. As discussed earlier the use of these models need not be limited to ultra-high end battery applications, but, can be used in everyday electronic applications as technology advances. The robustness of these models allow them to be easily ported to other battery chemistries and new theory can easily be incorporated into these models as will be shown in projects and communications to follow from this group. Monitoring and control of batteries form the next big step in heading towards a fully automated battery management system. Efforts are already underway to use these re-formulated models in controls environment.

Specific applications demand specific desirable characteristics from the battery, for example, a battery that is used in the PHEV would require short charging times, this can be achieved by 'tweaking' the battery chemistry for faster charging times without damaging the performance or life of the battery. Modeling helps in determining the factors that contribute to optimizing battery chemistries, more insight can be obtained by looking at the molecular properties. Information from the molecular level need to be translated into useable information at the continuum level for better engineered batteries. As shown in chapter 1, both the transport and stationary applications of the future would be some form of hybrid electrochemical system. When making control decisions or

optimized usage decisions for the use of these hybrid systems, it is of prime importance that the predictions from the management systems are accurate, especially considering the complex nature of the hybrid systems itself and the crossflow of information that needs to be accounted for.

From the general discussion presented above, we can derive three major subgroups of perspectives that could throw light on future endeavors in the field of modeling and simulation of battery systems and in general electrochemical power sources, using reformulated models. They are:

1. Multiscale modeling of battery systems
2. Hybrid system modeling
3. Monitoring and control of battery systems

Let us look at how the current work can impact each of these three aspects mentioned.

6.1. Multiscale Simulation of Battery Systems – Design of New Materials Using Simulation

Although in its relative infancy, multiscale simulation concepts have been around for a while now. The questions posed in Chapter 5 could be answered by applying multiscale simulation, Figure 6.1 shows a schematic of the different techniques at different time and length scales. The most common use of multiscale simulation in electrochemical systems has been in the semiconductor fabrication industry [88-92]. The major hindrance to multiscale modeling problems has been computational speed and power requirements. The multiscale modeling community as a whole, are looking for simpler algorithms to give them comparable results.

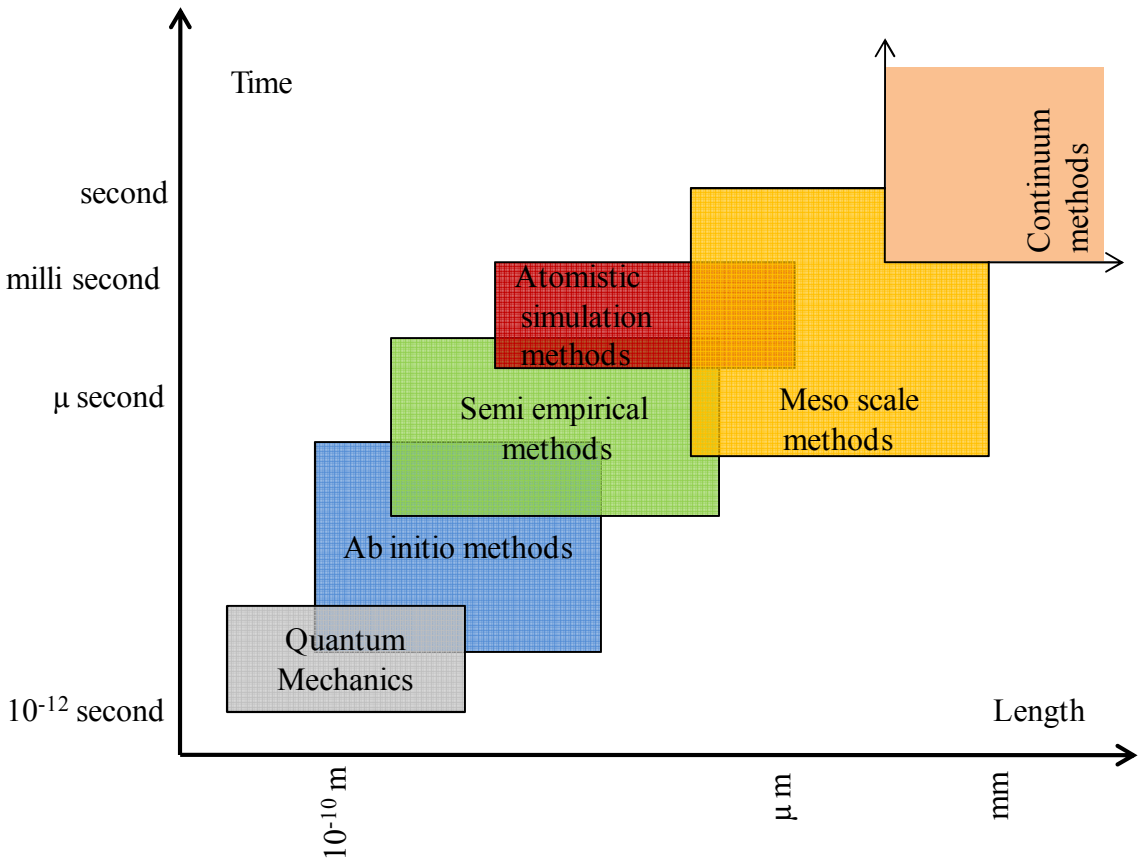

Figure 6.1: Simulation methods at varying time and length scales. Each method has its own independent attributes and can be used for specific purposes. Length scale and time scale overlap constitutes that there is flow of information between scales.

Understanding battery chemistries and helping develop custom battery materials for specific applications is a multiscale problem. Valuable information from the molecular level, for example, bond distances and bond energies, have a significant impact on the continuum design models. Most models at the molecular level are stochastic in nature, this introduces probability issues into the picture. Given the existing complex nature of the continuum models, computational time and memory would increase exponentially. The use of simplified engineering models would serve to simplify the computational time at the continuum scale of models, this would in turn reduce the

computational requirements at the continuum level and free up computational resources for the molecular models.

6.2. Hybrid Systems Modeling – Coupled Modeling of Various Power Sources

A hybrid system consists of two or more electrochemical power sources in series or parallel that contribute to the addition of power to a system. Most hybrid system modeling consists of using simple limiting models, such as, circuit models. This reduces the usability of these models for varied conditions. Using continuum models are a better choice given their versatility and robustness. Reformulated models not only fit in to the framework of hybrid systems modeling but also enable the framework to be a lot more flexible and robust. The time constants of the various electrochemical power sources, i.e., batteries, supercapacitors and fuel cells, are different and pose significant challenges to modeling the hybrid systems. It is proposed that using reformulated models that identify key dimensional groups will help solve part of the problem of understanding hybrid system models and their dynamics.

6.3. Monitoring and Control of Battery Systems – Extending the Life-time of Battery Systems

Monitoring and tracking batteries is an important task to prolong the life-time and prevent abuse of the battery. Most work in this field so far have been performed by electrical and electronics engineers. It is desired that control of Li-ion batteries be as robust as possible in very sensitive and expensive applications, for example, batteries used in satellites, military, etc. In these applications, wrong prediction could mean the loss of millions of dollars or loss of sensitive data or even loss of life.

Using engineering models for monitoring and control purposes involves parameter estimation. Difficulty arises when trying to estimate even a single parameter by using engineering models. The parameter estimation algorithms, for example, the Marquardt-Levenberg algorithm require large amounts of time for the estimation of one parameter. If engineering models have to be used in battery management systems, they need to be able to estimate and track more than one of these parameters to display the state-of-charge and state-of-health of the battery. Using these reformulated models, work has been done by colleages to estimate parameters for Li-ion batteries and they report a confidence level of 95% with considerable decrease in computational time and real-estate [94].

6.4. Conclusions

A simplification methodology for Lithium Ion battery models is presented. The models were benchmarked with the optimized full numeric finite difference models. The reformulated model is shown to retain the complexities of the original first principles based physics model. Excellent accuracy is seen between the simplified and finite difference numeric model. A numeric Symbolic solution (NSS) was discussed. The AC impedance response was simulated using NSS was found to predict with good accuracy when benchmarked with analytical solutions and rigorous numeric solutions. A novel Monte Carlo method that possesses a simple framework is presented. Discharge behavior for two cathode materials ($LiCoO_2$ and $LiFePO_4$), were predicted. The results obtained were in agreement with reports from literature. The methods and strategies proposed in this work have resulted in significant reduction in computational time and resources.

BIBLIOGRAPHY

[1] D. Linden, and T. B. Reddy, *Handbook of Batteries*, 3rd ed., McGraw Hill (2002)

[2] W. S. Harris, Ph.D. Dissertation, University of California – Berkeley (1958)

[3] M. S. Whittingham, "The role of ternary phases in cathode reactions", *J. Electrochem. Soc.*, **123**(3), 315-320 (1976)

[4] J. B. Goodenough, and M. S. Whittingham, "Solid state chemistry of energy conversion and storage", Proceedings of the Symposium, New York, N.Y., April 5-8, (1976)

[5] J. B. Goodenough, H. Y. P. Hong, and J. A. Kafalas, "Fast sodium(1+) ion transport in skeleton structures", *Mat. Res. Bull.*, **11**(2), 203-20 (1976)

[6] http://www.sony.net/SonyInfo/News/Press/200502/05-006E/index.html (accessed 02/23/09)

[7] W. A. van Schakwijk and B. Scrosati (Eds.), *Advances in Lithium-ion batteries*, Kluwer Academic / Plenum publishers, New York (2002)

[8] M. S. Whittingham, "Lithium Batteries and Cathode Materials", *Chem. Rev.*, **104**(10), 4271–4302 (2004)

[9] R. A. Huggins, *Advances Batteries – Material Science Aspects*, Springer science, New York (2008)

[10] M. Wakihara and O. Yamamoto (Eds.), *Lithium Ion Batteries – Fundamentals and Performance*, Wiley, Weinheim (1998)

[11] P. Arora and Z. (John) Zhang, "Battery separators", *Chem. Rev.*, **104** (10), 4419–4462 (2004)

[12] B. Scrosati, "Recent advances in lithium ion battery materials", *Electrochim. Acta*, **45**(15-16), 2461 (2000)

[13] D. Aurbach, E. Zinigrad, Y. Cohen, and H. Teller, "A short review of failure mechanisms of lithium metal and lithiated graphite anodes in liquid electrolyte solutions", *Solid State Ionics*, **148**(3-4), 405-416 (2002)

[14] P. P. Soo, B. Huang, Y-I. Jang, Y-M. Chiang, D. R. Sadoway and A. M. Mayes, "Rubbery block copolymer electrolytes for solid-state rechargeable lithium batteries", *J. Electrochem. Soc*., **146**(1), 32-37 (1999)

[15] A. Blazejczyk, W. Wieczorek, R. Kovarsky, D. Golodnitsky, E. Peled, L. G. Scanlon, G. B. Appetecchi and B. Scrosati, "Novel solid polymer electrolytes with single lithium-ion transport", *J. Electrochem. Soc*., **151**(10), A1762-A1766 (2004)

[16] M. Winter and R. J. Brodd, "What Are Batteries, Fuel Cells, and Supercapacitors?", *Chem. Rev.*, **104** (10), 4245–4270 (2004)

[17] Goals for advanced EV batteries (online document from www.uscar.org, accessed 02/16/2009): http://www.uscar.org/commands/files_download.php?files_id=27

[18] GM-Chevrolet: http://www.chevrolet.com/electriccar/ (accessed 02/20/2009)

[19] V. Pop, H. J. Bergveld, D. Danilov, P. P. L. Regtien, and P. H. L. Notten, *Battery Management Systems - Accurate State-of-Charge Indication for Battery-Powered Applications*, Springer Science, (2008)

[20] V. Pop, H. J. Bergveld, P. H. L. Notten and P. P. L. Regtien, State-of-the-art of State-of-Charge determination, *Measurement Science and Technology Journal*, **16**(12), R93–R110 (2005)

[21] H. J. Bergveld, W. S. Kruijt and P. H. L. Notten, *Battery Management Systems – Design by Modelling*, Philips Research Book Series, **1**, Kluwer Academic Publishers, Boston (2002)

[22] Texas Instruments, High-performance battery monitor IC with Coulomb counter, voltage, and temperature measurements, Doc. I.D. SLUS521A (2002)

[23] S. Grewal, D. A. Grant, "A novel technique for modelling the state of charge of lithium ion batteries using artificial neural networks", Proc. Int. Telecommunications, Energy Conf. (IEEE), **484**, 14–18 (2001)

[24] A. J. Salkind, C. Fennie, P. Singh, T. Atwater and D. E. Reisner, "Determination of state-of-charge and state-of-health of batteries by fuzzy logic methodology", *J. Power Sources*, **80**(1-2), 293–300 (1999)

[25] G. Plett, "Extended Kalman filtering for battery management systems of LiPB based HEV battery packs: Part 1. Background", *J. Power Sources*, **134**(2), 252–261 (2004)

[26] G. Plett, "Extended Kalman filtering for battery management systems of LiPB based HEV battery packs: Part 2. Modeling and identification", *J. Power Sources*, **134**(2), 262–276 (2004)

[27] G. Plett, "Extended Kalman filtering for battery management systems of LiPB based HEV battery packs: Part 3. State and parameter estimation", *J. Power Sources*, **134**(2), 277–292 (2004)

[28] G. G. Botte, V. R. Subramanian, R. E. White, "Mathematical modeling of secondary lithium batteries", *Electrochim. Acta*, **45**(15-16), 2595–2609 (2000)

[29] M. Doyle and J. Newman, "The use of mathematical modeling in the design of lithium/polymer battery systems", *Electrochim. Acta*, **40**(13-14), 2191-2196 (1995)

[30] P. M. Gomadam, J. W. Weidner, R. A. Dougal, R. E. White, "Mathematical modeling of lithium-ion and nickel battery systems", *J. Power Sources*, **110**(2), 267–284 (2002)

[31] P. Nelson, I. Bloom, K. Amine, and G. Henriksen, "Design modeling of lithium-ion battery performance", *J. Power Sources,* **110**(2)**,** 437–444 (2002)

[32] M. W. Verbrugge, D. R. Baker and B. J. Koch, "Mathematical modeling of high-power-density insertion electrodes for lithium ion batteries", *J. Power Sources* **110**(2), 295–309 (2002)

[33] J. Newman and K. E. Thomas-Alyea, *Electrochemical Systems,* 3rd edition. Hoboken, N. J., Wiley-Interscience (2004)

[34] R. B. Bird, W. E. Stewart, and E. N. Lightfoot, *Transport Phenomena*, John Wiley and Sons, New York (2007)

[35] A. J. Bard and L. R. Faulkner, *Electrochemical Methods; Fundamentals and Applications*, Wiley (1980)

[36] J O'M Bockris, A. K. N. Reddy and M. E. Gamboa-Aldeco (Eds.), *Modern Electrochemistry*, 2nd ed., Plenum Press, New York (2007)

[37] J. Newman and W. Tiedemann, "Porous-Electrode Theory with Battery Applications", *AIChE J.*, **21**(1), 25-41 (1975)

[38] M. Doyle, T. F. Fuller and J. Newman, "Modeling the Galvanostatic Charge and Discharge of the Lithium/Polymer/Insertion", *J. Electrochem. Soc.*, **140**(6), 1526-1533 (1993)

[39] T. Fuller, M. Doyle and J. Newman, "Simulation and Optimization of the Dual Lithium Ion Insertion Cell", *J. Electrochem. Soc*., **141**(1), 1-10 (1994)

[40] M. Doyle, J. Newman, A. S. Gozdz, C. N. Schmutz, and J-M. Tarascon "Comparison of Modeling Predictions with Experimental Data from Plastic Lithium Ion", *J. Electrochem. Soc*., **143**(12), 1890-1903 (1996)

[41] M. Doyle and J. Newman, "Modeling the performance of rechargeable lithium-based cells: design correlations for limiting cases", *J. Power Sources*, **54**(1), 46-51 (1995)

[42] P. De Vidts and R. E. White, "Governing Equations for Transport in Porous Electrodes", *J. Electrochem. Soc*., **144**(4), 1343-1353 (1997)

[43] R. Darling and J. Newman, "Modeling a Porous Intercalation Electrode with Two Characteristic Particle Sizes", *J. Electrochem. Soc*., **144**(12), 4201-4208 (1997)

[44] P. De Vidts Sabelle, *Mathematical modeling of a nickel/hydrogen cell*, Ph.D. dissertation, Texas A&M University, College Station, TX (1995)

[45] I. Nozad, H. G. Carbonell, and S. Whitaker, "Heat conduction in multiphase systems - II. Experimental method and results for three-phase systems", *Chem. Eng. Sci.*, **40**(5), 857-853 (1985)

[46] C. M. Doyle, *Design and Simulation of Lithium Rechargeable Batteries*, Ph.D. dissertation, University of California – Berkeley (1995)

[47] G. G. Botte and R. E. White, "Modeling Lithium Intercalation in a Porous Carbon Electrode", *J. Electrochem. Soc.,* **148**(1), A54-A66 (2001)

[48] P. Arora, M. Doyle and R. E. White, "Mathematical Modeling of the Lithium Deposition Overcharge Reaction in Lithium-Ion Batteries Using Carbon-Based Negative Electrodes", *J. Electrochem. Soc.,* **146**(10), 3543-3553 (1999)

[49] Mathematical Modeling of Lithium Batteries (with Karen E. Thomas and Robert M. Darling). Walter A. van Schalkwijk and Bruno Scrosati, eds., *Advances in Lithium-Ion Batteries* (New York: Kluwer Academic/Plenum Publishers, 2002) pp. 345-392

[50] M. Doyle and Y. Fuentes, "Computer Simulations of a Lithium-Ion Polymer Battery and Implications for Higher Capacity Next-Generation Battery Designs", *J. Electrochem. Soc.*, **150**(6), A706-A713 (2003)

[51] J. H. Ferziger and M. Peric, *Computational methods for fluid dynamics*,3rd ed., Springer-Verlag, Berlin 2002

[52] BANDJ - http://www.cchem.berkeley.edu/jsngrp/fortran_files/band.f (accessed 02/23/09)

[53] DASSL – Linda Petzold

[54] H. A. Kooijman, *Dynamic nonequilibrium column simulation*, Ph.D. dissertation, Clarkson University (1995)

[55] http://www.comsol.com/ (accessed 02/23/09)

[56] V. Boovaragavan and V. R. Subramanian, "A quick and efficient method for consistent initialization of battery models", *Electrochem. Comm.*, **9**(7), 1772–1777 (2007)

[57] V. Balakotaiah and S. Chakraborty, "Averaging Theory and Low-dimensional Models for Chemical Reactors and Reacting Flows", *Chem. Eng. Sci.*, **58**(21), 4769-4786 (2003)

[58] V. Balakotaiah and H-C. Chang, "Hyperbolic homogenized models for thermal and solutal dispersion", *SIAM J. Appl. Math.*, **63**(4), 1231-1258 (2003)

[59] F. A. Howes and S. Whitaker, "The Spatial Averaging Theorem Revisited", *Chem. Eng. Sci.*, **40**(8)**,** 1387-1392 (1985)

[60] K. E. Thomas and J. Newman, "Thermal Modeling of Porous Insertion Electrodes", *J. Electrochem. Soc*., **150**(2), A176-A192 (2003)

[61] V. R. Subramanian, V. D. Diwakar, and D. Tapriyal, "Efficient macro-micro scale coupled simulation of batteries", *J. Electrochem. Soc.*, **152**(10), A2002-A2008 (2005)

[62] V. Srinivasan and C. Y. Wang, "Analysis of Electrochemical and Thermal Behavior of Li-Ion Cells", *J. Electrochem. Soc*., **150**(1), A98-A106 (2003)

[63] C. Y. Wang and V. Srinivasan, "Computational battery dynamics (CBD)—electrochemical/thermal coupled modeling and multi-scale modeling", *J. Power Sources* **110**(2), 364–376 (2002)

[64] Q. Guo, V. R. Subramanian, J. W. Weidner and R. E. White, "Estimation of diffusion coefficient of lithium in carbon using AC impedance technique", *J. Electrochem. Soc.*, **149**(3), A307-A318 (2002)

[65] J. P. Meyers, M. Doyle, R. M. Darling and J. Newman, "The impedance response of a porous electrode composed of intercalation particles", *J. Electrochem. Soc.,* **147**(8), 2930-2940 (2000)

[66] S. Devan, V. R. Subramanian and R. E. White, "Analytical Solution for the Impedance of a Porous Electrode", *J. Electrochem. Soc.*, **151**(6), A905-A913 (2004)

[67] A. Varma and M. Morbidelli, *Mathematical Methods in Chemical Engineering*, Oxford University Press, New York (1997)

[68] http://www.maplesoft.com/

[69] V. R. Subramanian and R. E. White, "Symbolic solutions for boundary value problems using Maple", *Comp. Chem. Eng.*, **24**(11), 2405-2416 (2000)

[70] V. R. Subramanian and R. E. White, "Semianalytical method of lines for solving elliptic partial differential equations", *Chem. Eng. Sci.,* **59**(4), 781-788 (2004)

[71] P. Englezos and N. Kalogerakis, *Applied Parameter Estimation for Chemical Engineers*, Marcel Dekker, New York (2001)

[72] K. Mizushima, P. C. Jones, P. C. Wiseman and J. B. Goodenough, "Lithium cobalt oxide (Li_xCoO_2) ($0<x\leq1$): a new cathode material for batteries of high energy density", *Mater. Res. Bull.* **15**(6), 783-789 (1980)

[73] A. K. Padhi, K. S. Nanjundaswamy and J. B. Goodenough, "Phospho-olivines as positive-electrode materials for rechargeable lithium batteries", *J. Electrochem. Soc.,* **144**(4), 1188-1194 (1997)

[74] N. Ravert, Y. Chouinard, J. F. Magnan, S. Besner, M. Gauthier and M. Armand, "Electroactivity of natural and synthetic triphylite", *J. Power Sources*, **97-98**, 503-507 (2001)

[75] Z. Chen and J. R. Dahn, "Reducing carbon in LiFePO4/C composite electrodes to maximize specific energy, volumetric energy, and tap density", *J. Electrochem. Soc.*, **149**(9), A1184-A1189 (2002)

[76] H. Huang, S.C.Yin and L.F.Nazar, *Electrochem. Solid – State Lett*., "Approaching theoretical capacity of $LiFePO_4$ at room temperature at high rates", **4**(10), A170-A172 (2001)

[77] F. Croce, A. D'Epifanio, J. Hassoun, A. Deptula, T. Olczac and B. Scrosati," **"**A novel concept for the synthesis of an improved $LiFePO_4$ lithium battery cathode", *Electrochem. Solid – State Lett*., **5**(3), A47-A50 (2002)

[78] S. Franger, F. Le Cras, C. Bourbon and H. Rouault, "Comparison between different $LiFePO_4$ synthesis routes and their influence on its physico-chemical properties", *J. Power Sources*, **119-121**, 252-257 (2003)

[79] S. Franger, F. Le Cras, C. Bourbon and H. Rouault, "$LiFePO_4$ Synthesis Routes for Enhanced Electrochemical Performance", *Electrochem. Solid – State Lett*., **5**(10)**,** A231-A233 (2002)

[80] S. Franger, C. Bourbon and F. Le Cras, "Optimized lithium iron phosphate for high-rate electrochemical applications", *J. Electrochem. Soc.,* **151**(7)**,** A1024-A1027 (2004)

[81] J. Newman, K. E. Thomas, H. Hafezi and D. R. Wheeler, "Modeling of lithium-ion batteries", *J. Power Sources*, **119-121,** 838-843 (2003)

[82] M. W. Verbrugge, D. R. Baker and B. J. Koch, "Mathematical modeling of high-power-density insertion electrodes for lithium ion batteries", *J. Power Sources*, **110**(2), 295-309 (2002)

[83] X-C. Zhang, W. Shyy, and A. M. Sastry, "Numerical Simulation of Intercalation-Induced Stress in Li-Ion Battery Electrode Particles", *J. Electrochem. Soc*., **154**(10), A910-A916 (2007)

[84] W. F. Howard and R. M. Spotnitz, “Theoretical evaluation of high-energy lithium metal phosphate cathode materials in Li-ion batteries”, *J. Power Sources*, **165**(2), 887-891 (2007)

[85] V. Srinivasan and J. Newman, “Existence of Path-dependence in the LiFePO4 Electrode”, *Electrochem. Solid – State Lett*., **9**(3), A110-A114 (2006)

[86] V. Srinivasan and J. Newman, “Design and Optimization of a Natural Graphite/Iron Phosphate Lithium-ion Cell”, *J. Electrochem. Soc.*, **151**(10), A1530-A1538 (2004)

[87] R. Darling and J. Newman, “Dynamic Monte Carlo Simulations of Diffusion in $Li_yMn_2O_4$”, *J. Electrochem. Soc*., **146**(10), 3765-3772 (1999)

[88] R. D. Braatz, R. C. Alkire, E. Seebauer, E. Rusli, R. Gunawan, T. O. Drews, X. Li and Y. He, "Perspectives on the design and control of multiscale systems", *J. Process Control*, **16**(3), 193-204 (2006)

[89] T. O. Drews, S. Krishnan, J. C. Alameda, D. Gannon, R. D. Braatz and R. C. Alkire, "Multiscale simulations of copper electrodeposition onto a resistive substrate", *IBM Journal of Research & Development*, **49**, 49-63 (2005)

[90] T. O. Drews, R. Aleksandar, J. Erlebacher, R. D. Braatz, P. C. Searson and R. C. Alkire, "Stochastic simulation of the early stages of kinetically limited electrodeposition", *J. Electrochem. Soc*., **153**(6), C434-C441 (2006)

[91] T. Drews, E. Webb, D. Ma, J. Alameda, R. Braatz, and R. Alkire, “Coupled Mesoscale-Continuum Simulations of Copper Electrodeposition in a Trench”, *A.I.Ch.E. J.*, **50**(1), 226-240 (2004)

[92] R. Alkire, “Processing Nanostructured Materials: The Need to Integrate Experimental Data with Multiscale Continuum/Non-Continuum Simulations”, *J. Electroanalytical Chem.*, **559**, 3-12 (2003)

[93] A. Marquez and P. B. Balbuena, "Molecular Dynamics study of graphite/electrolyte interfaces", *J. Electrochem. Soc.*, **148**, A624-A635 (2001)

[94] V. Boovaragavan, S. Harinipriya and V. R. Subramanian, “Towards accurate real-time (milliseconds) parameter estimation of Lithium-ion batteries using reformulated physics based models”, *J. Power Sources*, **183**(1), 361-365 (2008)

[95] V. R. Subramanian, V. Boovaragavan V. Ramadesigan and M. Arabandi, “Mathematical Model Reformulation for Lithium-ion Battery Simulation: Galvanostatic Boundary Conditions”, *J. Electrochem. Soc.*, **156**(4), A260-A271 (2009)

APPENDIX A: Summary of Governing equations and boundary conditions for a Li-ion Battery

Region	Eq. No.	Governing equations	Boundary conditions
Cathode	1	$\varepsilon_{\mathrm{p}}\frac{\partial c}{\partial t}=D_{\mathrm{eff,p}}\frac{\partial^2 c}{\partial x^2}+a_{\mathrm{p}}\left(1-t_+\right)j_{\mathrm{p}}$ initial condition $c\big\vert_{t=0}=c_0$	$-D_{\mathrm{eff,p}}\left.\frac{\partial c}{\partial x}\right\vert_{x=0}=0$ & $-D_{\mathrm{eff,p}}\left.\frac{\partial c}{\partial x}\right\vert_{x=l_p,-}=-D_{\mathrm{eff,s}}\left.\frac{\partial c}{\partial x}\right\vert_{x=l_{\mathrm{p}},+}$
	2	$-\sigma_{\mathrm{eff,p}}\frac{\partial \Phi_1}{\partial x}-\kappa_{\mathrm{eff,p}}\frac{\partial \Phi_2}{\partial x}+\frac{2\kappa_{\mathrm{eff,p}}RT}{F}\left(1-t_+\right)\frac{\partial \ln c}{\partial x}=I$	$-\kappa_{\mathrm{eff,p}}\left.\frac{\partial \Phi_2}{\partial x}\right\vert_{x=0}=0$ & $-\kappa_{\mathrm{eff,p}}\left.\frac{\partial \Phi_2}{\partial x}\right\vert_{x=l_p,-}=-\kappa_{\mathrm{eff,s}}\left.\frac{\partial \Phi_2}{\partial x}\right\vert_{x=l_{\mathrm{p}},+}$
	3	$\sigma_{\mathrm{eff,p}}\frac{\partial^2 \Phi_1}{\partial x^2}=a_{\mathrm{p}}Fj_{\mathrm{p}}$	$\left.\frac{\partial \Phi_1}{\partial x}\right\vert_{x=0}=-\frac{I}{\sigma_{\mathrm{eff,p}}}$ & $-\sigma_{\mathrm{eff,p}}\left.\frac{\partial \Phi_1}{\partial x}\right\vert_{x=l_{\mathrm{p}}}=0$
	4	$\frac{\partial c_{\mathrm{s}}}{\partial t}=\frac{D_{\mathrm{s,p}}}{r^2}\frac{\partial}{\partial r}\left(r^2\frac{\partial c_{\mathrm{s}}}{\partial r}\right)$ initial condition $c_s\big\vert_{t=0}=0.5c_{s,\max,p}$	$\left.\frac{\partial c_{\mathrm{s}}}{\partial r}\right\vert_{r=0}=0$ & $j_{\mathrm{p}}=-D_{\mathrm{s,p}}\left.\frac{\partial c_{\mathrm{s}}}{\partial r}\right\vert_{r=R_{\mathrm{p}}}$
Separator	5	$\varepsilon_{\mathrm{s}}\frac{\partial c}{\partial t}=D_{\mathrm{eff,s}}\frac{\partial^2 c}{\partial x^2}$	$-D_{\mathrm{eff,p}}\left.\frac{\partial c}{\partial x}\right\vert_{x=l_p,-}=-D_{\mathrm{eff,s}}\left.\frac{\partial c}{\partial x}\right\vert_{x=l_p,+}$ & $-D_{\mathrm{eff,s}}\left.\frac{\partial c}{\partial x}\right\vert_{x=l_p+l_s,-}=-D_{\mathrm{eff,n}}\left.\frac{\partial c}{\partial x}\right\vert_{x=l_p+l_s,+}$
	6	$I=-\kappa_{\mathrm{eff,s}}\frac{\partial \Phi_2}{\partial x}+\frac{2\kappa_{\mathrm{eff,s}}RT}{F}\left(1-t_+\right)\frac{\partial \ln c}{\partial x}$	$-\kappa_{\mathrm{eff,p}}\left.\frac{\partial \Phi_2}{\partial x}\right\vert_{x=l_p,-}=-\kappa_{\mathrm{eff,s}}\left.\frac{\partial \Phi_2}{\partial x}\right\vert_{x=l_p,+}$ & $-\kappa_{\mathrm{eff,s}}\left.\frac{\partial \Phi_2}{\partial x}\right\vert_{x=l_p+l_s,-}=-\kappa_{\mathrm{eff,n}}\left.\frac{\partial \Phi_2}{\partial x}\right\vert_{x=l_p+l_s,+}$
Anode	7	$\varepsilon_{\mathrm{n}}\frac{\partial c}{\partial t}=D_{\mathrm{eff,n}}\frac{\partial^2 c}{\partial x^2}+a_{\mathrm{n}}\left(1-t_+\right)j_{\mathrm{n}}$ initial condition $c\big\vert_{t=0}=c_0$	$-D_{\mathrm{eff,s}}\left.\frac{\partial c}{\partial x}\right\vert_{x=l_{\mathrm{p}}+l_s,-}=-D_{\mathrm{eff,n}}\left.\frac{\partial c}{\partial x}\right\vert_{x=l_{\mathrm{p}}+l_s,+}$ & $-D_{\mathrm{eff,n}}\left.\frac{\partial c}{\partial x}\right\vert_{x=l_{\mathrm{p}}+l_{\mathrm{s}}+l_{\mathrm{n}}}=0$
	8	$-\sigma_{\mathrm{eff,n}}\frac{\partial \Phi_1}{\partial x}-\kappa_{\mathrm{eff,n}}\frac{\partial \Phi_2}{\partial x}+\frac{2\kappa_{\mathrm{eff,n}}RT}{F}\left(1-t_+\right)\frac{\partial \ln c}{\partial x}=I$	$-\kappa_{\mathrm{eff,s}}\left.\frac{\partial \Phi_2}{\partial x}\right\vert_{x=l_{\mathrm{p}}+l_s,-}=-\kappa_{\mathrm{eff,n}}\left.\frac{\partial \Phi_2}{\partial x}\right\vert_{x=l_{\mathrm{p}}+l_s,+}$ & $\Phi_2\big\vert_{x=l_{\mathrm{p}}+l_{\mathrm{s}}+l_{\mathrm{n}}}=0$
	9	$\sigma_{\mathrm{eff,n}}\frac{\partial^2 \Phi_1}{\partial x^2}=a_{\mathrm{n}}Fj_{\mathrm{n}}$	$-\sigma_{\mathrm{eff,n}}\left.\frac{\partial \Phi_1}{\partial x}\right\vert_{x=l_{\mathrm{p}}+l_s}=0$ & $\left.\frac{\partial \Phi_1}{\partial x}\right\vert_{x=l_{\mathrm{p}}+l_{\mathrm{s}}+l_{\mathrm{n}}}=-\frac{I}{\sigma_{\mathrm{eff,n}}}$
	10	$\frac{\partial c_{\mathrm{s}}}{\partial t}=\frac{D_{\mathrm{s,n}}}{r^2}\frac{\partial}{\partial r}\left(r^2\frac{\partial c_{\mathrm{s}}}{\partial r}\right)$ initial condition $c_s\big\vert_{t=0}=0.85c_{s,\max,n}$	$\left.\frac{\partial c_{\mathrm{s}}}{\partial r}\right\vert_{r=0}=0$ & $j_{\mathrm{n}}=-D_{\mathrm{s,n}}\left.\frac{\partial c_{\mathrm{s}}}{\partial r}\right\vert_{r=R_{\mathrm{n}}}$

VITA

Vinten D. Diwakar was born on 14 October 1978 in Madras (now, Chennai), India, to Dr. Joseph E. Diwakar and Mary E. Poornakumari. He obtained a Bachelor of Engineering degree in Chemical Engineering from Bangalore University, India, in 2000. He completed a Master of Science degree in Chemical Engineering in 2004 from Tennessee Technological University, Cookeville. Vinten is currently a candidate for Doctor of Philosophy in Engineering.